Low-frequency vibrations of strongly inhomogeneous multicomponent elastic structures

Olga Sergushova

Submitted in partial fulfilment of the requirements of the degree of Doctor of Philosophy

School of Computing and Mathematics, University of Keele.

October 2018

Declaration

I certify that this thesis submitted for the degree of Doctor of Philosophy is the result of my own research, except where otherwise acknowledged, and that this thesis (or any part of the same) has not been submitted for a higher degree to any other university or institution.

Signed: .....
(Olga Sergushova)

Date: .....

Acknowledgements

I want to gratitude all who have helped me during this project.

Firstly, I am grateful to both of my supervisors. My appreciation goes out to Prof. Julius Kaplunov, for the continuous support of my Ph.D study, for his patience, motivation, and immense knowledge. His guidance helped me in all the time of research and writing of this thesis. I also would like to thank Dr. Danila Prikazchikov for the patient guidance, encouragement and advice he has provided throughout my time as his student. I have been extremely lucky to have supervisors who cared so much about my work, and who responded to my questions and queries so promptly.

Finally, I would like to express my sincere gratitude to my family and friends for supporting me throughout writing this thesis and my life in general. Especially I would like to thank my parents, whose love and guidance are with me in what ever I pursue.

Abstract

The thesis deals with 1D and 2D scalar equations governing dynamic behaviour of strongly inhomogeneous layered structures. Harmonic vibrations of a composite rod and antiplane shear motions of a cylindrical body consisting of several components are studied paying particular attention to the lowest frequencies. The main focus is on a strong contrast between the parameters characterising structure components, including their sizes, material stiffness, and densities.

We start with a multi-parametric analysis of the near-rigid body motions of rods and cylindrical bodies with piecewise uniform properties. The listed problems allow exact analytical solutions demonstrating that the values of all lowest eigenfrequencies tend to zero at large/small ratios of material and geometric parameters. The low-frequency behaviour is considered for so-called global and local regimes, and simple explicit conditions on the problem parameters, underlying each of the regimes, are derived.

Further, we present a perturbation procedure for a more general setup based on the evaluation of the almost rigid body motions of ″stronger″ components assuming a high contrast of material parameters. The proposed approach is extended to structures of arbitrary shape, with variable material parameters, as well as to multi-component structures. We obtain asymptotic formulae for the lowest natural frequencies and also present illustrative examples for each of the studied problems. Many of asymptotic estimations are compared with exact solutions. The results of the thesis are applicable to a mathematical justification of shear deformation theories for multi-layered plates and shells with a strong transverse inhomogeneity.

Contents

List of Figures

1 Introduction

Composite elastic structures have many applications within the industry since long ago. For example, both commercial and military aircraft, aerospace, automotive, and civil engineering use a large amount of multi-layered structures, e.g. see Milton (2002), Berthelot (2012), and references therein. In addition, geomechanics and biomechanics adapt composite material technology, see Ramakrishna et al (2001), Salernitano and Migliaresi (2003), and Borja (2011).

In recent years, new applications associated with the development of multi-layered structures with high contrast in the geometrical and mechanical properties appear and revive interest to the subject. Various structural components may have contrast material and geometric characteristics, including stiffness, volume density, and size. As a typical example, sandwich plates can be mentioned. Sandwich structures are widely used in civil and mechanical engineering and are therefore intensively studied, see for instance Vinson (1999).

Another area that promises to increase significantly the number of potential applications is related to the fast developing field of metamaterials. The unique properties of metamaterials are often originated from the combined performance of periodically arranged phases having extremely high contrast, see e.g. Perrins and McPhedran (2010), Helsing et al (2011), and Martin et al (2012). In particular, acoustic metamaterials are associated with the wave motion problems. These local resonators demonstrate a specific macroscopic behaviour such as a negative density. Among possible applications of acoustic metamaterials are non-invasive probing, high-resolution tomography in medical imaging, acoustic camouflaging and seismic protection, see for example Craster and Guenneau (2012), Titovich (2015).

Therefore, mechanical vibrations of multi-layered elastic structures composed of parts with high-contrast material and geometrical characteristics is an important scientific problem having multiple innovative industrial applications. It is well known that high-frequency vibrations are very desirable in a view of their high energy content.

However, low-frequency mechanical vibrations arise naturally in a variety of environments, such as body movements (footsteps or heartbeat), wind, thermal generated vibrations, or air flow. Thus, due to their omnipresent character, low-frequency modes are of much greater interest for investigation. Broad general studies of low-frequency dynamics of composite structures can be found in Graff (1975), Le (2012), and Wang and Wang (2013).

The present thesis deals with low-frequency vibrations of elastic structures composed of parts with contrast properties. The analysis is performed for free vibrations of elastic multi-component rods and antiplane shear motions of elastic multi-component cylindrical bodies. It is worth noting that 2D equations describing antiplane shear motions of cylinders with fixed boundaries are identical to those for membranes. A large amount of numerical approaches for solving this type of problems exist, see Zhang and Yang (2009), Sayyad and Ghugal (2015), and references therein. However, we use asymptotic methods, rather than numerical solutions. The use of asymptotic methods provides a better understanding of the connection between the lowest eigenfrequencies of a structure and the contrast in parameters of its components. The analysis presented in this work based on asymptotic approach mainly involves perturbations in a small parameter, e.g. see Nayfeh (2011), Simmonds and Mann (2013), and Kevorkian and Cole (2013), taking into consideration a multi-parametric nature of the problem.

The main motivation of this study is to deduce the conditions on the structure parameters supporting the low-frequency regime. We aim to show a clear link between the contrast in parameters of composite structures and the lowest eigenfrequencies. We deduce that under certain restrictions on material and geometrical parameters the lowest natural frequencies become small tending to zero at the limit of large/small contrasts. The basic problem parameters include the ratios of elastic moduli, densities, and typical linear sizes of the components.

Two possible types of low-frequency motions are subject to a multi-parametric analysis. The so-called global low-frequency regime assumes the quasi-static behaviour of both stiffer and softer structure components. Another type, namely local low-frequency regime, describes the quasi-static profile of stiffer components and does not

prevent oscillating behaviour of softer parts. The studied local low-frequency behaviour is similar to process of homogenization of contrast periodic media. In each case explicit asymptotic formulae for the lowest eigenfrequencies as well as the associated displacement profiles are presented. Where it is possible the accuracy of the established approximations is tested by comparison with exact solutions. The developed methodology is not restricted to 1D and 2D problems considered in the thesis. It has a potential to be extended to the framework of 3D elasticity. In particular, the lowest cut-off frequencies of sandwich plates and shells could be analysed with help of the obtained results.

1.1 Industrial applications

Composite rods, membranes, and sandwich plates find numerous applications in various constructions under dynamics loading. As an example, a mathematical model of a human body experiencing oscillatory motion can be considered as a 1D system of multi-component rods whose material properties similar to the properties of the body, see Yermolayev (1992). Another possible application is related to the analysis of chain segment lengths of molecular systems. Polymers have a low eigenfrequency proportional to a chain length. Thus, investigation of longitudinal acoustic modes in a long chain polymer considered as a composite rod with perturbing forces at the ends helps to deduce lengths of molecular segments, see Hsu and Krimm (1976), Hsu et al (1977).

The propagation of longitudinal waves in smart periodic structures is another possible field of research. A rod with shunted piezoelectric patches, periodically placed to control the longitudinal wave propagation, is considered in Thorp et al (2001). The described periodic structure allows filtering the propagation of waves over predetermined frequency bands. The shunting capabilities of piezoelectric materials provide high control flexibility in attenuation and localization of propagating waves. Another structure that is capable to control wave transmission is a rod composed of shape

memory alloy parts periodically inserted in a matrix material. By controlling Young's modulus of the shape memory alloy parts it is possible to prevent the wave propagation along the rods, see Ruzzene and Baz (2000).

Next, let us mention a rapidly growing area of energy harvesting. It aims to generate small amounts of electrical energy from mechanical vibrations appearing in most environments. Thus, self-sustaining micro- and nano-devices can use power harvested from mechanical vibrations. To maximize the harvested energy the resonant frequencies of the energy harvesting device should match ambient vibration frequencies, see Song et al (2006).

Textile fabric devices have been proposed for a very low-frequency (< 10 Hz) energy harvesting. In particular, low-frequency mechanical vibrations of textile fibers can be harvested through friction and are used in energy scavenging fabric devices, see Qin et al (2008), Nobili et al (2010). The problem can be described as free vibrations of a two-component string with high-contrast material parameters subject to a variety boundary conditions, see Kudaibergenov et al (2016).

Along with fibers, a membrane based energy harvesters are widely implemented, Dong et al (2015). For example, a circular membrane with low resonant frequencies was designed and analysed for implementation in polymer micro-structures with small size energy harvesters in Rezaeisaray et al (2014). Wang et al (2012) presented a piezoelectric circular membrane array for energy harvesting. Additionally, a theoretical model of a piezoelectric circular membrane under pressure fluctuations was considered to predict levels of harvested energy, see Mo et al (2014).

It is worth mentioning that membranes play an important role as basic elements in microelectronics, especially for acoustic microelectromechanical systems. Moreover, due to their numerous applications (musical instruments, condenser microphones, hearing aids, etc.) circular membranes are very widely used in comparison with other types of membranes. Among different applications in this field, we mention resonant systems, which are employed for navigation of drones, autonomous system, or bio-mimetic developments based on animal instincts. It is shown that the navigation principle using sound sources in complex environments can be applied to designing autonomous micro-

flying objects, see Alsahlani and Mukherjee (2013). Natural frequencies of acoustic resonant sensors can be set by controlling membrane parameters enabling good sensitivity and selectivity without employing any passive and electronic filters, making such systems ideal for bio-mimetic applications, see Sosa et al (2001), Ruffier et al (2011). Membrane based resonators are also exploited in accelerometric and gyroscopic sensors. Recent studies show that by incorporating nanometer-thin freestanding membranes it is possible to obtain resonators that are capable to measure pressure or small forces and masses with extremely high sensitivity, e.g. see Lee et al (2013), Schlicke et al (2016).

There are also various applications of composite membranes in the aerospace industry. Deployable multi-layered membrane structures are used in spacecraft systems, such as solar panels, antennas of satellites, or deployable roofs. Deployable spacecraft systems can vary from extremely lightweight, such as solar sails, to relatively thick rigid panels such as solar arrays of communications satellites, see Papa and Pellegrino (2008), Lee and Pellegrino (2014). In addition, deploying multi-layered membrane mirrors become a part of space-borne telescopes due to their lightness and quality optical imaging capabilities. However, undesirable vibrations can decrease the performance of membrane mirrors forcing to design a system of smart actuators to prevent vibrations, see Baruh (2001), Adetona et al (2003), Renno (2008).

Other widely used composite structures are sandwich panels. They are typically composed of two thin and stiff face sheets or skins separated by a thick lightweight layer or core. Commonly used materials for the sandwich skins are composite or wood laminates and metals, while polymeric expanded foams, metallic and non-metallic honeycombs or balsa wood are frequently used for the core. Sandwich panels have many advantages over conventional constructions, such as high strengths and stiffness, as well as good weight saving, see Zenkert (1995).

Therefore, sandwich composites are widely employed in modern mechanical design, where weight must be kept to a minimum. They are used not only in aeronautical and aerospace structures, where they have been initially implemented, see Baker (2004), but also in high-speed marine craft and trains, and racing cars, see Arbaoui et

al (2015). In Belingardi et al (2003) glass fiber composite-foam sandwich structures are investigated for the front shield of a high speed train, in Zinno et al (2010) and Kim and Chung (2007) properties of composite sandwich panels analysed in case of large scale test on a train, while Torre and Kenny (2000) discuss composite structures in application to train or buses body shells.

For more specific high-tech solutions, such as a solar aircraft, see Romeo et al (2004), solar cars or satellite solar panels, ultra-light photovoltaic sandwich structures are used. This is a new multifunctional lowest-cost structure concept that enables weight and thus energy to be saved, see Mines et al (1998), Rion (2008), and Beral (2007). Photovoltaic panels demonstrate high contrast in their material properties. In this case, the shear moduli ratio of a glass skin and a polymeric core with encapsulated solar cells varies from $10 \sim 5$ to $10 \sim 2$, depending on temperature and polymer type, see Schulze et al (2012), Aßmus et al (2016, 2017).

Other structures characterised by high contrast of material and geometrical properties of the layers are laminated glass beams and plates. The laminated glass used in automotive and civil engineering is usually composed of three layers, including two stiff relatively thick facings and a soft, thin polymeric core. This results in contrasts of core and skin layer thickness and stiffness, see Aşık and Tezcan (2005), Kaplunov et al (2017c).

Usually, sandwich structures are characterised by stiff facings. However, there are also important examples of composites with a soft skin and a stiff inner layer. An elastic sandwich plate with these characteristics is a good model for a precipitator plate, which is an important part of gas filters collecting dust particles from passing gas streams, see Tassicker (1972), Lee and Chang (1979).

1.2 Literature review

The present thesis is devoted to vibrations of elastic multi-component rods and antiplane shear motions of elastic multi-component cylinders of circular and arbitrary

cross sections focusing on the lowest frequencies. An asymptotic methodology is developed for analysing the lowest eigenvalues for 1D and 2D scalar equations governing dynamic behaviour of layered elastic structures in case of strong contrast between the parameters characterising each of the layers, including their sizes, material stiffness, and densities. It is worth noting that the eigenfrequencies of a composite rod considered within 1D setup correspond to the lowest cut-off frequencies for a plate or a shell within the framework of 3D elasticity. Thus, the current results can be also used for the analysis of the so-called long-wave high-frequency vibrations in composite plates and shells considered in the scope of 3D elasticity.

Mechanics of layered media is originated from studying the process of wave propagation in an infinite two-layered elastic media. The governing equations of this problem may be found in Ewing et al (1957). The numerical evaluation of the exact solution for a two-layered half-space is given in Abramovici and Alterman (1965). The first analytical investigation of bending and buckling in a sandwich plate seems to be presented by Reissner (1947). There the analysis relies on the assumption that the face-parallel stresses in the core and the face stresses over the thickness of the plate are negligible. The same analysis but in more general form with the derivation of the differential equations and boundary conditions for bending and buckling of a sandwich plate is carried out by Hoff (1950). In Eringen (1951), the partial differential equations for bending and buckling of a rectangular sandwich plate with an isotropic core and faces under different loadings and edge conditions were obtained. Later, the propagation of waves in elastic sandwich plates was investigated by Mindlin (1959) and Yu (1959). In Cheng (1961), the Reissner problem was modified and the equations for a sandwich plate with an orthotropic core were reduced to the bi-harmonic equation in the classical plate theory. The most of the solutions in this area were obtained with help of numerical computations, however, asymptotic results were also presented.

Numerous publications are dedicated to recent trends in dynamics of sandwich plates, shells, and beams. The relationship between the solutions of the classical theories of beams and plates and those arising from various shear deformation theories are studied in Wang et al (2000). Qatu (2004) textbook is devoted to linear free vibrations

of thin and thick composite shells, plates, and curved beams. Approximate theories and corresponding finite element models of laminated composite structures can be find in Reddy (2004). Finally, a substantial review devoted to the computational treatment of laminated composite and sandwich panels is presented in Kreja (2011).

Moreover, there is a large amount of studies devoted to vibrations of multi-component rods. In Elishakoff (2004), a summary of results for closed form solutions for vibrations and buckling of inhomogeneous rods, beams, columns, and plates, composed of materials with high contrast mechanical and geometrical properties, is presented. One of the chapters is devoted to vibrations of inhomogeneous rods, especially to the problem of construction of a rod that has the preselected fundamental and second mode. An approach based on Green function is proposed for the analysis of vibrations of a high-contrast two-component piecewise homogeneous string supported on a Winkler elastic foundation in Nobili (2012). A low-frequency asymptotic analysis of a viscoelastic inhomogeneous bar subject to end loads is applicable for modelling of railway dynamics, see Kaplunov et al (2015). Another insight on vibrations of inhomogeneous strings, rods, and membranes with continuously varying properties can be found in Horgan and Chan (1999). In this work closed-form exact solutions are derived for some specific examples and lower bounds for vibration frequencies are obtained through an integral-equation-based method.

A number of papers are specifically focused on dynamics of inhomogeneous membranes. For example, composite membranes with discontinuous property changes are analysed in Spence and Horgan (1983), Laura et al (1985), Cortinez and Laura (1992), Laura et al (1997). In Spence and Horgan (1983), the natural frequencies of a circular membrane with stepped radial density are estimated with an integral equation approach. Vibrations of a composite doubly connected membrane of regular polygonal shape with an inner circular core are studied with a conformal mapping approach in Laura et al (1985). In Cortinez and Laura (1992), the exact solution for the fundamental frequency of a two-layered rectangular membrane is compared with the results obtained by the Kantorovich method and shown to be in a good agreement. An integral equation method is implemented in Laura et al (1997) to find upper and lower

bounds for the eigenfrequencies of a circular membrane with a stepped radial density.

Although, mechanics of layered media being a field of thorough investigation for a long time, nevertheless, only several works have a special focus on high contrast problems for strongly inhomogeneous multi-component structures. However, in many cases, structural components may have contrast material and geometrical parameters, including stiffness, volume density, and size. Thus, it is worth also mentioning a number of recent asymptotic developments dealing with sandwich plates with high contrast in the problem parameters. Simplified models for wave motions in an unbounded sandwich plate with and without heavy fluid loading are compared with the results obtained by the use of the exact theory in Sorokin (2004). These models can be used in naval and aerospace engineering, as they accurately describe all propagating waves below high-frequency range. In Lutianov and Rogerson (2010), the long wave motion in a three-layered elastic plate under different boundary conditions is considered. The paper contains dispersion relations and the results of the long-wave asymptotic analysis. Chapman (2013) addresses finite product approximations for analysing wave propagation in a multi-layered plate. The approach results in a hierarchy of approximations to the exact Rayleigh–Lamb dispersion relation. In Naumenko and Eremeyev (2014), a generalized Timoshenko–Reissner type model is suggested for describing bending and free vibrations of a thin beam and a thin plate composed of a transversally isotropic linearly elastic material heterogeneous in the thickness direction. Structural analysis of the glass and aforementioned photovoltaic laminates is described. The paper provides a layer-wise theory that includes governing equations for individual layers, kinematical constraints, appropriate interaction forces, and results in a twelfth order system of partial differential equations. In Altenbach et al (2015), first-order shear deformation plate theory is applied to the analysis of laminates with thin and soft core layers. This research is useful for calculating effective material properties of laminated glasses and photovoltaic panels with high contrast in mechanical properties. Tovstik and Tovstik (2017) emphasises that in case of a strongly heterogeneous material or for a composite material with the large ratio between Young's moduli of layers the Kirchhoff–Love and Timoshenko–Reissner models are not effective.

Another modern engineering application of vibrations in inhomogeneous elastic structures is concerned with tailoring and design of structures with specified values of natural frequencies. In Elishakoff and Perez (2006), a closed form polynomial solution for free vibrations of an inhomogeneous bar with a tip mass is derived. The paper of Elishakoff and Yost (2010) is devoted to vibration tailoring of an axially graded elastically-constrained bar with a polynomial varying modulus of elasticity along the axial coordinate. Closed-form analytic and numeric solutions are given oriented to constructing a bar with pre-selected natural frequencies.

The design of waveguides with tailored filtering properties is based on using periodic structures. In Figotin and Kuchment (1998), two-dimensional photonic band gap structures are investigated for classical electromagnetic and acoustic waves in a high-contrast, two-component periodic medium. The asymptotic results relied on the high-contrast are developed for the frequency spectrum. To control filtering of electromagnetic, acoustic, and elastic waves the position and the width of the photonic/phononic band gaps have to be properly adjusted. Gei et al (2009) offers a method for controlling the stop bands for a prestressed piecewise homogeneous elastic beam on an elastic foundation via optimising prestress. Prestress can be incorporated into the model through the coefficients in the chosen governing equations. The mechanism in which frequency is controlled by prestress is illustrated by adapting Green's-function-based analysis. In Piccolroaz and Movchan (2014), dispersive waves, band-gaps and localised waveforms in prestressed Rayleigh beams on elastic foundations are studied. The method is especially useful for modelling high-frequency regimes.

Homogenization of high-contrast periodic composites is an another closely related field. The idea behind homogenization of periodic media is averaging of rapidly oscillatory material properties of a periodic medium on a fine microscale to get an equivalent homogeneous material with effective material parameters. The local low-frequency regime studied in the thesis is characterized by a quasi-static behaviour of stiffer components and oscillating profiles in other parts. Thus, it may be linked with recent results for homogenization of contrast periodic media. A similarity of the asymptotic procedures underlying the long wave dynamic behaviour of thin structures and

homogenization for periodic media is revealed in Craster et al (2014).

Among recent works on the topic, we can cite Cherednichenko et al (2006), Smyshlyaev (2009), Cherdantsev and Cherednichenko (2012), and Kaplunov and Nobili (2017). Cherednichenko et al (2006) is devoted to the homogenization of highly anisotropic conducting fibres embedded into an isotropic matrix with focus on a high contrast between conductivity along the fibres and the transverse conductivities. In Cherdantsev and Cherednichenko (2012), the emphasis is on an analytical framework for a high-contrast model with soft inclusions embedded into a stiff matrix. Smyshlyaev (2009) studies wave propagation in periodic elastic composites with highly contrasting and highly anisotropic stiffnesses along with moderately contrasting densities. It is proven that under certain conditions high anisotropy allows achieving wave propagation along several directions and attenuation along other directions. The paper by Kaplunov and Nobili (2017) concerns with periodic waveguides in the shape of an inhomogeneous string or beam supported by a uniform elastic Winkler foundation. The asymptotic analysis shows that under derived conditions on problem parameters, quasi-static uniform or linear microscale displacement profiles can exist at high-frequencies.

In view of the link between the current research and area of long-wave high-frequency vibrations in composite plates and shells, we provide an overview of this topic. A high-frequency long-wave profile can be characterised by a wave length much greater than the thickness of a plate or shell along with a sinusoidal variation across the thickness. There is a large amount of publications devoted to high-frequency long-wave vibrations emerged near thickness resonant frequencies. These studies include works devoted to pre-stressed and anisotropic structures. In particular, Kaplunov et al (2000) developed the method of direct asymptotic integration for a layer with the in-plane axis of transverse isotropy oriented to the vicinities of the cut-off frequencies. In Kaplunov et al (2002), the effect of pre-stress on the long-wave high-frequency two-dimensional motion in an incompressible elastic plate is investigated. Pichugin and Rogerson (2001) derive a general model for the extensional motion of a prestressed incompressible elastic layer in the vicinity of the shear resonance frequencies. In Pichugin and Rogerson (2002), the method of asymptotic integration is applied to analyse flex-

ural motion near the cutoff frequencies in a pre-stressed incompressible elastic plate. Analysis of forced vibrations and acoustic radiation of an elastic layer interacting with media with a special attention to the vicinities of stretch thickness resonances is presented in Kaplunov and Markushevich (1993). Kaplunov (1995) studies long-wave vibrations of a thin-walled body with fixed faces using an asymptotic method to derive appropriate two-dimensional equations. This study shows that such vibrations exist only at frequencies close to thickness resonances. Another paper dealing with long-wave dynamics of a structure with clamped faces is Kaplunov and Nolde (2002). The phenomenon of trapped high-frequency long-wave modes is considered in Kaplunov et al (2005) and in Gridin et al (2005) for linear isotropic elastic plates and rods.

In the content of current work, the eigenfrequencies of a three-component elastic rod could be associated with the cut-off frequencies of a three-layered elastic plate, e.g. see Kaplunov et al (1998). Within a high contrast framework, the lowest non-zero eigenfrequency of a composite rod corresponds to the lowest thickness shear resonance frequency of a plate with similar properties. The case of a coupling between the fundamental bending mode and the above-mentioned shear lowest mode in sandwich plates is investigated in Kaplunov et al (2017a), see also Ryazantseva and Antonov (2012), Prikazchikova et al (2018). The latter is a key challenge for shear deformation plate theories, e.g. see Noor and Burton (1989), Goldenveizer et al (1993), and references there in. In addition, the natural frequencies of antiplane motion of a two-component cylinder of arbitrary cross section correspond to the cut-off frequencies of elastic rods, see e.g. Le (2012). Thus, the asymptotic formulae for the antiplane low-frequency motion of two-layered cylindrical bodies of an arbitrary cross section are also actual for the lowest cut-off frequencies of high-contrast layered rods.

1.3 Basic equations

The governing equations of linear isotropic elasticity are summarised here. First, we give definitions of the deformation, and the strain and stress tensors, followed

by the balance of linear momentum, which provides us with Cauchy's first law of motion. Our initial concern is solid structures composed of homogeneous, isotropic, elastic materials. Thus, the related stress-strain relations are provided. Further, a one-dimensional equation of motion, that approximates vibrations in thin rods, is derived, as well as a two-dimensional equation of antiplane shear motion.

1.3.1 Deformation, stress tensor and balance of linear momentum

Consider $u(x, y, z, t)$, describing small displacements of particles in the fixed Cartesian system $Oxyz$ with t denoting time. Then, u_x, u_y, and u_z are components of the infinitesimal displacement vector. In Section 1.3, let indices $i, j, k, l \in \{x, y, z\}$ with a repeated index implies a summation. Thus, for the displacement vector u we can write down

$$u = u_i \vartheta_i = u_x \vartheta_x + u_y \vartheta_y + u_z \vartheta_z, \tag{1.1}$$

where ϑ_i are the base vectors.

The deformation is defined by the symmetric second order infinitesimal strain tensor ε, with components $\varepsilon_{ij} = \varepsilon_{ji}$. Then, the strain-displacement relations are determined by

$$\varepsilon_{ij} = \frac{1}{2}\left(\frac{\partial u_i}{\partial j} + \frac{\partial u_j}{\partial i}\right). \tag{1.2}$$

Next, we introduce the surface traction vector $\tau^{(n)}$, defining a force per unit area across a surface with a unit outward normal n. The surface traction may be represented through the stress tensor by Cauchy stress formula

$$\tau_i^{(n)} = \sigma_{ji} n_j, \tag{1.3}$$

where σ_{ji} are components of the stress tensor.

Suppose we have a body with a closed arbitrary region D. Γ is the boundary of D with an outward unit normal n. Then, in the linearised theory the balance of linear

momentum specifies that

$$\iint_{\Gamma} \tau_i^{(n)} dA + \iiint_{D} \rho b_i \, dV = \iiint_{D} \rho \frac{\partial^2 u}{\partial t^2} \, dV, \tag{1.4}$$

where b_i are the body forces per unit mass, ρ is the material density, and dA and dV indicate differential area and volume, respectively.

The surface integral can be transformed into the volume integral by the divergence theorem, see Spencer (2004). Substitution of (1.3) into (1.4), together with the last observation, provides us with

$$\iiint_{D} \left(\frac{\partial \sigma_{ji}}{\partial j} + \rho b_i - \rho \frac{\partial^2 u}{\partial t^2} \right) dV = 0. \tag{1.5}$$

Since (1.5) relations must hold in every arbitrary region D of the body, it implies that wherever the integrand is continuous, we obtain

$$\frac{\partial \sigma_{ji}}{\partial j} + \rho b_i = \rho \frac{\partial^2 u}{\partial t^2}, \tag{1.6}$$

which is Cauchy's first law of motion.

1.3.2 Stress-strain relations for homogeneous isotropic linearly elastic solid

The linear relation between components of the stress tensor and components of the strain tensor is described by analogue of Hooke's law for continuum media as

$$\sigma_{ij} = C_{ijkl} \varepsilon_{kl}, \tag{1.7}$$

where C_{ijkl} are components of the fourth-order elasticity tensor and

$$C_{ijkl} = C_{jikl} = C_{klij} = C_{ijlk}. \tag{1.8}$$

When coefficients C_{ijkl} are constants the medium is called elastically homogeneous. In case of elastic isotropy constants C_{ijkl} may be expressed as

$$C_{ijkl} = \lambda \delta_{ij} \delta_{kl} + \mu(\delta_{ik} \delta_{jl} + \delta_{il} \delta_{jk}), \tag{1.9}$$

see for example Achenbach (2012). In (1.9) λ and μ are Lamé elastic constants and δ_{ij} is known as Kronecker delta, whose components are defined as

$$\begin{aligned} \delta_{ij} &= 1, \qquad \text{if} \quad i = j, \\ \delta_{ij} &= 0, \qquad \text{if} \quad i \neq j. \end{aligned} \tag{1.10}$$

Expression (1.9) inserted into equation (1.7) provides us with another well-known form of Hooke's law

$$\sigma_{ij} = \lambda \delta_{ij} \varepsilon_{kk} + 2\mu \varepsilon_{ij}. \tag{1.11}$$

1.3.3 Equations of motion

1.3.3.1 Longitudinal stress

When components of the stress tensor and the body forces depend on one spatial variable x, the stress equations of motion (1.6) reduce to

$$\frac{\partial \sigma_{ix}}{\partial x} + \rho b_i = \rho \frac{\partial^2 u_i}{\partial t^2}. \tag{1.12}$$

To approximate wave motion in a thin rod we consider a one-dimensional state of stress. In this case the only non-vanishing stress component is the longitudinal normal stress σ_{xx}, which depends on x and t only. Setting the transverse normal stresses σ_{yy} and σ_{zz} to zero in (1.11) leads to the relations

$$\varepsilon_{yy} = \varepsilon_{zz} = -\frac{\lambda}{2(\lambda + \mu)} \varepsilon_{xx}. \tag{1.13}$$

The relation for σ_{xx} follows by substitution of (1.13) into (1.11)

$$\sigma_{xx} = E \varepsilon_{xx}, \tag{1.14}$$

where the constant E is called Young's modulus

$$E = \frac{\mu(3\lambda + 2\mu)}{\lambda + \mu}. \tag{1.15}$$

By substituting (1.14) into (1.12) and in absence of the body forces, we obtain equation of motion in the from

$$\frac{\partial \sigma_{xx}}{\partial x} = \rho \frac{\partial^2 u_x}{\partial t^2}. \tag{1.16}$$

Using (1.14) with (1.2), we can rewrite the previous equation in terms of deformation

$$\frac{\partial^2 u_x}{\partial x^2} = \frac{1}{c_x^2} \frac{\partial^2 u_x}{\partial t^2}, \tag{1.17}$$

where $c_x = \sqrt{E/\rho}$ is the wave velocity.

We seek solution of equation (1.17) in the following form

$$u_x(x,t) = U_x(x) e^{i\omega t}. \tag{1.18}$$

Hence, (1.17) can be rewritten as

$$\frac{\partial^2 U_x}{\partial x^2} - \frac{\omega^2}{c_x^2} U_x = 0, \tag{1.19}$$

where U_x is the displacement, which is a function of x only, and ω is the vibration frequency.

1.3.3.2 Antiplane shear

In two-dimensional problems components of the stress tensor and the body forces are dependent on two variables only, for example, x and y. Thus, the stress equations of motion can be obtained from (1.6) by setting $\dfrac{\partial}{\partial z}$ equals to zero. Therefore, we can separate the system of equations (1.6) into two uncoupled systems as

$$\frac{\partial \sigma_{xz}}{\partial x} + \frac{\partial \sigma_{yz}}{\partial y} + \rho b_z = \rho \frac{\partial^2 u_z}{\partial t^2}, \tag{1.20}$$

and

$$\begin{aligned} \frac{\partial \sigma_{xx}}{\partial x} + \frac{\partial \sigma_{xy}}{\partial y} + \rho b_x &= \rho \frac{\partial^2 u_x}{\partial t^2}, \\ \frac{\partial \sigma_{yx}}{\partial x} + \frac{\partial \sigma_{yy}}{\partial y} + \rho b_y &= \rho \frac{\partial^2 u_y}{\partial t^2}, \end{aligned} \tag{1.21}$$

where deformation described by the displacement $u_z(x, y, t)$ is known as antiplane shear deformation.

We can derive the desirable stress components from Hooke's law (1.11) as

$$\begin{aligned} \sigma_{xz} &= \mu \frac{\partial u_z}{\partial x}, \\ \sigma_{yz} &= \mu \frac{\partial u_z}{\partial y}. \end{aligned} \tag{1.22}$$

Hence, in absence of the body forces the scalar wave equation for $u_z(x, y, t)$ follows from substituting expressions for σ_{xz} and σ_{yz} into (1.20)

$$\frac{\partial^2 u_z}{\partial x^2} + \frac{\partial^2 u_z}{\partial y^2} = \frac{1}{c_z^2} \frac{\partial^2 u_z}{\partial t^2}, \tag{1.23}$$

where $c_z = \sqrt{\mu/\rho}$ is the associated shear wave speed.

In case of time-harmonic dependence

$$u_z(x, y, t) = U_z(x, y) e^{i\omega t}, \tag{1.24}$$

(1.23) can be reformulated as

$$\frac{\partial^2 U_z}{\partial x^2} + \frac{\partial^2 U_z}{\partial y^2} + \frac{\omega^2}{c_z^2} U_z = 0, \tag{1.25}$$

where U_z is the out-of-plane displacement, which depends on x and y only.

Let us now consider the equation (1.23) in the polar coordinate system. For two-dimensional problems we introduce two variables. They are the radial distance r and the polar angle θ, where

$$\begin{aligned} x &= r \cos\theta, \\ y &= r \sin\theta. \end{aligned} \tag{1.26}$$

Thus, rewriting function u_z in terms of new variables, we get from (1.23)

$$\frac{\partial^2 u_z}{\partial r^2} + \frac{1}{r} \frac{\partial u_z}{\partial r} + \frac{1}{r^2} \frac{\partial^2 u_z}{\partial \theta^2} = \frac{1}{c_z^2} \frac{\partial^2 u_z}{\partial t^2}. \tag{1.27}$$

In this case

$$u_z(r, \theta, t) = U_z(r) e^{im\theta} e^{i\omega t}, \tag{1.28}$$

hence, (1.27) becomes

$$r^2\frac{\partial^2 U_z}{\partial r^2} + r\frac{\partial U_z}{\partial r} + \left(\frac{\omega^2 r^2}{c_z^2} - m^2\right) U_z = 0, \tag{1.29}$$

where U_z is the displacement function of r only, and $m = 0, 1, 2, 3 \ldots$.

The same equations describe vibrations in circular elastic membranes, however, they are based on very different physical principles.

1.4 Outline of thesis

The structure of the thesis is presented here. Chapter 1 contains an introduction to the topic. Chapter 2 is dedicated to vibrations of a composite elastic rod. We start with the reviewing of the problem for an elastic homogeneous rod with fixed or free ends in Section 2.1. An appropriate scaling for frequencies and space variables is introduced. In Section 2.2 vibrations of a three-component rod with piecewise uniform properties are analysed. In this case, we present the exact solution of the problem for three types of boundary conditions. They are fixed ends, free ends, and mixed boundary conditions, meaning a rod with one fixed end and one free end. In each case, a multi-parametric analysis is performed to determine the dependence of the lowest natural frequencies on the ratios of material and geometric parameters. We divide the low-frequency behaviour into global and local regimes and study them separately. Section 2.3 focuses on dynamics of a three-component rod with variable material parameters. Here a perturbation technique oriented to a more general setup of a rod composed of inhomogeneous materials is developed. The last section is concerned with a more general asymptotic model for a multi-component rod. Derivation of the model and several examples are given.

In Chapter 3 antiplane shear motion of a composite elastic body with a circular cross section is examined with the focus placed on low frequencies. The classical problem of antiplane shear motion of a homogeneous cylinder is reviewed in Section 3.1. In Section 3.2 the attention is first drawn to the model problem of low-frequency

vibrations of a two-component piecewise-homogeneous body. This problem allows a straightforward analytical treatment. A global low-frequency regime is obtained for certain conditions on the problem parameters. In Section 3.3 this analysis is generalized to a non-uniform two-component body with variable material parameters. Here we use a perturbation procedure to estimate low natural frequencies and related displacement profile since a straightforward analytical approach is no longer possible. Section 3.4 contains a general asymptotic model for a body with an arbitrary number of components, which is similar to that presented for a multi-layered rod in Chapter 2. It is worth noting that similar equations describe dynamic behaviour of circular membranes. Therefore, any fixed boundary problem of this chapter can be considered as a problem of vibrations of an elastic circular membrane.

In Chapter 4 antiplane shear motion of a composite elastic body with an arbitrary cross section is studied. Section 4.1 revises vibrations of a homogeneous body with a square cross section. In Section 4.2 a two-component hollow body of arbitrary shape is considered. The problem assumes either free or fixed inner and outer boundaries, together with perfect continuity conditions at the interfaces. Following the scheme of the previous chapter, a perturbation procedure is developed for evaluating the vibration modes associated with a global low-frequency regime, corresponding to a quasi-static behaviour of both stiffer and softer structure components. In Section 4.3, to illustrate the efficiency of the developed scheme, we present two examples including a hollow cylinder of a square cross section with a circular annular inclusion and a hollow cylinder of a circular cross section with a rectangular annular inclusion. Such problem does not allow a simple analytical solution. However, we manage to derive explicit asymptotic formulae for the lowest natural frequencies and associated displacements.

In Chapter 5 a discussion on the main results obtained in the thesis is presented. The potential developments and extensions of the obtained outcomes are also provided.

2 Vibrations of a composite elastic rod

This chapter describes low-frequency vibrations in a thin strongly inhomogeneous elastic rod. First, we review vibrations of a homogeneous elastic rod with ends being fixed or free. To do this we introduce appropriate scaling for frequencies together with corresponding dimensionless spatial variables. Then, we present the outcomes of a multi-parametric analysis of the near-rigid body motions of a three-component elastic rod with piecewise uniform properties. It is observed that the values of the associated lowest eigenfrequencies tend to zero at large/small ratios of material and geometric parameters. We derive conditions supporting low-frequency behaviour, which could be considered under global and local regimes. For a more general scheme of a rod having variable material parameters, we develop a perturbation procedure. In the last section an asymptotic model for a rod with arbitrary number of components is presented.

2.1 A homogeneous rod

Time-harmonic vibrations of an elastic homogeneous rod are revised in this section.

2.1.1 Statement of the problem

We consider a finite rod that occupies the region $|x| \leq l$, with the origin O located in the center, see Figure 2.1.

The governing equation is given by

$$\frac{d^2u}{dx^2} + \frac{\omega^2}{c^2}u = 0, \tag{2.1}$$

where u is the transverse displacement, ω is the vibration frequency, and $c = \sqrt{E/\rho}$ is the longitudinal wave speed, with E and ρ denoting Young's modulus and the material density, respectively.

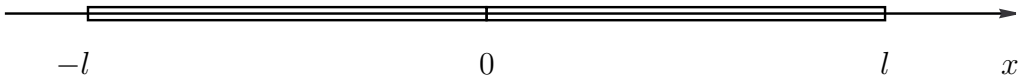

Figure 2.1: Geometry of the problem

We consider three types of boundary conditions, including fixed ends, with zero displacements imposed on the ends

$$u|_{|x|=l} = 0, \tag{2.2}$$

free ends, with zero stresses prescribed on both ends of the rod

$$\left.\frac{du}{dx}\right|_{|x|=l} = 0, \tag{2.3}$$

and mixed boundary conditions, meaning a fixed left and a free right end of the rod

$$\begin{aligned} u|_{x=-l} &= 0, \\ \left.\frac{du}{dx}\right|_{x=l} &= 0. \end{aligned} \tag{2.4}$$

Below we use the dimensionless longitudinal variable

$$X = \frac{x}{l}, \tag{2.5}$$

and the scaled frequency

$$\Omega = \frac{\omega l}{c}. \tag{2.6}$$

Hence, (2.1) can be reformulated as

$$\frac{d^2u}{dX^2} + \Omega^2 u = 0, \tag{2.7}$$

and (2.2)-(2.4) take the form

$$u|_{|X|=1} = 0, \tag{2.8}$$

$$\left.\frac{du}{dX}\right|_{|X|=1} = 0, \tag{2.9}$$

and

$$\begin{aligned} u|_{X=-1} &= 0, \\ \left.\frac{du}{dX}\right|_{X=1} &= 0, \end{aligned} \tag{2.10}$$

respectively. The displacement is found as

$$u = A\cos\Omega X + B\sin\Omega X, \tag{2.11}$$

where A and B are arbitrary constants.

2.1.2 Free ends

The sought-for linear algebraic system can be obtained by substituting (2.11) into the boundary conditions (2.9). Thus,

$$\Omega(A\sin\Omega \pm B\cos\Omega) = 0. \tag{2.12}$$

Let us assume first that $\Omega \neq 0$. By solving (2.12) we deduce the frequency equations describing symmetric and antisymmetric vibrations of the rod, i.e.

$$A = 0 \quad \text{and} \quad B\cos\Omega = 0, \qquad \text{with} \quad \Omega = -\frac{\pi}{2} + \pi n, \tag{2.13}$$

and

$$B = 0 \quad \text{and} \quad A\sin\Omega = 0, \qquad \text{with} \quad \Omega = \pi n, \tag{2.14}$$

respectively, where mode number $n = 1, 2, 3, \ldots$.

For the lowest natural frequencies the displacement profile takes the form

$$u = A\cos\pi X, \tag{2.15}$$

or

$$u = B\sin\frac{\pi}{2}X. \tag{2.16}$$

Along with (2.13)-(2.14) the system (2.12) provides the zero eigenfrequency solution ($\Omega = 0$), associated with the rigid body motion of a rod with free ends

$$u = A. \tag{2.17}$$

2.1.3 Fixed ends

Substituting (2.11) into the boundary conditions (2.8) for a rod with fixed ends we arrive at

$$A\cos\Omega \pm B\sin\Omega = 0. \tag{2.18}$$

The system above provides us with the same set of solutions (2.13)-(2.14) as in the previous subsection, except for the zero-frequency one, i.e.

$$B = 0 \quad \text{and} \quad A\cos\Omega = 0, \qquad \text{with} \quad \Omega = -\frac{\pi}{2} + \pi n, \tag{2.19}$$

and

$$A = 0 \quad \text{and} \quad B\sin\Omega = 0, \qquad \text{with} \quad \Omega = \pi n, \tag{2.20}$$

where mode number $n = 1, 2, 3, \ldots$.

Then, for the lowest eigenfrequencies the displacement profile is given by

$$u = A\cos\frac{\pi}{2}X, \tag{2.21}$$

or

$$u = B\sin\pi X. \tag{2.22}$$

2.1.4 Mixed boundary conditions

Using (2.11) with the boundary conditions (2.10) we can write down the linear algebraic system as

$$\begin{gathered} A\cos\Omega - B\sin\Omega = 0, \\ \Omega(A\sin\Omega - B\cos\Omega) = 0. \end{gathered} \tag{2.23}$$

The vibrations in this case can not be split to symmetric and antisymmetric. Thus, solving (2.23), we obtain the frequencies as

$$A = -B, \qquad \text{with} \quad \Omega = -\frac{\pi}{4} + \pi n, \qquad n = 1, 2, 3, \ldots, \tag{2.24}$$

and

$$A = B, \qquad \text{with} \quad \Omega = \frac{\pi}{4} + \pi m, \qquad m = 0, 1, 2, \ldots. \tag{2.25}$$

For the lowest natural frequencies the displacement profile can be derived as

$$u = A\left(\cos\frac{3\pi X}{4} - \sin\frac{3\pi X}{4}\right), \tag{2.26}$$

or

$$u = A\left(\cos\frac{\pi X}{4} + \sin\frac{\pi X}{4}\right). \tag{2.27}$$

2.2 A three-component piecewise-homogeneous rod

Consider now time-harmonic vibrations of an elastic geometrically symmetric rod composed of three homogeneous parts of the same cross-sectional area.

2.2.1 Statement of the problem

We study a finite rod with the outer parts having free or fixed ends, and continuity assumed between the components. The axis Ox is chosen such that the origin O is located in the middle of the inner part. The rod is geometrically symmetric, with the inner part occupying the region $|x| \le l_1$, and the outer parts specified by $l_1 \le |x| \le l_1 + l_2$, see Figure 2.2.

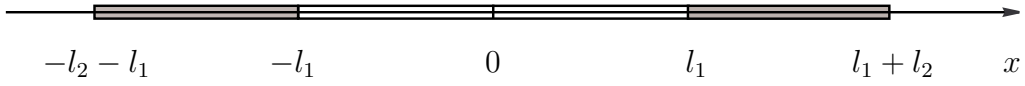

Figure 2.2: A three-component piecewise-homogeneous rod

The governing equations are written in the form

$$\frac{d^2u_i}{dx^2} + \frac{\omega^2}{c_i^2}u_i = 0, \qquad i = 1, 2, \tag{2.28}$$

where u_i are the displacements, ω is the vibration frequency, and $c_i = \sqrt{E_i/\rho_i}$ are the longitudinal wave speeds, with E_i denoting Young's module, and ρ_i denoting the material densities. Here and below in this section, the indices 1 and 2 correspond to the inner and outer components, respectively.

We introduce dimensionless longitudinal variables

$$X_i = \frac{x}{l_i}, \qquad i = 1, 2. \tag{2.29}$$

This scaling allows to simplify equations for the subsequent consideration of a rod with any finite number of components. The dimensionless parameters are taken as

$$E = \frac{E_1}{E_2}, \qquad \rho = \frac{\rho_1}{\rho_2}, \qquad c = \frac{c_1}{c_2}, \qquad l = \frac{l_1}{l_2}, \tag{2.30}$$

along with the scaled frequencies

$$\Omega_i = \frac{\omega l_i}{c_i}, \qquad i = 1, 2. \tag{2.31}$$

Thus, the dimensionless equations of motion can be formulated as

$$\frac{d^2 u_i}{dX_i^2} + \Omega_i^2 u_i = 0, \qquad i = 1, 2. \tag{2.32}$$

We consider the continuity of displacements and stresses at the interfaces, i.e.

$$u_1\big|_{|X_1|=1} = u_2\big|_{|X_2|=l}\,, \tag{2.33}$$

and

$$\frac{E}{l}\frac{du_1}{dX_1}\bigg|_{|X_1|=1} = \frac{du_2}{dX_2}\bigg|_{|X_2|=l}, \tag{2.34}$$

respectively.

We assume three types of boundary conditions on the outer ends, namely free ends

$$\frac{du_2}{dX_2}\bigg|_{|X_2|=l+1} = 0, \tag{2.35}$$

fixed ends

$$u_2\big|_{|X_2|=l+1} = 0, \tag{2.36}$$

and mixed boundary conditions being a combination of the previous two cases

$$\begin{aligned} u_3|_{X_3=-l-1} &= 0, \\ \left.\frac{du_2}{dX_2}\right|_{X_2=l+1} &= 0. \end{aligned} \tag{2.37}$$

For the first two types of boundary conditions it is sufficient to consider only $x \geq 0$ to derive the sought-for frequency equations since the rod is geometrically symmetric. Thus, symmetric and antisymmetric cases can be considered separately. For symmetric and antisymmetric vibrations the displacement of the inner part is given by

$$u_1 = A\cos\Omega_1 X_1, \qquad |X_1| \leq 1, \tag{2.38}$$

and

$$u_1 = B\sin\Omega_1 X_1, \qquad |X_1| \leq 1, \tag{2.39}$$

respectively, following from (2.32). The displacement of the outer part is written as

$$u_2 = C\cos\Omega_2 X_2 + D\sin\Omega_2 X_2, \qquad l \leq |X_2| \leq l+1, \tag{2.40}$$

where A, B, C and D are arbitrary constants.

For the mixed boundary conditions all three parts of the rod should be considered, and vibrations can no longer be classified as symmetric and antisymmetric ones. The displacement then is provided in the form

$$\begin{aligned} u_3 &= F\cos\Omega_2 X_3 + G\sin\Omega_2 X_3, && -l-1 \leq X_3 \leq -l, \\ u_1 &= A\cos\Omega_1 X_1 + B\sin\Omega_1 X_1, && -1 \leq X_1 \leq 1, \\ u_2 &= C\cos\Omega_2 X_2 + D\sin\Omega_2 X_2, && l \leq X_2 \leq l+1. \end{aligned} \tag{2.41}$$

2.2.2 Antisymmetric vibrations of a rod with free ends

Consider now antisymmetric vibrations of a rod subject to the boundary conditions (2.35).

Substituting (2.39) and (2.40) into (2.33), (2.34), and (2.35), we arrive at

$$\begin{aligned} B\sin\Omega_1 - C\cos\Omega_2 l - D\sin\Omega_2 l &= 0,\\ B\frac{E}{c}\cos\Omega_1 + C\sin\Omega_2 l - D\cos\Omega_2 l &= 0,\\ C\sin\big(\Omega_2(l+1)\big) - D\cos\big(\Omega_2(l+1)\big) &= 0. \end{aligned} \tag{2.42}$$

The linear algebraic system (2.42) possesses non-trivial solutions as long as the associate determinant vanishes, resulting in the frequency equation

$$\tan\Omega_1 \tan\Omega_2 = \frac{E}{c}. \tag{2.43}$$

From now on, we will use U_i, $i = 1, 2, \ldots$, to denote the scaled dimensionless displacements corresponding to displacements u_i, $i = 1, 2, \ldots$. Hereinafter, $U = U_1$ for $|x| \le l_1$ and $U = U_2$ for $l_1 \le |x| \le l_1 + l_2$. Using (2.42), the scaled displacement profile can be expressed as

$$\begin{aligned} U_1 &= \sin\Omega_1 X_1,\\ U_2 &= \frac{\sin\Omega_1 \cos\big(\Omega_2(l+1-X_2)\big)}{\cos\Omega_2}. \end{aligned} \tag{2.44}$$

The studied low-frequency motion may be classified into the global low-frequency regime ($\Omega_1 \ll 1$, $\Omega_2 \ll 1$), and also the local low-frequency behaviour ($\Omega_1 \ll 1$, $\Omega_2 \gtrsim 1$) or ($\Omega_1 \gtrsim 1$, $\Omega_2 \ll 1$). The local low-frequency regimes are in some-sense similar to problems of homogenization of periodic contrast media, see e.g. Cherednichenko et al (2006) and Cherdantsev et al (2013).

2.2.2.1 Global low-frequency regime

Global low-frequency regime can be characterised by $\Omega_1 \ll 1$ and $\Omega_2 \ll 1$, which associates with the quasi-static behaviour of both inner and outer components of the rod. We reduce the frequency equation (2.43) to the following approximate form

$$\Omega_1\Omega_2 = \frac{E}{c}. \tag{2.45}$$

In a view of the relation between the dimensionless frequency parameters $c\Omega_1 = l\Omega_2$, (2.45) leads to

$$\Omega_1^2 = \rho l, \tag{2.46}$$

and

$$\Omega_2^2 = \frac{E}{l}. \tag{2.47}$$

Using the formulae (2.46)-(2.47) together with the strong inequalities $\Omega_1 \ll 1$ and $\Omega_2 \ll 1$, we derive

$$E \ll l \ll \rho^{-1}, \tag{2.48}$$

which imply an estimate for the material parameters supporting the global low-frequency regime.

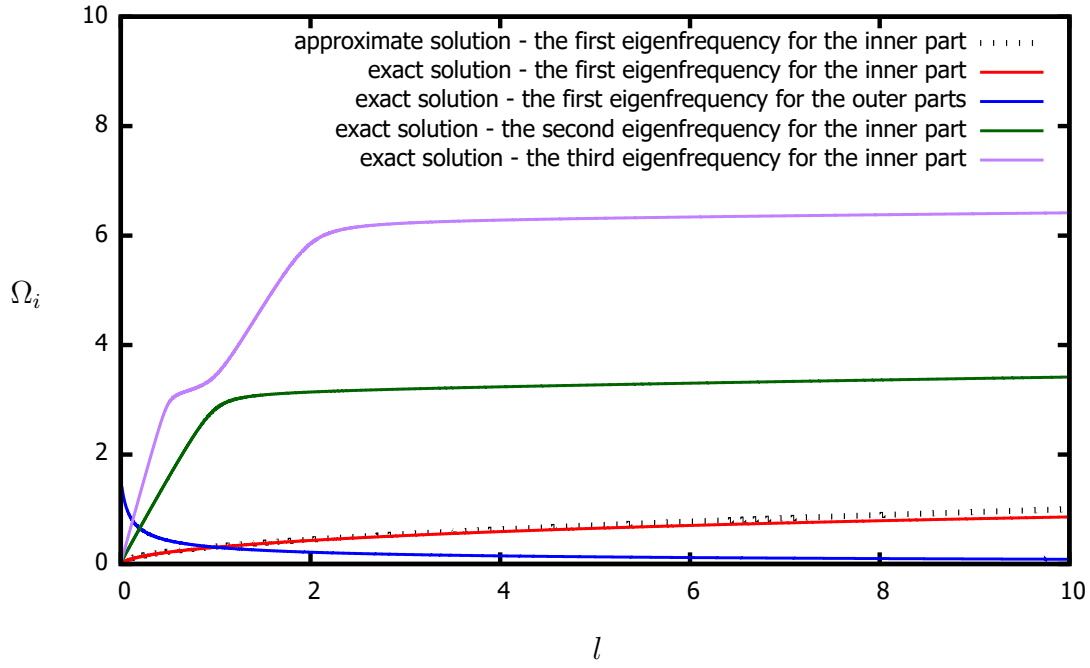

Figure 2.3: Frequency vs relative thickness l for antisymmetric vibrations of a rod with free ends; $E = 0.1$, $\rho = 0.1$

Figure 2.3 displays dependence of the scaled frequencies on the relative length l, including the asymptotic approximation (2.46) for the inner part, and the decreasing function given by (2.47) for the outer part. The curves of the first three eigenfrequencies for the inner part are defined by (2.43). It is readily observed from Figure 2.3 that Ω_1 and Ω_2 are both small if l satisfies condition (2.48). We also observe a good agreement between the lowest value of Ω_1 defined by (2.43) and its approximation (2.46).

The large distance between the first and second natural frequencies notable from the graph can be significant for the dispersion analysis of sandwich plates composed of layers with contrast properties. As was mentioned in the introduction, the frequencies obtained here within a 1D problem correspond to the cut-off frequencies of an elastic plate, see for example Kaplunov et al (1998). We assume that the small first cut-off frequency implies a coupling effect between the fundamental mode and the first harmonic in a plate, see e.g. Noor and Burton (1989), Goldenveizer et al (1993), Le (2012), and Kaplunov et al (2017a).

Noting that the condition $0 \leq (l + 1 - X_2)\Omega_2 \ll 1$ holds true for the outer part, we approximate the scaled displacement profile to the form

$$\begin{aligned} U_1 &= X_1, \\ U_2 &= 1, \end{aligned} \tag{2.49}$$

see Figure 2.4. It may be observed from Figure 2.4 that the outer parts at leading order perform a rigid body motion, whereas the inner part undergoes an almost homogeneous deformation, i.e. $dU_1/dX_1 = 1$.

It is also worth mentioning that in the intersection of the curves for Ω_1 and Ω_2 in Figure 2.3, over the low frequency region $\Omega_1 = \Omega_2 = \Omega \ll 1$, implies $l = c$ and

$$\Omega^2 = \sqrt{E\rho}. \tag{2.50}$$

Therefore, now we analyse the low-frequency regime in terms of the small parameter $E\rho \ll 1$, see Figure 2.5, which may be interpreted physically as the condition underlying a ‶weaker″ inner and ‶stronger″ outer components. It can be seen from Figure 2.5 that the first eigenfrequency of the equation (2.43) decreases and the distance between

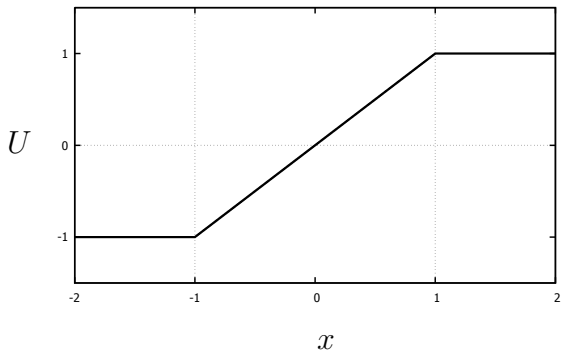

Figure 2.4: Global low-frequency regime (2.49); $l = 1$

the first and second eigenfrequencies increases as $E\rho \to 0$. In addition, we can note that the accuracy of the asymptotic approximation (2.50) enhances as $E\rho \to 0$.

2.2.2.2 Local low-frequency regime for the inner part

The local low-frequency regime of $\Omega_1 \ll 1$ and $\Omega_2 \gtrsim 1$ allows wave-like phenomena in the outer parts and restricts those in the inner part of the rod.

The approximate frequency equation is then presented as

$$\tan \Omega_2 = \frac{E}{l\Omega_2}. \tag{2.51}$$

The corresponding scaled natural form is derived as

$$\begin{aligned} U_1 &= X_1, \\ U_2 &= \frac{\cos\left(\Omega_2(l+1-X_2)\right)}{\cos \Omega_2}. \end{aligned} \tag{2.52}$$

The frequency equation (2.51) allows analytical treatment for several particular cases.

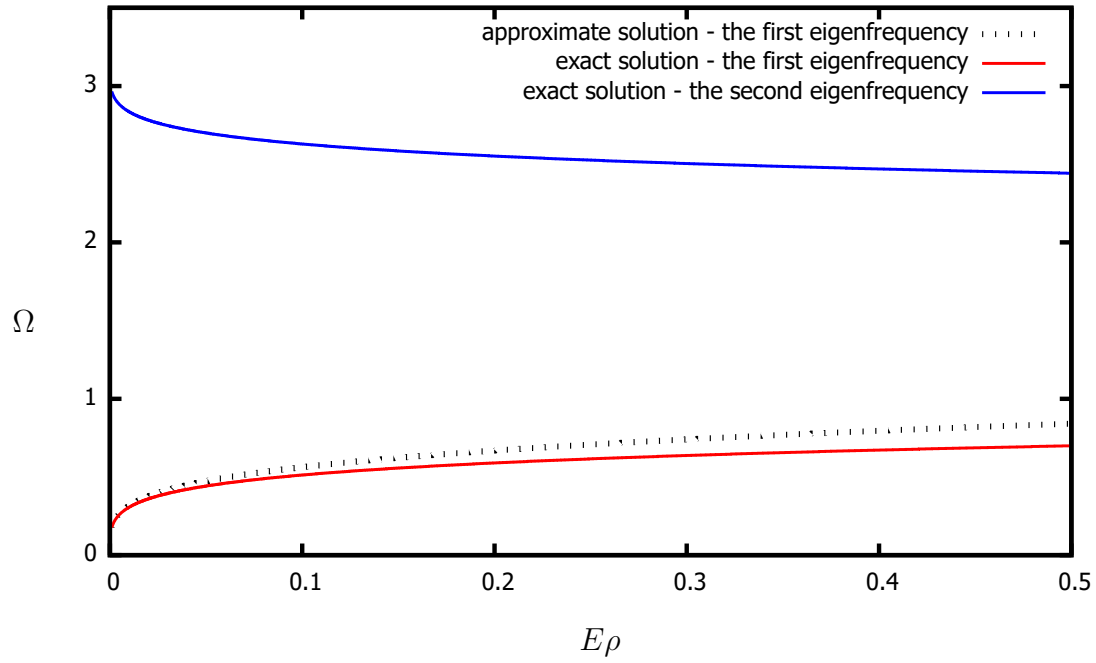

Figure 2.5: Variation of the frequency Ω vs the parameter $E\rho$ for antisymmetric vibrations of a rod with free ends

Case 1. If $E \ll l\Omega_2$, then, from the frequency equation (2.51), $|\tan\Omega_2| \ll 1$. Hence,

$$\Omega_2 \approx \pi n, \qquad \text{with} \quad n = 1, 2, 3, \ldots. \tag{2.53}$$

Remarking that $\Omega_1 \ll 1$ and $E \ll l\Omega_2$, we infer

$$\frac{E}{l} \ll n \ll \frac{c}{l}. \tag{2.54}$$

The scaled displacement takes the form

$$\begin{aligned} U_1 &= X_1, \\ U_2 &= \cos\big(\pi n(l - X_2)\big). \end{aligned} \tag{2.55}$$

The resulting profile for the first two modes is given on Figure 2.6.

One of the possible physical interpretations of the limiting case $|\tan\Omega_2| \ll 1$ corresponds to resonant frequencies of the ˝stronger˝ outer parts with free ends. Indeed,

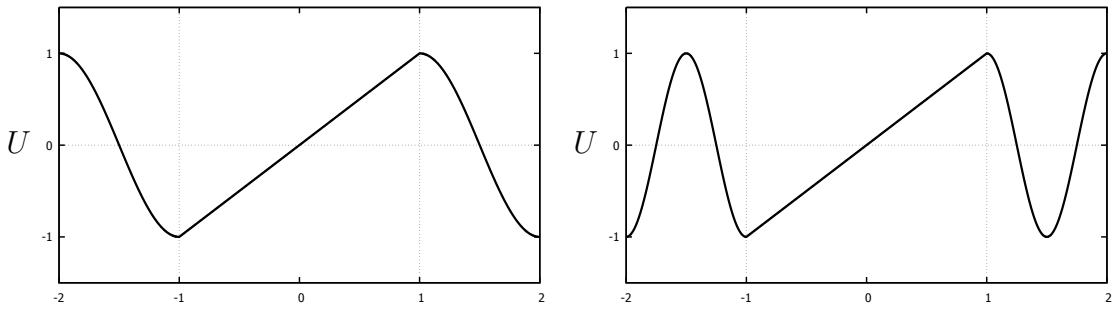

Figure 2.6: Local low-frequency regime for the inner part (2.55); $l = 1$

$E \ll l\Omega_2$ or $E \ll c\Omega_1$ leads to $E_1\rho_1 \ll E_2\rho_2$. This can be explained as a "weaker" inner part, being not able to prevent the vibrations of "stronger" outer parts. At the same time, $\Omega_2 = \pi n$ indeed gives a set of natural frequencies of a homogeneous rod with free ends, see Section (2.1.2).

Case 2. If $E \gg l\Omega_2$, then, (2.51) provides

$$\Omega_2 \approx \frac{\pi(2n-1)}{2}, \qquad \text{with} \quad n = 1, 2, 3, \ldots. \tag{2.56}$$

Using the conditions $\Omega_1 \ll 1$ and $E \gg l\Omega_2$, we derive

$$n \ll \min\left[\frac{c}{l}, \frac{E}{l}\right]. \tag{2.57}$$

The scaled displacement is now given in the form

$$\begin{aligned} U_1 &= X_1, \\ U_2 &= \cos\frac{\pi(2n-1)(l-X_2)}{2} - \tan\Omega_2 \sin\frac{\pi(2n-1)(l-X_2)}{2}. \end{aligned} \tag{2.58}$$

From initial assumption of this case $|\tan\Omega_2| \gg 1$ and

$$U_2 \sim -\tan\Omega_2 \sin\frac{\pi(2n-1)(l-X_2)}{2}, \tag{2.59}$$

with the first term in (2.58) behaving similarly to a boundary layer, smoothing the discontinuity at $X_2 = l$. The overall profile for the first two modes is shown on Figure 2.7.

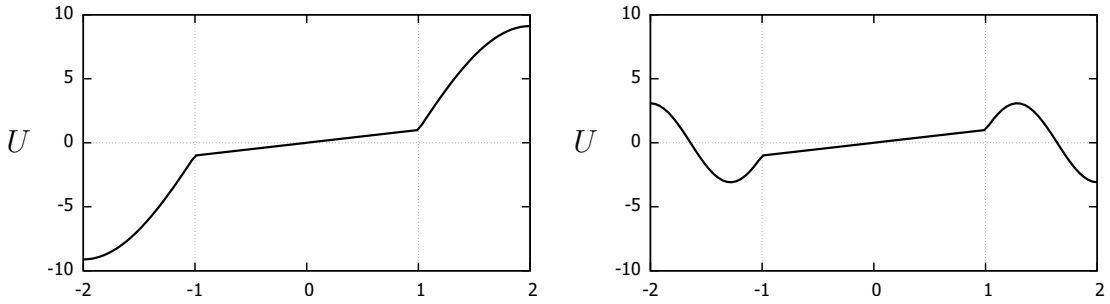

a) n=1 b) n=2

Figure 2.7: Local low-frequency regime for the inner part (2.58); $l = 1$

Similarly to the Case 1, a possible physical interpretation of the limiting Case 2 is related to resonant frequencies of the outer parts. Now, the condition $E \gg l\Omega_2$ implies $E_1\rho_1 \gg E_2\rho_2$. This relation describes a "stronger" inner part, which results in vibrations of the outer parts under mixed boundary conditions with the eigenfrequencies $\Omega_2 = \dfrac{\pi(2n-1)}{2}$.

Case 3. If $E \sim l\Omega_2$, then, there is no simple explicit solution for Ω_2, with the conditions for Ω_2 reducing to

$$\Omega_2 \sim \frac{E}{l} \ll \frac{c}{l}. \tag{2.60}$$

2.2.2.3 Local low-frequency regime for the outer parts

The conditions $\Omega_1 \gtrsim 1$ and $\Omega_2 \ll 1$ describes the local low-frequency regime of the outer parts.

The frequency equation is then given by

$$\tan \Omega_1 = \frac{\rho l}{\Omega_1}, \tag{2.61}$$

and the corresponding scaled displacement profile is written as

$$\begin{aligned} U_1 &= \sin \Omega_1 X_1, \\ U_2 &= \sin \Omega_1. \end{aligned} \tag{2.62}$$

Similarly to the previous section, we split the problem into several cases.

Case 1. If $\rho l \ll \Omega_1$, then, $|\tan \Omega_1| \ll 1$. Thus,

$$\Omega_1 \approx \pi n, \qquad \text{with} \quad n = 1, 2, 3, \ldots. \tag{2.63}$$

Inequalities $\Omega_2 \ll 1$ and $\rho l \ll \Omega_1$ imply

$$\rho l \ll n \ll \frac{l}{c}. \tag{2.64}$$

The eigenform is then reduced to

$$\begin{aligned} U_1 &= \sin \pi n X_1, \\ U_2 &= 0, \end{aligned} \tag{2.65}$$

see Figure 2.8 for numerical illustrations corresponding to the first two modes.

Case 2. If $\rho l \gg \Omega_1$, then, from (2.61) we obtain

$$\Omega_1 \approx \frac{\pi(2n-1)}{2}, \qquad \text{with} \quad n = 1, 2, 3, \ldots. \tag{2.66}$$

Using the conditions $\Omega_2 \ll 1$ and $\rho l \gg \Omega_1$, we get

$$n \ll \min\left[\rho l, \frac{l}{c}\right]. \tag{2.67}$$

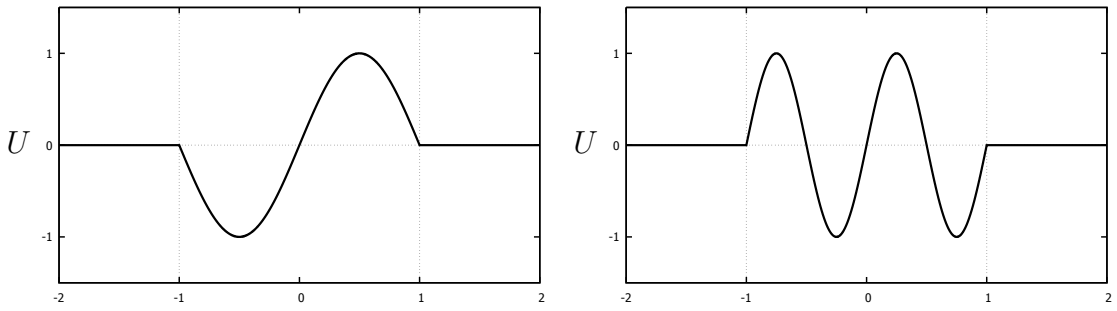

Figure 2.8: Local low-frequency regime for the outer parts (2.65); $l = 1$

Then, the scaled displacement is expressed as

$$U_1 = \sin \frac{\pi(2n-1)X_1}{2}, \qquad U_2 = (-1)^{n+1}, \tag{2.68}$$

see Figure 2.9.

The limiting Cases 1 and 2 correspond to an oscillatory behaviour for the inner part of the rod and a polynomial dependence for the outer components. Moreover, Case 1 would be associated with the condition $\Omega_2 \gg \rho c$, thus, $E_1\rho_1 \ll E_2\rho_2$. Therefore, a ˝weaker˝ inner part will be under a homogeneous deformation, with $\Omega_1 = \pi n$ providing a set of natural frequencies of this part with fixed ends. Case 2 may be interpreted physically as a ˝stronger˝ inner part having free ends.

Case 3. If $\rho l \sim \Omega_1$, the conditions allowing low-frequency regime, are derived in the form

$$\Omega_1 \sim \rho l \ll \frac{l}{c}. \tag{2.69}$$

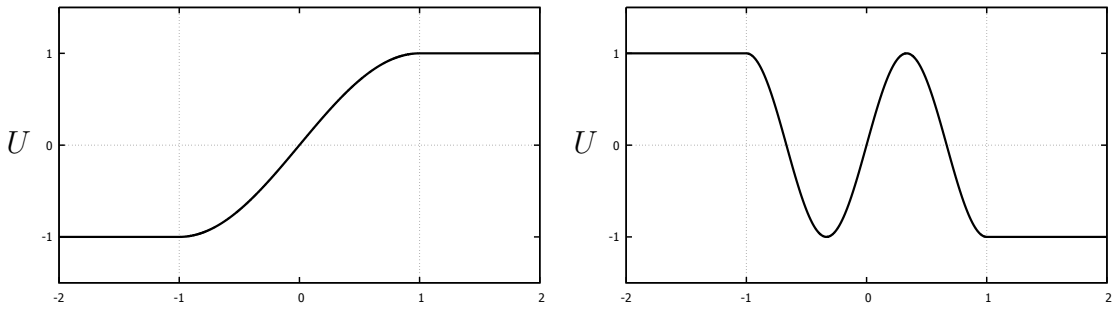

a) n=1 b) n=2

Figure 2.9: Local low-frequency regime for the outer parts (2.68); $l = 1$

2.2.3 Symmetric vibrations of a rod with free ends

Let us now study symmetric vibrations of a rod with free ends, see boundary conditions (2.35).

By substituting (2.38) and (2.40) into (2.33), (2.34), and (2.35), we get the linear algebraic system

$$\begin{gathered} A\cos\Omega_1 - C\cos\Omega_2 l - D\sin\Omega_2 l = 0, \\ \Omega_1\Big(A\frac{E}{c}\sin\Omega_1 - C\sin\Omega_2 l + D\cos\Omega_2 l\Big) = 0, \\ \Omega_1\Big(C\sin\big(\Omega_2(l+1)\big) - D\cos\big(\Omega_2(l+1)\big)\Big) = 0. \end{gathered} \tag{2.70}$$

Solving (2.70), we obtain the frequency equation

$$-\cot\Omega_1\tan\Omega_2 = \frac{E}{c}. \tag{2.71}$$

Then, using (2.70), we can write down the eigenform as

$$\begin{aligned} U_1 &= \cos\Omega_1 X_1, \\ U_2 &= \frac{\cos\Omega_1\cos\big(\Omega_2(l+1-X_2)\big)}{\cos\Omega_2}. \end{aligned} \tag{2.72}$$

In this case the system also has zero-frequency solution with $A = C$ and

$$U_1 = U_2 = 1, \tag{2.73}$$

corresponding to the rigid body motion typical for a rod with free ends.

By assuming $\Omega_1 \ll 1$ and $\Omega_2 \ll 1$ and simplifying the frequency equation (2.71) to an approximate form it can be easily shown that this problem does not allow the global low-frequency regime. However, the local low-frequency regimes are possible.

2.2.3.1 Local low-frequency regime for the inner part

Now, we consider the case of the local low-frequency regime for the inner part assuming the conditions $\Omega_1 \ll 1$ and $\Omega_2 \gtrsim 1$.

The sought-for approximate equation following from (2.71) is given by

$$\tan \Omega_2 = -l\rho\Omega_2. \tag{2.74}$$

The scaled displacement profile can be approximated as

$$\begin{aligned} U_1 &= 1, \\ U_2 &= \frac{\cos\big(\Omega_2(l+1-X_2)\big)}{\cos \Omega_2}. \end{aligned} \tag{2.75}$$

Case 1. In case of $l\rho\Omega_2 \ll 1$, the frequency equation (2.74) leads to $|\tan \Omega_2| \ll 1$. This results in

$$\Omega_2 \approx \pi n, \qquad \text{with} \quad n = 1, 2, 3, \ldots. \tag{2.76}$$

In view of $\Omega_1 \ll 1$ and $l\rho\Omega_2 \ll 1$, the conditions for n can be written down as

$$n \ll \min\left[\frac{1}{l\rho}, \frac{c}{l}\right]. \tag{2.77}$$

The scaled displacement takes the form

$$\begin{aligned} U_1 &= 1, \\ U_2 &= \cos\big(\pi n(l - X_2)\big). \end{aligned} \tag{2.78}$$

see Figure 2.10.

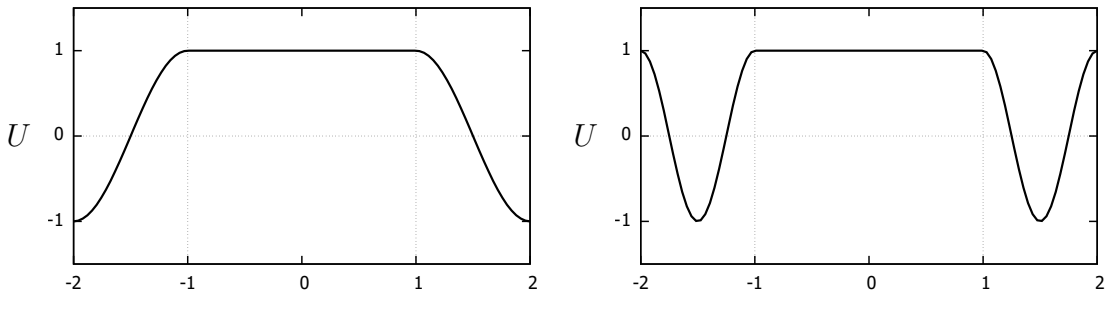

Figure 2.10: Local low-frequency regime for the inner part (2.78); $l = 1$

Case 2. If $l\rho\Omega_2 \gg 1$, then, from (2.74) we obtain $|\tan\Omega_2| \gg 1$ and

$$\Omega_2 \approx \frac{\pi(2n-1)}{2}, \qquad \text{with} \quad n = 1, 2, 3, \ldots. \tag{2.79}$$

The conditions $\Omega_1 \ll 1$ and $l\rho\Omega_2 \gg 1$ imply

$$\frac{1}{l\rho} \ll n \ll \frac{c}{l}. \tag{2.80}$$

The scaled displacement is given by

$$\begin{aligned} U_1 &= 1, \\ U_2 &= \cos\frac{\pi(2n-1)(l-X_2)}{2} - \tan\Omega_2 \sin\frac{\pi(2n-1)(l-X_2)}{2}. \end{aligned} \tag{2.81}$$

Figure 2.11 shows the eigenform for the first two modes.

In Case 1 the condition $\rho l\Omega_2 \ll 1$ or $c\rho\Omega_1 \ll 1$ signifies that the inner part is "weaker" with $E_1\rho_1 \ll E_2\rho_2$ and is not able to prevent the vibrations of the outer parts. In Case 2 the condition $\rho l\Omega_2 \gg 1$ transforms to $E_1\rho_1 \gg E_2\rho_2$ meaning a "stronger" inner part. The behaviour is very similar to the antisymmetric vibrations of the rod with fixed ends.

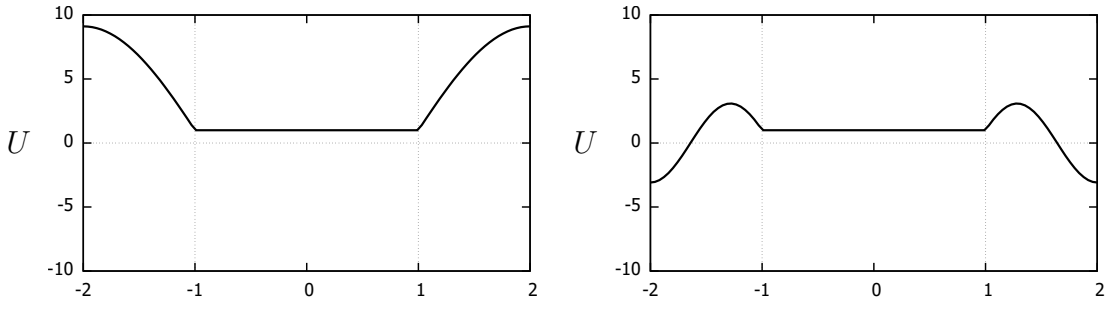

Figure 2.11: Local low-frequency regime for the inner part (2.81); $l = 1$

Case 3. If $l\rho\Omega_2 \sim 1$, the conditions for Ω_2 take the form

$$\Omega_2 \sim \frac{1}{l\rho} \ll \frac{c}{l}. \tag{2.82}$$

2.2.3.2 Local low-frequency regime for the outer parts

In case of the local low-frequency regime for the outer parts the studied conditions are given by $\Omega_1 \gtrsim 1$ and $\Omega_2 \ll 1$. Then, the approximate frequency equation is reduced to

$$\cot\Omega_1 = -\frac{l\rho}{\Omega_1}, \tag{2.83}$$

with the corresponding approximate natural form is deduced as

$$\begin{aligned} U_1 &= \cos\Omega_1 X_1, \\ U_2 &= \cos\Omega_1. \end{aligned} \tag{2.84}$$

Case 1. Assuming $l\rho \ll \Omega_1$, we infer $|\cot\Omega_1| \ll 1$, thus,

$$\Omega_1 \approx \frac{\pi(2n-1)}{2}, \qquad \text{with} \quad n = 1, 2, 3, \ldots. \tag{2.85}$$

Using $\Omega_2 \ll 1$ and $l\rho \ll \Omega_1$, we obtain

$$l\rho \ll n \ll \frac{l}{c}. \tag{2.86}$$

Then, the eigenform can be reformulated as

$$\begin{aligned} U_1 &= \cos\frac{\pi(2n-1)X_1}{2}, \\ U_2 &= 0, \end{aligned} \tag{2.87}$$

see Figure 2.12 presenting the first two modes.

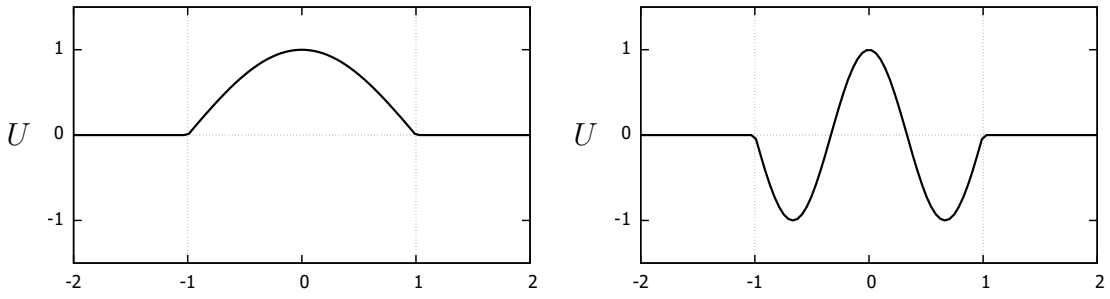

a) n=1 b) n=2

Figure 2.12: Local low-frequency regime for the outer parts (2.87); $l = 1$

Case 2. Using (2.83) with $l\rho \gg \Omega_1$, we can infer that

$$\Omega_1 \approx \pi n, \qquad \text{with} \quad n = 1, 2, 3, \ldots. \tag{2.88}$$

The conditions $\Omega_2 \ll 1$ and $l\rho \gg \Omega_1$ provide

$$n \ll \min\left[l\rho, \frac{l}{c}\right]. \tag{2.89}$$

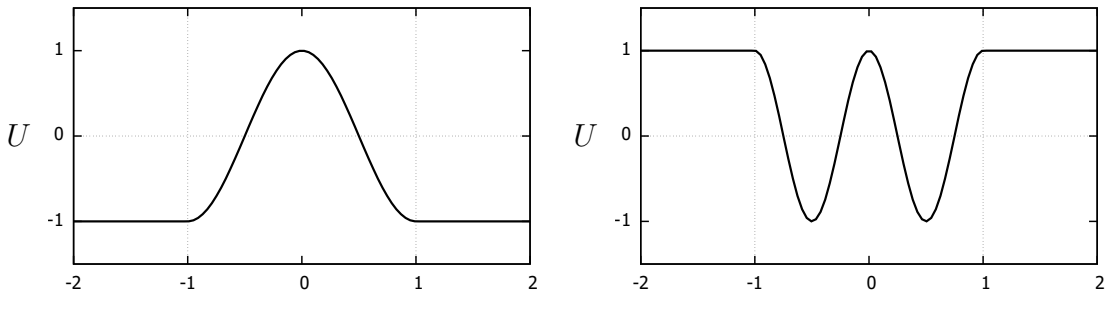

Figure 2.13: Local low-frequency regime for the outer parts (2.90); $l = 1$

Then, the approximate scaled displacement profile follows in the form

$$\begin{aligned} U_1 &= \cos \pi n X_1, \\ U_2 &= (-1)^n, \end{aligned} \tag{2.90}$$

see Figure 2.13.

Displacement profiles in both cases show expected due to the conditions $\Omega_1 \gtrsim 1$ and $\Omega_2 \ll 1$ oscillatory behaviour for the inner section of the rod along with the polynomial dependence for the outer components. Case 1 can be associated with $E_1\rho_1 \ll E_2\rho_2$ or a ‶weaker″ inner part with fixed ends. Case 2 corresponds to a ‶stronger″ inner part with free ends. The conditions on scaled frequencies are similar to those for antisymmetric vibrations with changes taking place in displacement profiles.

Case 3. If $l\rho \sim \Omega_1$, the conditions for Ω_1 can be formulated as

$$\Omega_1 \sim l\rho \ll \frac{l}{c}. \tag{2.91}$$

2.2.4 Antisymmetric vibrations of a rod with fixed ends

Antisymmetric motions of a rod with fixed ends are considered in this section, see (2.36).

We derive a frequency equation by substituting (2.39) and (2.40) into the conditions (2.33), (2.34), and (2.36), resulting in

$$\begin{gathered} B\sin\Omega_1 - C\cos\Omega_2 l - D\sin\Omega_2 l = 0, \\ B\frac{E}{c}\cos\Omega_1 + C\sin\Omega_2 l - D\cos\Omega_2 l = 0, \\ C\cos\big(\Omega_2(l+1)\big) + D\sin\big(\Omega_2(l+1)\big) = 0. \end{gathered} \tag{2.92}$$

The solvability of this system implies

$$-\tan\Omega_1\cot\Omega_2 = \frac{E}{c}. \tag{2.93}$$

The scaled displacement profile can be presented as

$$\begin{aligned} U_1 &= \sin\Omega_1 X_1, \\ U_2 &= \frac{\sin\Omega_1\sin\big(\Omega_2(l+1-X_2)\big)}{\sin\Omega_2}. \end{aligned} \tag{2.94}$$

It can be verified by taking $\Omega_1 \ll 1$ and $\Omega_2 \ll 1$ and then simplifying the frequency equation (2.93) to an approximate form that this problem again does not have the global low-frequency regime.

2.2.4.1 Local low-frequency regime for the inner part

In view of the local low-frequency regime of $\Omega_1 \ll 1$ and $\Omega_2 \gtrsim 1$ the equation (2.93) is approximated to the form

$$\cot\Omega_2 = -\frac{E}{l\Omega_2}. \tag{2.95}$$

The associated eigenform is obtained as

$$\begin{aligned} U_1 &= X_1, \\ U_2 &= \frac{\sin\big(\Omega_2(l+1-X_2)\big)}{\sin\Omega_2}. \end{aligned} \tag{2.96}$$

Case 1. Assuming $E \ll l\Omega_2$, we get the condition $|\cot \Omega_2| \ll 1$, which provides

$$\Omega_2 \approx \frac{\pi(2n-1)}{2}, \qquad \text{with} \quad n = 1, 2, 3, \ldots. \tag{2.97}$$

Inequalities $\Omega_1 \ll 1$ and $E \ll l\Omega_2$ allow to write conditions on n as

$$\frac{E}{l} \ll n \ll \frac{c}{l}. \tag{2.98}$$

Then, the natural form is reduced to

$$\begin{aligned} U_1 &= X_1, \\ U_2 &= \cos \frac{\pi(2n-1)(l-X_2)}{2}, \end{aligned} \tag{2.99}$$

see Figure 2.14 for the first two modes.

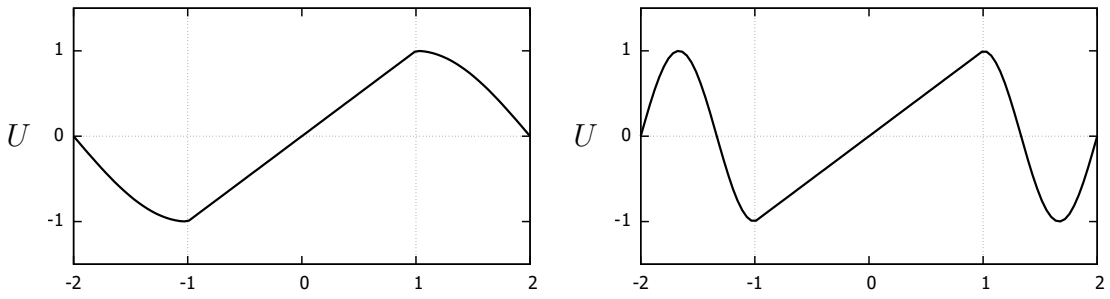

a) n=1 b) n=2

Figure 2.14: Local low-frequency regime for the inner part (2.99); $l = 1$

The limiting case $|\cot \Omega_2| \ll 1$ implies $\sqrt{E\rho} \ll \Omega_1$ or the rod with the ˝stronger˝ outer parts under mixed boundary conditions.

Case 2. If $E \gg l\Omega_2$, then, from (2.95) we deduce

$$\Omega_2 \approx \pi n, \qquad \text{with} \quad n = 1, 2, 3, \ldots. \tag{2.100}$$

The conditions $\Omega_1 \ll 1$ and $E \gg l\Omega_2$ lead to

$$n \ll \min\left[\frac{c}{l}, \frac{E}{l}\right]. \tag{2.101}$$

The scaled displacement is now approximated to

$$\begin{aligned} U_1 &= X_1, \\ U_2 &= \cos\big(\pi n(l - X_2)\big) + \cot\Omega_2 \sin\big(\pi n(l - X_2)\big), \end{aligned} \tag{2.102}$$

where $|\cot\Omega_2| \gg 1$. Figure 2.15 shows the overall profile for the first two modes.

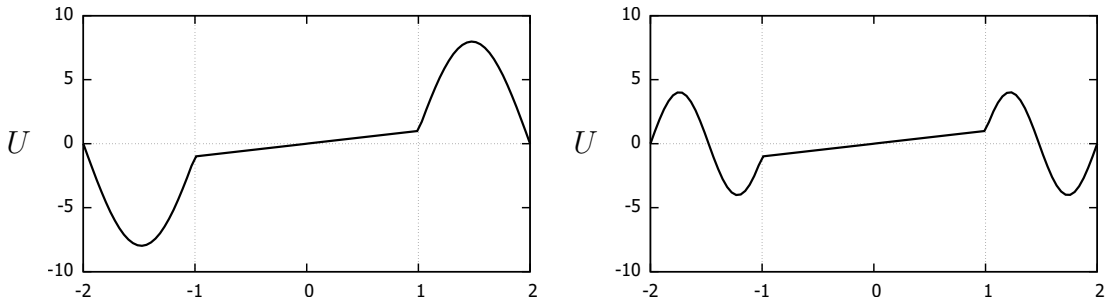

a) n=1 b) n=2

Figure 2.15: Local low-frequency regime for the inner part (2.102); $l = 1$

The condition $E \gg l\Omega_2$ of the limiting Case 2 implies $E_1\rho_1 \gg E_2\rho_2$. This relation is associated with ˝weaker˝ outer parts. Thus, we can observe vibrations of the outer parts under fixed boundary conditions with the eigenfrequencies $\Omega_2 = \pi n$.

Case 3. If $E \sim l\Omega_2$, then, the conditions on Ω_2 are formulated as

$$\Omega_2 \sim \frac{E}{l} \ll \frac{c}{l}. \tag{2.103}$$

2.2.4.2 Local low-frequency regime for the outer parts

The local low-frequency regime of the outer parts $\Omega_1 \gtrsim 1$ and $\Omega_2 \ll 1$ allows to reduce the frequency equation to the form

$$\tan \Omega_1 = -\frac{E\Omega_1}{l}. \tag{2.104}$$

The corresponding natural form is approximated to

$$\begin{aligned} U_1 &= \sin \Omega_1 X_1, \\ U_2 &= (l + 1 - X_2) \sin \Omega_1. \end{aligned} \tag{2.105}$$

Case 1. If $E\Omega_1 \ll l$, then, (2.104) provides $|\tan \Omega_1| \ll 1$. Hence,

$$\Omega_1 \approx \pi n, \qquad \text{with} \quad n = 1, 2, 3, \ldots. \tag{2.106}$$

Using $\Omega_2 \ll 1$ and $E\Omega_1 \ll l$, we can write down for n

$$n \ll \min \left[\frac{l}{c}, \frac{l}{E} \right]. \tag{2.107}$$

Then, the natural form is given by

$$\begin{aligned} U_1 &= \sin \pi n X_1, \\ U_2 &= 0, \end{aligned} \tag{2.108}$$

see Figure 2.16 for n equals 1 and 2.

Case 1 corresponds to the condition $E_1\rho_1 \ll E_2\rho_2$ implying a ″weaker″ inner part having fixed ends.

Case 2. If $E\Omega_1 \gg l$, then, from (2.104) we infer

$$\Omega_1 \approx \frac{\pi(2n-1)}{2}, \qquad \text{with} \quad n = 1, 2, 3, \ldots. \tag{2.109}$$

From $\Omega_2 \ll 1$ and $E\Omega_1 \gg l$ the conditions on n follow as

$$\frac{l}{E} \ll n \ll \frac{l}{c}. \tag{2.110}$$

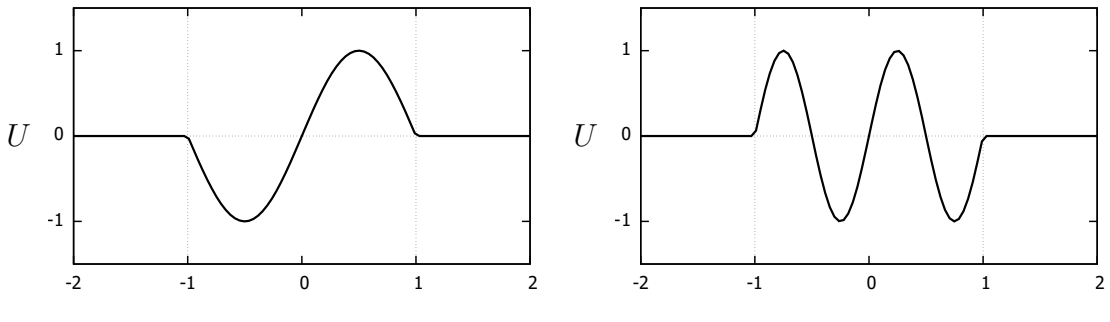

a) n=1 b) n=2

Figure 2.16: Local low-frequency regime for the outer parts (2.108); $l = 1$

We simplify the expressions for the eigenform as

$$U_1 = \sin \frac{\pi(2n-1)X_1}{2}, \qquad U_2 = (-1)^{n+1}(l+1-X_2), \tag{2.111}$$

see Figure 2.17.

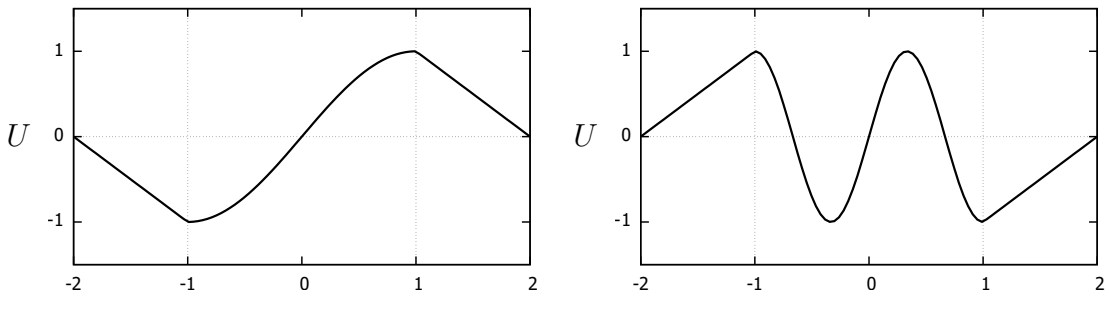

a) n=1 b) n=2

Figure 2.17: Local low-frequency regime for the outer parts (2.111); $l = 1$

Possible physical interpretation of the Case 2 may be formulated as a ˝stronger˝

inner part with free ends having a set of vibration frequencies $\dfrac{\pi(2n-1)}{2}$.

Case 3. Assuming $\rho l \sim \Omega_1$, we derive the conditions allowing the low-frequency regime in the form

$$\Omega_1 \sim \rho l \ll \frac{l}{c}. \tag{2.112}$$

2.2.5 Symmetric vibrations of a rod with fixed ends

Here we study symmetric vibrations of a rod with fixed ends, see boundary conditions (2.36).

The system of linear equations follows from the conditions (2.33), (2.34), and (2.36) with the displacements (2.38) and (2.40) as

$$\begin{aligned} A\cos\Omega_1 - C\cos\Omega_2 l - D\sin\Omega_2 l &= 0,\\ A\frac{E}{c}\sin\Omega_1 - C\sin\Omega_2 l + D\cos\Omega_2 l &= 0,\\ C\cos\big(\Omega_2(l+1)\big) + D\sin\big(\Omega_2(l+1)\big) &= 0. \end{aligned} \tag{2.113}$$

The frequency equation is obtained from (2.113) in the form

$$\cot\Omega_1 \cot\Omega_2 = \frac{E}{c}. \tag{2.114}$$

Then, the scaled displacement profile is given by

$$\begin{aligned} U_1 &= \cos\Omega_1 X_1,\\ U_2 &= \frac{\cos\Omega_1 \sin\big(\Omega_2(l+1-X_2)\big)}{\sin\Omega_2}. \end{aligned} \tag{2.115}$$

The consideration may be split into the global low-frequency regime ($\Omega_1 \ll 1$, $\Omega_2 \ll 1$), and also the local low-frequency behaviour for the inner part ($\Omega_1 \ll 1$, $\Omega_2 \gtrsim 1$), and the outer parts ($\Omega_1 \gtrsim 1$, $\Omega_2 \ll 1$).

2.2.5.1 Global low-frequency regime

The low-frequency approximation of the frequency equation (2.114) results in

$$\Omega_1\Omega_2 = \frac{c}{E}, \tag{2.116}$$

following by

$$\Omega_1^2 = \frac{l}{E}, \tag{2.117}$$

and

$$\Omega_2^2 = \frac{1}{\rho l}. \tag{2.118}$$

The conditions on material parameters associated with the low-frequency vibrations in all rod components are deduced as

$$\rho^{-1} \ll l \ll E. \tag{2.119}$$

We derive the corresponding approximate eigenform as

$$\begin{aligned} U_1 &= 1, \\ U_2 &= l + 1 - X_2, \end{aligned} \tag{2.120}$$

see Figure 2.18.

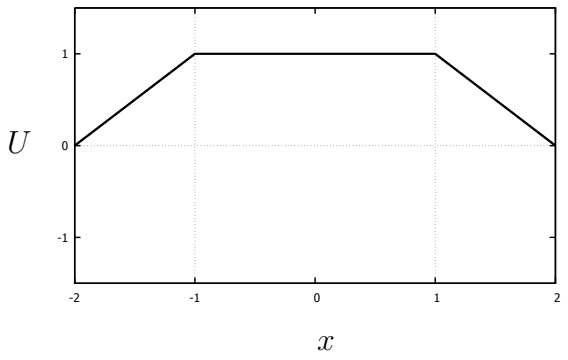

Figure 2.18: Global low-frequency regime (2.120); $l = 1$

Considering $\Omega_1 = \Omega_2 = \Omega \ll 1$, we obtain the approximate solution for $\Omega \ll 1$ as

$$\Omega^2 = \sqrt{\frac{1}{E\rho}}. \tag{2.121}$$

Figure 2.19 confirms that the first eigenfrequency defined by (2.121) decreases as $E\rho \longrightarrow \infty$. The large values of $E\rho$ can be interpreted as a composite rod having a "stronger" inner component and "weaker" outer components.

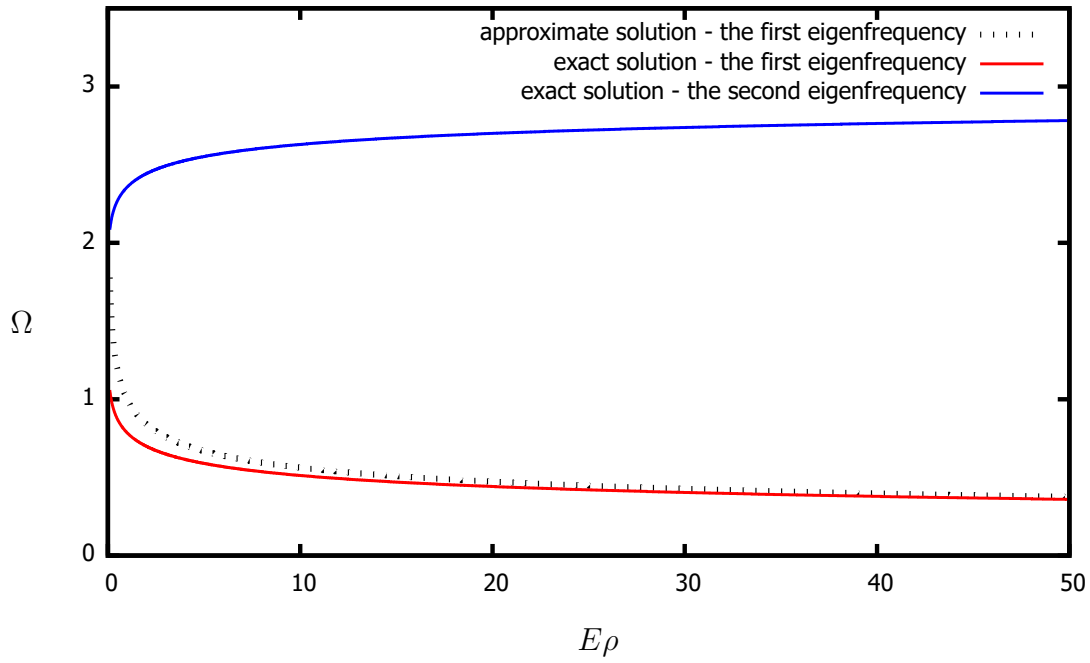

Figure 2.19: Dependence of the frequency Ω on the parameter $E\rho$ for symmetric vibrations of a rod with fixed ends

2.2.5.2 Local low-frequency regime for the inner part

Now, the local low-frequency regime for the inner part is considered. Using the conditions $\Omega_1 \ll 1$ and $\Omega_2 \gtrsim 1$, we derive the approximate frequency equation as

$$\cot \Omega_2 = \rho l \Omega_2. \tag{2.122}$$

The sought-for scaled displacement profile is found in the form

$$\begin{aligned} U_1 &= 1, \\ U_2 &= \frac{\sin\big(\Omega_2(l+1-X_2)\big)}{\sin\Omega_2}. \end{aligned} \tag{2.123}$$

Case 1. Taking $\rho l\Omega_2 \ll 1$, we have $|\cot\Omega_2| \ll 1$ meaning that

$$\Omega_2 \approx \frac{\pi(2n-1)}{2}, \qquad \text{with} \quad n = 1, 2, 3, \ldots. \tag{2.124}$$

We use $\Omega_1 \ll 1$ and $\rho l\Omega_2 \ll 1$ to derive the conditions on n as

$$n \ll \min\left[\frac{c}{l}, \frac{1}{\rho l}\right]. \tag{2.125}$$

The scaled displacement profile takes the form

$$\begin{aligned} U_1 &= 1, \\ U_2 &= (-1)^{n+1}\sin\frac{\pi(2n-1)(l+1-X_2)}{2}, \end{aligned} \tag{2.126}$$

see Figure 2.20.

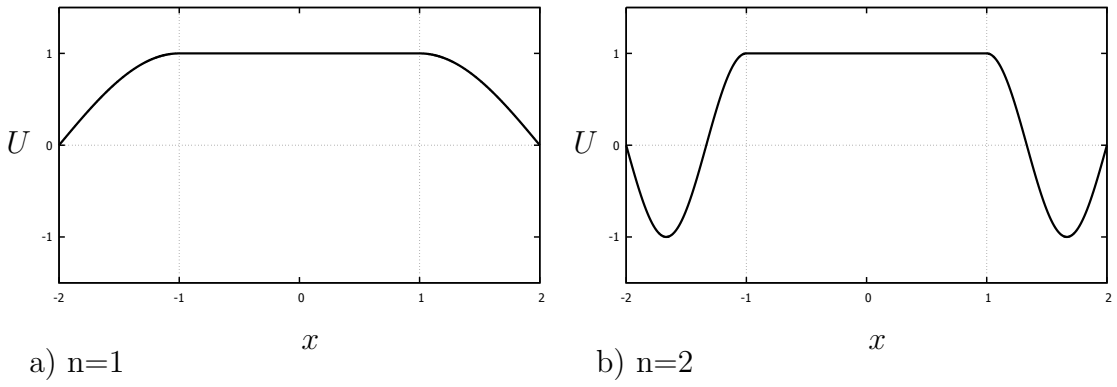

Figure 2.20: Local low-frequency regime for the inner part (2.126); $l = 1$

Case 2. Setting $\rho l\Omega_2 \gg 1$, we derive

$$\Omega_2 \approx \pi n, \qquad \text{with} \quad n = 1, 2, 3, \ldots. \tag{2.127}$$

The conditions $\Omega_1 \ll 1$ and $\rho l\Omega_2 \gg 1$ lead to

$$\frac{1}{\rho l} \ll n \ll \frac{c}{l}. \tag{2.128}$$

Then, the eigenform is given by

$$\begin{aligned} U_1 &= 1, \\ U_2 &= \cot\Omega_2 \sin\big(\pi n(l - X_2)\big) + \cos\big(\pi n(l - X_2)\big), \end{aligned} \tag{2.129}$$

where $\cot\Omega_2 \gg 1$. Figure 2.21 shows the displacement profile for the first two modes.

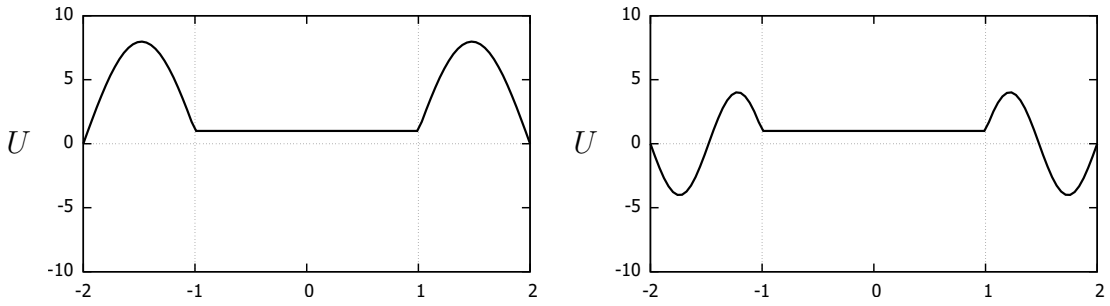

a) n=1 b) n=2

Figure 2.21: Local low-frequency regime for the inner part (2.129); $l = 1$

Case 3. Having $\rho l\Omega_2 \sim 1$, we can write down the conditions for Ω_2 in the form

$$\Omega_2 \sim \frac{1}{\rho l} \ll \frac{c}{l}. \tag{2.130}$$

2.2.5.3 Local low-frequency regime for the outer parts

The local low-frequency regime for the outer parts provides us with the conditions $\Omega_1 \gtrsim 1$ and $\Omega_2 \ll 1$ leading to the simplified frequency equation

$$\cot \Omega_1 = \frac{E}{l}\Omega_1, \tag{2.131}$$

with the corresponding approximate natural form

$$\begin{aligned} U_1 &= \cos \Omega_1 X_1, \\ U_2 &= (l + 1 - X_2) \cos \Omega_1. \end{aligned} \tag{2.132}$$

Case 1. For $E\Omega_1 \ll l$ the equation (2.131) implies

$$\Omega_1 \approx \frac{\pi(2n-1)}{2}, \qquad \text{with} \quad n = 1, 2, 3, \ldots. \tag{2.133}$$

In view of $\Omega_2 \ll 1$ and $E\Omega_1 \ll l$, we deduce

$$n \ll \min\left[\frac{l}{E}, \frac{l}{c}\right]. \tag{2.134}$$

Then, the scaled displacement profile takes the form

$$\begin{aligned} U_1 &= \cos \frac{\pi(2n-1)X_1}{2}, \\ U_2 &= 0, \end{aligned} \tag{2.135}$$

see Figure 2.22 presenting the first two modes.

Case 2. Assuming $E\Omega_1 \gg l$, we can infer that

$$\Omega_1 \approx \pi n, \qquad \text{with} \quad n = 1, 2, 3, \ldots. \tag{2.136}$$

From the conditions $\Omega_2 \ll 1$ and $E\Omega_1 \gg l$ we obtain

$$\frac{l}{E} \ll n \ll \frac{l}{c}. \tag{2.137}$$

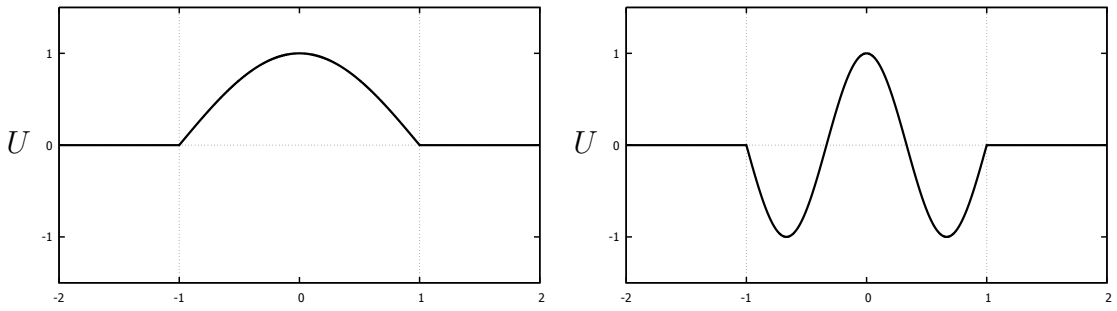

a) n=1 b) n=2

Figure 2.22: Local low-frequency regime for the outer parts (2.135); $l = 1$

Then, the approximate eigenform can be reformulated as

$$\begin{aligned} U_1 &= \cos \pi n X_1, \\ U_2 &= (-1)^n (l + 1 - X_2), \end{aligned} \tag{2.138}$$

see Figure 2.23.

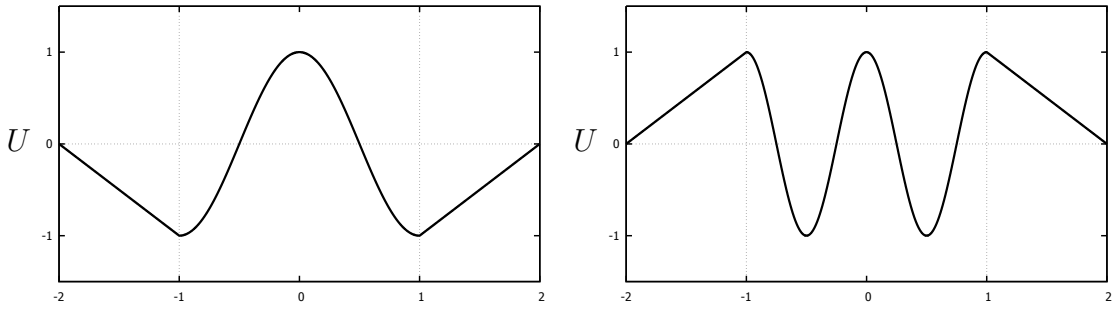

a) n=1 b) n=2

Figure 2.23: Local low-frequency regime for the outer parts (2.138); $l = 1$

Case 3. If $E\Omega_1 \sim l$, the conditions for Ω_1 can be formulated as

$$\Omega_1 \sim \frac{l}{E} \ll \frac{l}{c}. \tag{2.139}$$

The local low-frequency regimes described in this section are very similar to those of previous section for the antisymmetric vibrations of the rod with fixed ends.

2.2.6 Vibrations of a rod with mixed boundary conditions

Now, a rod subject to mixed boundary conditions is analysed. Using (2.33), (2.34), and (2.37) with (2.41), we get the system

$$\begin{gathered}
A\cos\Omega_1 + B\sin\Omega_1 - C\cos\Omega_2 l - D\sin\Omega_2 l = 0,\\
A\cos\Omega_1 - B\sin\Omega_1 - F\cos\Omega_2 l + G\sin\Omega_2 l = 0,\\
A\frac{E}{c}\sin\Omega_1 - B\frac{E}{c}\cos\Omega_1 - C\sin\Omega_2 l + D\cos\Omega_2 l = 0,\\
A\frac{E}{c}\sin\Omega_1 + B\frac{E}{c}\cos\Omega_1 - F\sin\Omega_2 l - G\cos\Omega_2 l = 0,\\
C\sin\big(\Omega_2(l+1)\big) - D\cos\big(\Omega_2(l+1)\big) = 0,\\
F\cos\big(\Omega_2(l+1)\big) - G\sin\big(\Omega_2(l+1)\big) = 0.
\end{gathered} \tag{2.140}$$

Hence, the frequency equation is obtained in the form

$$2\cot 2\Omega_1 \cot 2\Omega_2 = \frac{E}{c} + \frac{c}{E}. \tag{2.141}$$

The scaled displacement profile is then derived as

$$U_3 = \frac{\frac{E}{c}\sin\big(\Omega_2(l+1+X_3)\big)}{\sin\Omega_1\cos\Omega_2 + \frac{E}{c}\cos\Omega_1\sin\Omega_2},$$

$$U_1 = \frac{\sin\big(\Omega_1(1+X_1)\big)\cos\Omega_2 + \frac{E}{c}\cos\big(\Omega_1(1+X_1)\big)\sin\Omega_2}{\sin\Omega_1\cos\Omega_2 + \frac{E}{c}\cos\Omega_1\sin\Omega_2}, \tag{2.142}$$

$$U_2 = \frac{\cos\big(\Omega_2(X_2-l)\big)(\sin 2\Omega_1\cos\Omega_2 + \frac{E}{c}\cos 2\Omega_1\sin\Omega_2)}{\sin\Omega_1\cos\Omega_2 + \frac{E}{c}\cos\Omega_1\sin\Omega_2}.$$

Further analysis of the problem can be split into cases of the global and local low-frequency regimes.

2.2.6.1 Global low-frequency regime

Having $\Omega_1 \ll 1$ and $\Omega_2 \ll 1$, we approximate the frequency equation to the form

$$\frac{1}{2\Omega_1\Omega_2} = \frac{E}{c} + \frac{c}{E}, \tag{2.143}$$

which results in

$$\Omega_1^2 = \frac{l}{2(E+\rho^{-1})}, \tag{2.144}$$

and

$$\Omega_2^2 = \frac{l^{-1}}{2(E^{-1}+\rho)}. \tag{2.145}$$

Combining the latter together with the inequalities $\Omega_1 \ll 1$ and $\Omega_2 \ll 1$, we arrive at the following restrictions on the parameters

$$(E^{-1}+\rho)^{-1} \ll l \ll E+\rho^{-1}, \tag{2.146}$$

supporting the global low-frequency regime.

The approximate profile of the scaled displacement is written as

$$U_3 = \frac{\frac{E}{l}(l+1+X_3)}{1+\frac{E}{l}},$$

$$U_1 = \frac{1+X_1+\frac{E}{l}}{1+\frac{E}{l}}, \tag{2.147}$$

$$U_2 = \frac{2+\frac{E}{l}}{1+\frac{E}{l}},$$

see Figure 2.24 for $\frac{E}{l} \ll 1$ and $\frac{E}{l} \gg 1$.

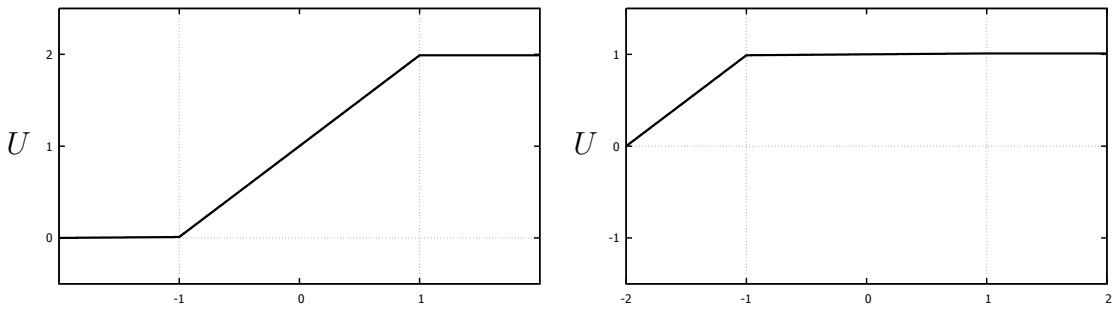

a) E = 0.01 b) E = 100

Figure 2.24: Global low-frequency regime (2.147); $l = 1$

If $\Omega_1 = \Omega_2 = \Omega \ll 1$, the approximate solution for $\Omega \ll 1$ is given by

$$\Omega^2 = \frac{\sqrt{E\rho}}{2(E\rho+1)}, \qquad (\sqrt{E\rho} + \sqrt{(E\rho)^{-1}} \gg 1). \tag{2.148}$$

Figure 2.25 illustrates the behaviour of the first two eigenfrequencies described by (2.141). The approximate solution for the first eigenfrequency (2.148) is also given on

the graph. We can note that the first eigenfrequency decreases in both limits $E\rho \to 0$ and $E\rho \to \infty$. This display a potential of global low-frequency vibrations arising in a rod with mixed boundary conditions in both cases, i.e. a ˝weaker˝ inner part and ˝stronger˝ outer parts, or a ˝stronger˝ inner part and ˝weaker˝ outer parts.

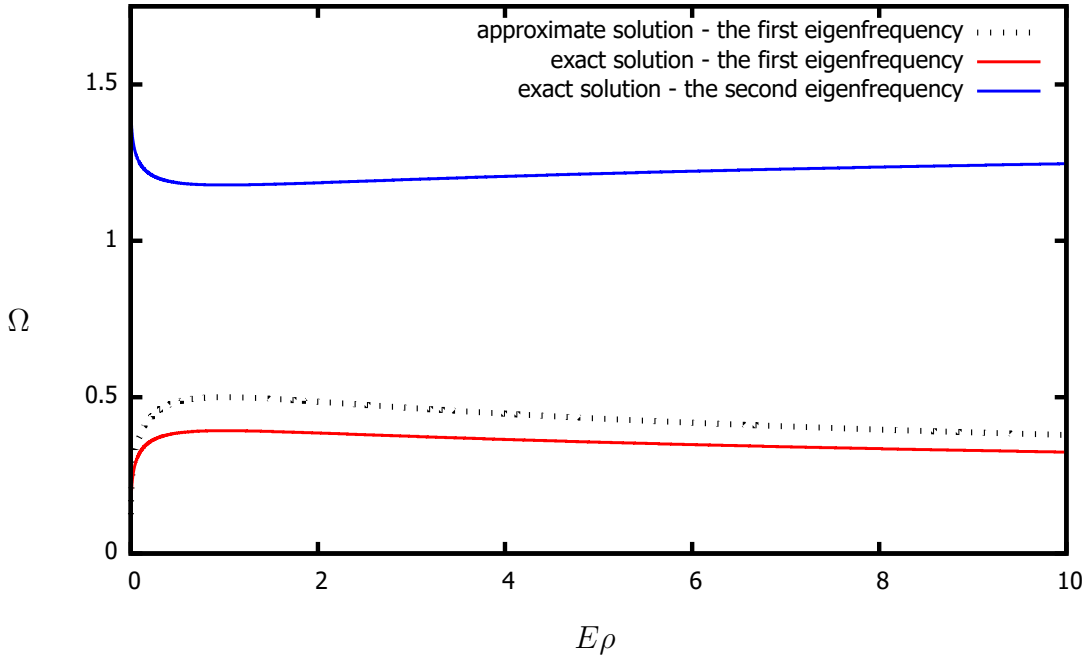

Figure 2.25: Variation of the frequency Ω vs the parameter $E\rho$ for the case of mixed boundary conditions

2.2.6.2 Local low-frequency regime for the inner part

For the case of $\Omega_1 \ll 1$ and $\Omega_2 \gtrsim 1$ the frequency equation can be approximated to the following form

$$\cot 2\Omega_2 = l(\rho + E^{-1})\Omega_2. \tag{2.149}$$

The natural form is given by

$$
\begin{aligned}
U_3 &= \frac{\sin\left(\Omega_2(l+1+X_3)\right)}{\dfrac{l}{E}\Omega_2\cos\Omega_2+\sin\Omega_2},\\
U_1 &= \frac{\dfrac{l}{E}\Omega_2(1+X_1)\cos\Omega_2+\sin\Omega_2}{\dfrac{l}{E}\Omega_2\cos\Omega_2+\sin\Omega_2},\\
U_2 &= \frac{\cos\left(\Omega_2(X_2-l)\right)\left(2\dfrac{l}{E}\Omega_2\cos\Omega_2+\sin\Omega_2\right)}{\dfrac{l}{E}\Omega_2\cos\Omega_2+\sin\Omega_2}.
\end{aligned}
\tag{2.150}
$$

Case 1. If $l(\rho+E^{-1})\Omega_2 \ll 1$, from the frequency equation (2.149) we get

$$
\Omega_2 \approx \frac{\pi(2n-1)}{4}, \qquad \text{with} \quad n=1,2,3,\ldots. \tag{2.151}
$$

Noting that $\Omega_1 \ll 1$ and $l(\rho+E^{-1})\Omega_2 \ll 1$, we obtain conditions on n as

$$
n \ll \min\left[\frac{1}{l(\rho+E^{-1})}, \frac{c}{l}\right]. \tag{2.152}
$$

The corresponding natural form is transformed to

$$
\begin{aligned}
U_3 &= \frac{\sin\dfrac{\pi(2n-1)(l+1+X_3)}{4}}{\sin\dfrac{\pi(2n-1)}{4}},\\
U_1 &= 1,\\
U_2 &= \cos\frac{\pi(2n-1)(X_2-l)}{4}.
\end{aligned}
\tag{2.153}
$$

Figure 2.26 presents the resulting profile.

This case of $l(\rho+E^{-1})\Omega_2 \ll 1$ or $(\sqrt{E\rho}+\sqrt{(E\rho)^{-1}})\Omega_1 \ll 1$ corresponds to a rod without high contrast in components parameters.

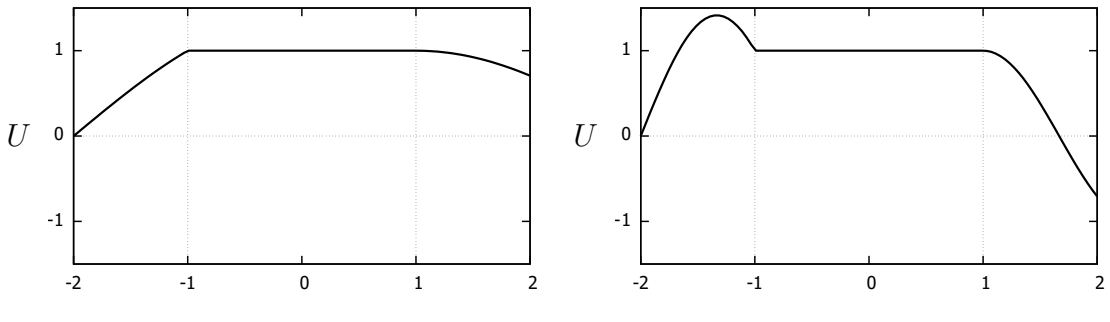

a) n=1 b) n=2

Figure 2.26: Local low-frequency regime for the inner part (2.153); $l = 1$

Case 2. Inequality $l(\rho + E^{-1})\Omega_2 \gg 1$ together with (2.149) implies

$$\Omega_2 \approx \pi n, \qquad \text{with} \quad n = 1, 2, 3, \ldots, \tag{2.154}$$

and

$$\Omega_2 \approx \frac{\pi(2m-1)}{2}, \qquad \text{with} \quad m = 1, 2, 3, \ldots. \tag{2.155}$$

Remarking that $\Omega_1 \ll 1$ and $l(\rho + E^{-1})\Omega_2 \gg 1$, we can write down for n and m

$$\frac{1}{l(\rho + E^{-1})} \ll n, m \ll \frac{c}{l}. \tag{2.156}$$

In this case the condition $l(\rho + E^{-1})\Omega_2 \gg 1$ or $(\sqrt{E\rho} + \sqrt{(E\rho)^{-1}})\Omega_1 \gg 1$ implies a high contrast with either a "stronger" inner part or "stronger" outer parts.

Let us first assume that $lE^{-1}\Omega_2 \gg 1$ and $\rho \ll E^{-1}$, which corresponds to a rod with the "stronger" outer parts. Then, the scaled displacement (2.150) takes the forms

$$\begin{aligned} U_3 &= 0, \\ U_1 &= 1 + X_1, \\ U_2 &= 2\cos\big(\pi n(X_2 - l)\big), \end{aligned} \tag{2.157}$$

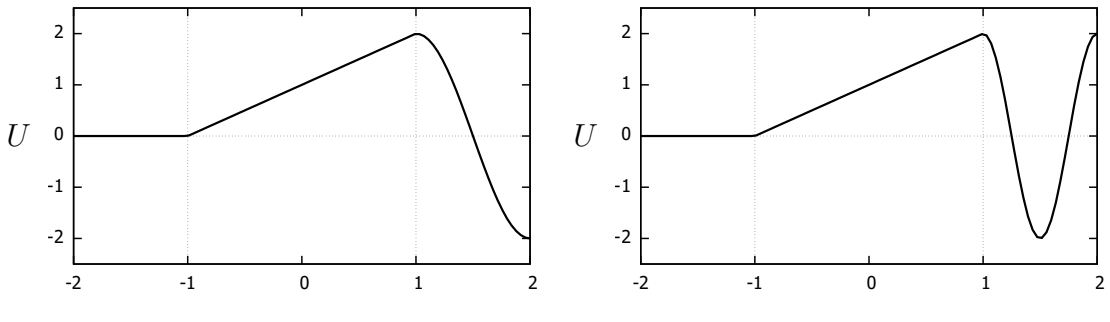

a) n=1 b) n=2

Figure 2.27: Local low-frequency regime for the inner part (2.157); $l = 1$

and

$$\begin{aligned} U_3 &= (-1)^{m+1} 2 \sin \frac{\pi(2m-1)(l+1+X_3)}{2}, \\ U_1 &= 1 - X_1, \\ U_2 &= 0, \end{aligned} \tag{2.158}$$

for (2.154) and (2.155) values of Ω_2, respectively. The eigenforms (2.157) and (2.158) are presented on Figure 2.27 and Figure 2.28, respectively, for the first two modes.

If $l\rho\Omega_2 \gg 1$ and $E^{-1} \ll \rho$ we consider a rod with the "stronger" inner part. In case of $\Omega_2 \approx \pi n$ let us first assume that $lE^{-1}\Omega_2 \gtrsim 1$. Then, the scaled displacement can be simplified to the form

$$\begin{aligned} U_3 &= \frac{(-1)^n E}{l\Omega_2} \sin\big(\pi n(l+1+X_3)\big), \\ U_1 &= 1 + X_1, \\ U_2 &= 2\cos(\pi n(X_2 - l)), \end{aligned} \tag{2.159}$$

see Figure 2.29 for the first two modes. If $lE^{-1}\Omega_2 \ll 1$, then, multiplying U_i by

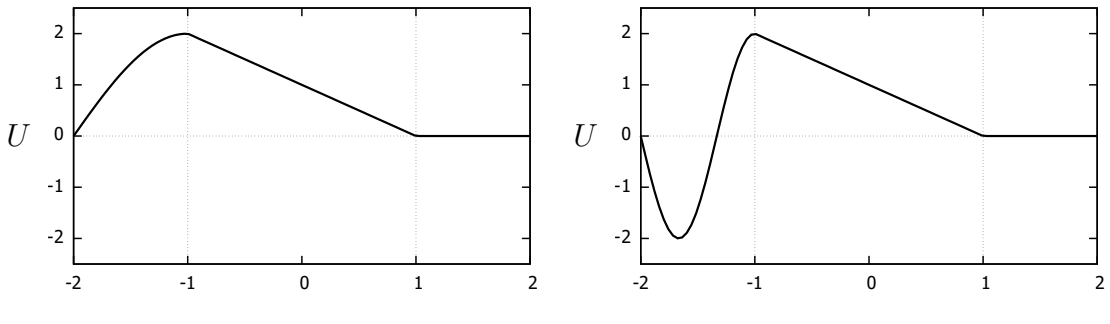

a) m=1 b) m=2

Figure 2.28: Local low-frequency regime for the inner part (2.158); $l = 1$

$\left[\dfrac{l\Omega_2}{E} + \dfrac{1}{2l\rho\Omega_2}\right]$ we derive the eigenform as

$$\begin{aligned} U_3 &= (-1)^n \sin\big(\pi n(l+1+X_3)\big), \\ U_1 &= 0, \\ U_2 &= 0, \end{aligned} \tag{2.160}$$

see Figure 2.30.

When $\Omega_2 \approx \dfrac{\pi(2m-1)}{2}$ the scaled displacement is given by

$$\begin{aligned} U_3 &= (-1)^{m+1} \sin \frac{\pi(2m-1)(l+1+X_3)}{2}, \\ U_1 &= 1, \\ U_2 &= \cos \frac{\pi(2m-1)(X_2-l)}{2}, \end{aligned} \tag{2.161}$$

see Figure 2.31.

Case 3. If $l(\rho + E^{-1})\Omega_2 \sim 1$, we can write down for Ω_2

$$\Omega_2 \sim \frac{1}{l(\rho + E^{-1})} \ll \frac{l}{c}. \tag{2.162}$$

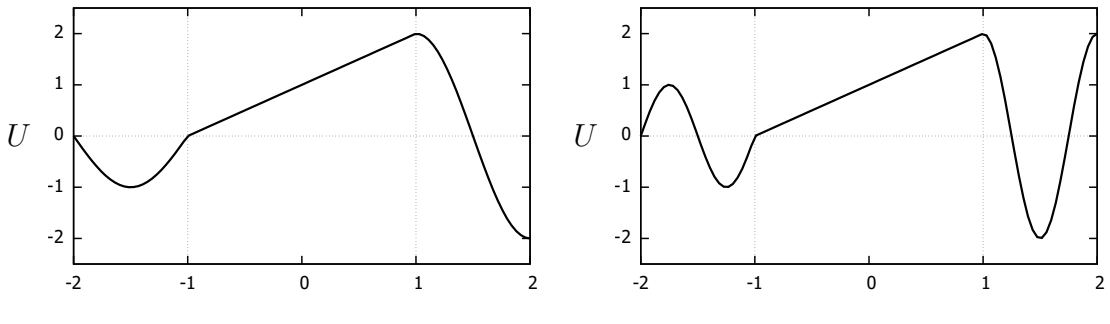

a) n=1 b) n=2

Figure 2.29: Local low-frequency regime for the inner part (2.159); $l = 1$, $\dfrac{E}{\Omega_2} = 1$

2.2.6.3 Local low-frequency regime for the outer parts

The conditions $\Omega_1 \gtrsim 1$ and $\Omega_2 \ll 1$ characterise the local low-frequency regime for the outer parts. The frequency equation is then written as

$$\cot 2\Omega_1 = \frac{E + \rho^{-1}}{l}\Omega_1, \tag{2.163}$$

with the approximate natural form given by

$$U_3 = \frac{\dfrac{E}{l}\Omega_1(l + 1 + X_3)}{\sin\Omega_1 + \dfrac{E}{l}\Omega_1\cos\Omega_1},$$

$$U_1 = \frac{\sin\big(\Omega_1(1 + X_1)\big) + \dfrac{E}{l}\Omega_1\cos\big(\Omega_1(1 + X_1)\big)}{\sin\Omega_1 + \dfrac{E}{l}\Omega_1\cos\Omega_1}, \tag{2.164}$$

$$U_2 = \frac{\sin 2\Omega_1 + \dfrac{E}{l}\Omega_1\cos 2\Omega_1}{\sin\Omega_1 + \dfrac{E}{l}\Omega_1\cos\Omega_1}.$$

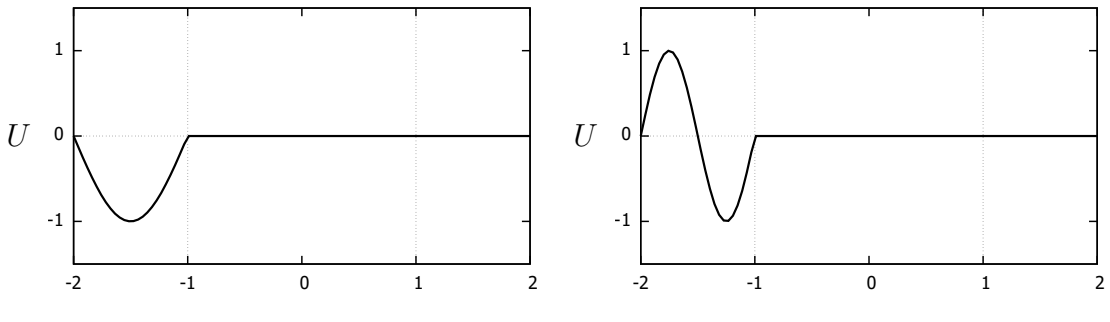

Figure 2.30: Local low-frequency regime for the inner part (2.160); $l = 1$

Case 1. Assuming $(E + \rho^{-1})\Omega_1 \ll l$, we infer that $|\cot 2\Omega_1| \ll 1$ and

$$\Omega_1 \approx \frac{\pi(2n-1)}{4}, \qquad \text{with} \quad n = 1, 2, 3, \ldots. \tag{2.165}$$

From the conditions $\Omega_2 \ll 1$ and $E + \rho^{-1}\Omega_1 \ll l$ we deduce

$$n \ll \min\left[\frac{l}{E+\rho^{-1}}, \frac{l}{c}\right]. \tag{2.166}$$

Then, the eigenform is reduced to

$$\begin{aligned} U_3 &= 0, \\ U_1 &= \frac{\sin\dfrac{\pi(2n-1)(1+X_1)}{4}}{\sin\dfrac{\pi(2n-1)}{4}}, \\ U_2 &= 2\cos\frac{\pi(2n-1)}{4}. \end{aligned} \tag{2.167}$$

Figure 2.32 illustrates the profile.

Similarly to the previous section, the Case 1 characterised by $(E + \rho^{-1})\Omega_1 \ll l$ describes local low-frequency vibrations in a rod without high contrast in material parameters of components.

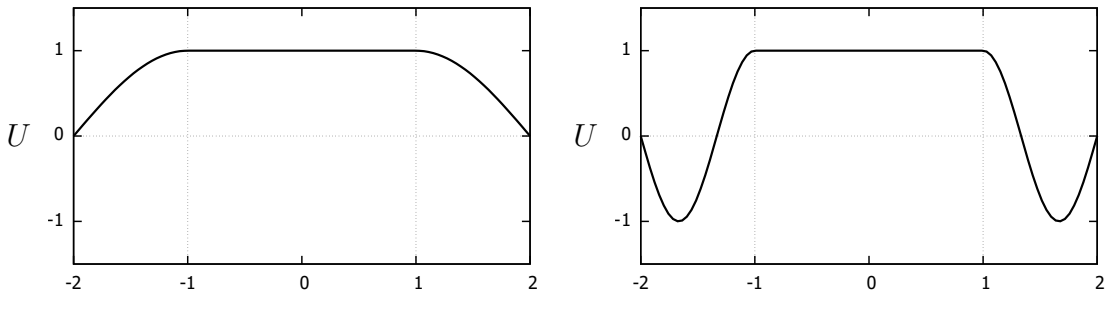

a) m=1 b) m=2

Figure 2.31: Local low-frequency regime for the inner part (2.161); $l = 1$

Case 2. If $(E + \rho^{-1})\Omega_1 \gg l$, then, (2.163) leads to

$$\Omega_1 \approx \pi n, \qquad \text{with} \quad n = 1, 2, 3, \ldots, \tag{2.168}$$

and

$$\Omega_1 \approx \frac{\pi(2m-1)}{2}, \qquad \text{with} \quad m = 1, 2, 3, \ldots. \tag{2.169}$$

Using the conditions $\Omega_2 \ll 1$ and $E + \rho^{-1}\Omega_1 \gg l$, we obtain

$$\frac{l}{E + \rho^{-1}} \ll n, m \ll \frac{l}{c}. \tag{2.170}$$

In the Case 2 the condition $(E+\rho^{-1})\Omega_1 \gg l$ allows either a rod with a ″stronger″ inner part or with ″stronger″ outer parts.

If a rod has the ″stronger″ inner part we assume that $E\Omega_1 \gg l$ and $\rho^{-1} \ll E$. Then for (2.168) values of Ω_1 we simplify the scaled displacement to the form

$$\begin{aligned} U_3 &= l + 1 + X_3, \\ U_1 &= \cos\big(\pi n(1 + X_1)\big), \\ U_2 &= 1, \end{aligned} \tag{2.171}$$

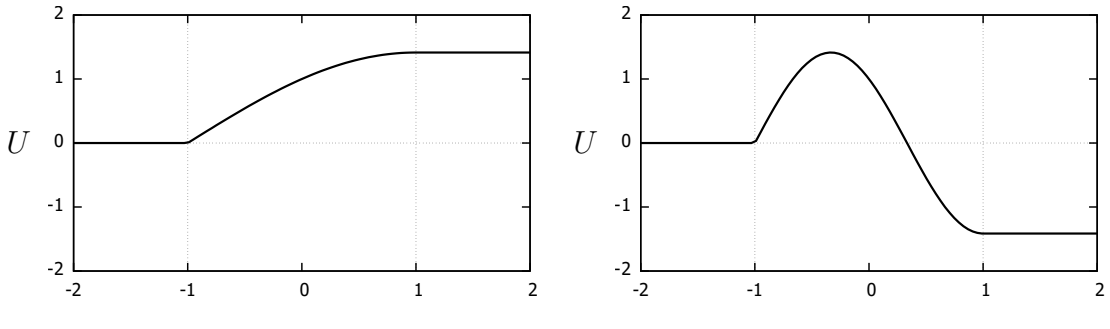

a) n=1 b) n=2

Figure 2.32: Local low-frequency regime for the outer parts (2.167); $l = 1$

see Figure 2.33 for the first two modes. If $\Omega_1 \approx \dfrac{\pi(2m-1)}{2}$ we divide U_i by $2El^{-1}\Omega_1$ to derive the approximate scaled displacement as

$$\begin{aligned} U_3 &= l + 1 + X_3, \\ U_1 &= \cos\frac{\pi(2m-1)(1+X_1)}{2}, \\ U_2 &= -1, \end{aligned} \tag{2.172}$$

see Figure 2.34. In (2.171), (2.172), and all further cases of current subsection we omit the common factor $(-1)^n$ if $\Omega_1 \approx \pi n$ and $(-1)^{m+1}$ if $\Omega_1 \approx \dfrac{\pi(2m-1)}{2}$.

If $\rho^{-1}\Omega_1 \gg l$ and $E \ll \rho^{-1}$, then, a rod has the "stronger" outer parts. Let us first consider $E\Omega_1 \gtrsim l$. For (2.168) the scaled displacement takes the form

$$\begin{aligned} U_3 &= l + 1 + X_3, \\ U_1 &= \frac{l}{E\Omega_1}\sin\big(\pi n(1+X_1)\big) + \cos\big(\pi n(1+X_1)\big), \\ U_2 &= 1, \end{aligned} \tag{2.173}$$

see Figure 2.35. For (2.169) dividing U_i by $El^{-1}\Omega_1$ we obtain the approximate eigenform

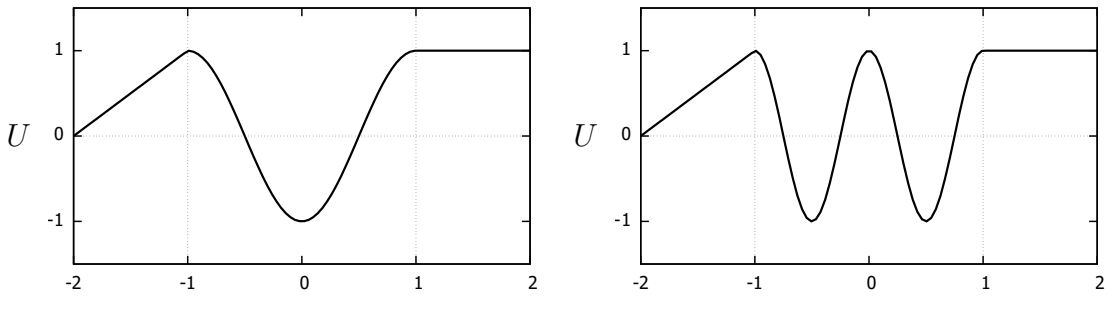

a) n=1 b) n=2

Figure 2.33: Local low-frequency regime for the outer parts (2.171); $l = 1$

as

$$\begin{aligned} U_3 &= l + 1 + X_3, \\ U_1 &= \frac{l}{E\Omega_1} \sin \frac{\pi(2m-1)(1+X_1)}{2} + \cos \frac{\pi(2m-1)(1+X_1)}{2}, \\ U_2 &= -1, \end{aligned} \tag{2.174}$$

see Figure 2.36.

If $E\Omega_1 \ll l$ for $\Omega_1 \approx \pi n$ we multiply U_i by $\left[\frac{E\Omega_1}{l} + \frac{l\rho}{2\Omega_1}\right]$ and approximate the scaled displacement to the form

$$\begin{aligned} U_3 &= 0, \\ U_1 &= \sin\big(\pi n(1+X_1)\big), \\ U_2 &= 0, \end{aligned} \tag{2.175}$$

see Figure 2.37. When $\Omega_1 \approx \dfrac{\pi(2m-1)}{2}$ the eigenform is derived as

$$\begin{aligned} U_3 &= 0, \\ U_1 &= \sin \frac{\pi(2m-1)(1+X_1)}{2}, \\ U_2 &= 0, \end{aligned} \tag{2.176}$$

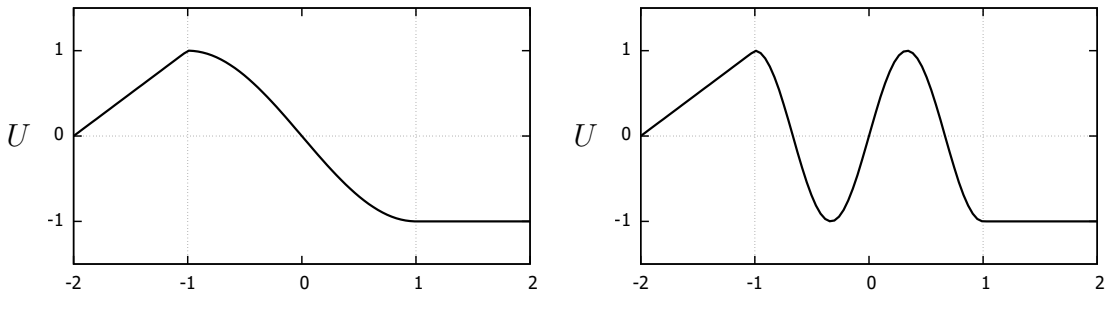

a) m=1 b) m=2

Figure 2.34: Local low-frequency regime for the outer parts (2.172); $l = 1$

see Figure 2.38.

Case 3. If $(E + \rho^{-1})\Omega_1 \sim l$, the conditions for Ω_1 can be written down as

$$\Omega_1 \sim \frac{l}{E + \rho^{-1}} \ll \frac{l}{c}. \tag{2.177}$$

2.3 A three-component rod with variable material parameters

Next, our analysis is extended to a three-component rod with the densities and Young's moduli of parts depending on the coordinate. Since the exact solution could not be found in this case, below we adapt a more general perturbation technique.

2.3.1 Statement of the problem

Consider an elastic rod composed of three inhomogeneous parts. The axis Ox is chosen such that the origin O is located in the middle of the inner part. The rod

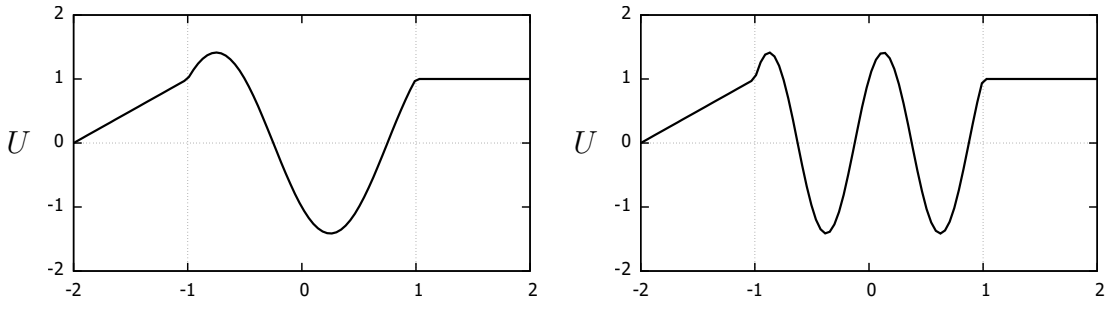

Figure 2.35: Local low-frequency regime for the outer parts (2.173); $l = 1$, $\dfrac{1}{E\Omega_1} = 1$

is finite, with the outer parts having free or fixed ends. Continuity is assumed at the interfaces. The inner part of the rod occupies the region $|x| \le l_1$, with the outer parts specified by $-l_1 - l_3 \le x \le -l_1$ and $l_1 \le x \le l_1 + l_2$, see Figure 2.39.

The governing equations are written in the form

$$\frac{d}{dx}\left(E_i(x)\frac{du_i}{dx}\right) + \rho_i(x)\omega^2 u_i = 0, \qquad i = 1, 2, 3, \tag{2.178}$$

where u_i are the displacements, ω is the vibration frequency, $E_i(x)$ are Young's moduli, $\rho_i(x)$ are the material densities. Here the indices 1, 2, and 3 correspond to the inner, right outer, and left outer parts, respectively.

We introduce dimensionless longitudinal variables

$$X_i = \frac{x}{l_i}, \qquad i = 1, 2, 3. \tag{2.179}$$

The variable material parameters are taken as

$$E_i(X_i) = E_i^* \tilde{E}_i(X_i), \quad \rho_i(X_i) = \rho_i^* \tilde{\rho}_i(X_i), \quad c_i(X_i) = c_i^* \tilde{c}_i(X_i), \quad i = 1, 2, 3, \tag{2.180}$$

where $c_i(X_i) = \sqrt{E_i(X_i)/\rho_i(X_i)}$ are the longitudinal wave speeds and E_i^*, ρ_i^*, and c_i^* are typical values of the associated quantities.

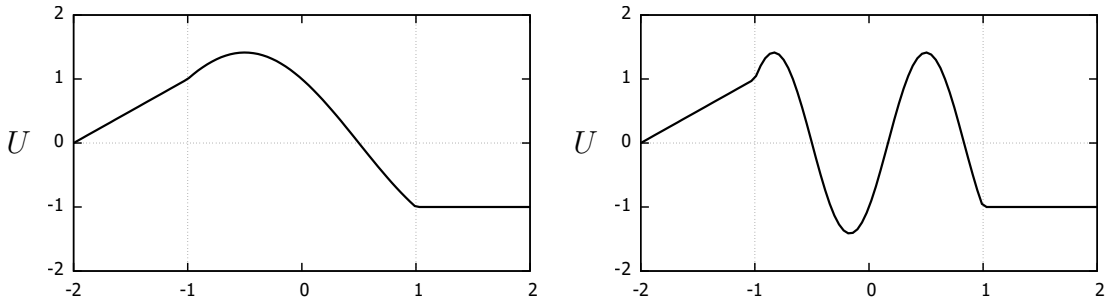

a) m=1 b) m=2

Figure 2.36: Local low-frequency regime for the outer parts (2.174); $l = 1$, $\dfrac{1}{E\Omega_1} = 1$

The dimensionless parameters are given by

$$E_{ij} = \frac{E_i^*}{E_j^*}, \qquad \rho_{ij} = \frac{\rho_i^*}{\rho_j^*}, \qquad c_{ij} = \frac{c_i^*}{c_j^*}, \qquad l_{ij} = \frac{l_i}{l_j}, \qquad i,j = 1,2,3, \tag{2.181}$$

along with the scaled frequencies

$$\Omega_i = \frac{\omega l_i}{c_i^*}, \qquad i = 1,2,3. \tag{2.182}$$

Thus, the dimensionless equations of motion follow from (2.178) as

$$\frac{d}{dX_i}\left(\tilde{E}_i(X_i)\frac{du_i}{dX_i}\right) + \tilde{\rho}_i(X_i)\Omega_i^2 u_i = 0, \qquad i = 1,2,3. \tag{2.183}$$

The continuity conditions for displacements and stresses are formulated as

$$\begin{aligned} u_1|_{X_1=-1} &= u_3|_{X_3=-l_{13}}\,, \\ u_1|_{X_1=1} &= u_2|_{X_2=l_{12}}\,, \end{aligned} \tag{2.184}$$

and

$$\begin{aligned} E_{13}l_{31}\tilde{E}_1(X_1)\left.\frac{du_1}{dX_1}\right|_{X_1=-1} &= \tilde{E}_3(X_3)\left.\frac{du_3}{dX_3}\right|_{X_3=-l_{13}}\,, \\ E_{12}l_{21}\tilde{E}_1(X_1)\left.\frac{du_1}{dX_1}\right|_{X_1=1} &= \tilde{E}_2(X_2)\left.\frac{du_2}{dX_2}\right|_{X_2=l_{12}}\,. \end{aligned} \tag{2.185}$$

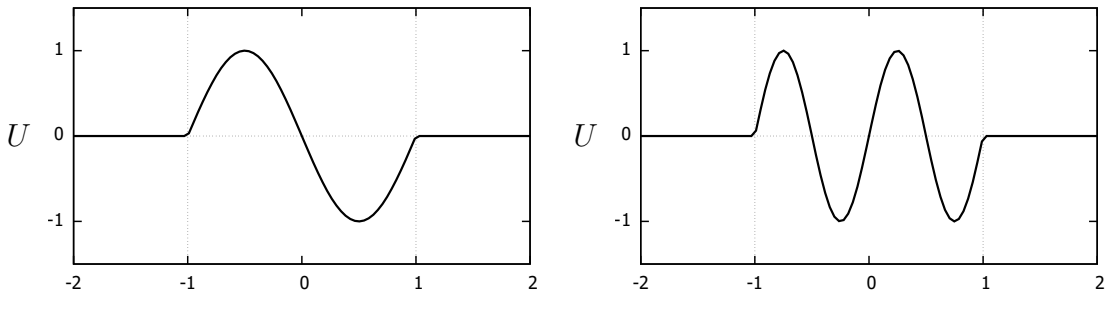

Figure 2.37: Local low-frequency regime for the outer parts (2.175); $l = 1$

We consider the boundary conditions at free ends

$$\begin{aligned} \left.\frac{du_3}{dX_3}\right|_{X_3=-l_{13}-1} &= 0, \\ \left.\frac{du_2}{dX_2}\right|_{X_2=l_{12}+1} &= 0, \end{aligned} \tag{2.186}$$

and fixed ends

$$\begin{aligned} u_3|_{X_3=-l_{13}-1} &= 0, \\ u_2|_{X_2=l_{12}+1} &= 0. \end{aligned} \tag{2.187}$$

Now, we introduce a small parameter $\epsilon \ll 1$ associated with contrast material properties of the components. Then, the global low-frequency regime is considered in the form $\Omega_1^2 \sim \Omega_2^2 \sim \Omega_3^2 \sim \epsilon$, with the frequencies and the displacements expanded as asymptotic series

$$\Omega_i^2 = \epsilon(\Omega_{i0}^2 + \epsilon\Omega_{i1}^2 + \epsilon^2\Omega_{i2}^2 + \ldots), \tag{2.188}$$

and

$$u_i = u_{i0} + \epsilon u_{i1} + \epsilon^2 u_{i2} + \ldots \ . \tag{2.189}$$

Below, we analyse this problem for several cases of different boundary conditions and small parameter.

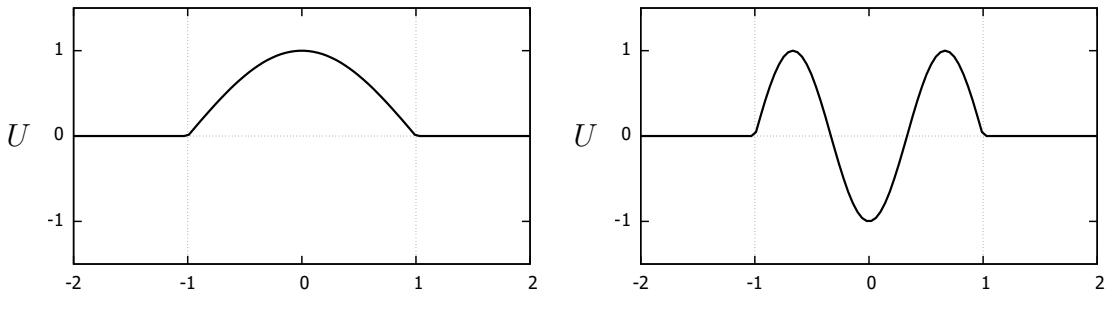

Figure 2.38: Local low-frequency regime for the outer parts (2.176); $l = 1$

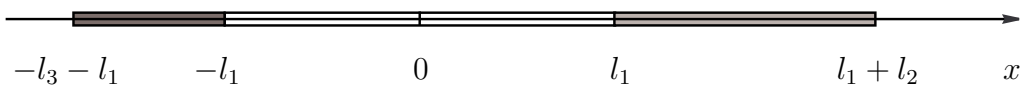

Figure 2.39: A three-component inhomogeneous rod

2.3.2 Free ends

In this section low-frequency vibrations of a rod with variable material parameters and free ends are studied.

2.3.2.1 "Weaker" inner part

First, the small parameter is chosen as $\epsilon = E_{12}l_{21}$. Thus, if $l_{21} = O(1)$, then $E_1 \ll E_2$ corresponding to a "weaker" inner part of the rod. Here and below, we also assume that $E_{23}l_{32} = O(1)$.

On substituting the expansion (2.189) into the equation of motion (2.183) for the

"stronger" outer parts, at leading order ϵ^0 we obtain

$$\frac{d}{dX_i}\left(\tilde{E}_i(X_i)\frac{du_{i0}}{dX_i}\right) = 0, \qquad i = 2, 3, \tag{2.190}$$

subject to

$$\begin{aligned} \left.\frac{du_{30}}{dX_3}\right|_{X_3=-l_{13}-1} &= 0, \\ \left.\frac{du_{30}}{dX_3}\right|_{X_3=-l_{13}} &= 0, \end{aligned} \tag{2.191}$$

and

$$\begin{aligned} \left.\frac{du_{20}}{dX_2}\right|_{X_2=l_{12}} &= 0, \\ \left.\frac{du_{20}}{dX_2}\right|_{X_2=l_{12}+1} &= 0. \end{aligned} \tag{2.192}$$

Integrating (2.190) over X_3 ($-l_{13} - 1 \leq X_3 \leq -l_{13}$) and X_2 ($l_{12} \leq X_2 \leq l_{12} + 1$), we deduce

$$\frac{du_{i0}}{dX_i} = \frac{C_i}{\tilde{E}_i(X_i)}, \qquad i = 2, 3, \tag{2.193}$$

where C_i are constants. From (2.191) and (2.192) we can conclude that

$$\begin{aligned} u_{30} &= C_L, \\ u_{20} &= C_R, \end{aligned} \tag{2.194}$$

where C_L and C_R are constants.

The leading order problem for the inner displacement is written as

$$\frac{d}{dX_1}\left(\tilde{E}_1(X_1)\frac{du_{10}}{dX_1}\right) = 0, \tag{2.195}$$

with

$$\begin{aligned} u_{10}|_{X_1=-1} &= C_L, \\ u_{10}|_{X_1=1} &= C_R. \end{aligned} \tag{2.196}$$

Integrating (2.195) over X_1 ($-1 \leq X_1 \leq 1$) and employing (2.196), we have

$$u_{10} = C_L + \int_{-1}^{X_1} \frac{C_R - C_L}{\tilde{E}_1(X_1)e_1} dX_1, \tag{2.197}$$

where

$$e_1 = \int_{-1}^{1} \tilde{E}_1^{-1}(X_1) dX_1. \tag{2.198}$$

It is worth mentioning that the leading order displacement (2.194) and (2.197) correlates with (2.49) obtained above, see also Figure 2.4.

Frequency estimations and a relation between C_L and C_R can be obtained by analysing the outer parts at next order ϵ. The problem is formulated as follows

$$\frac{d}{dX_i}\left(\tilde{E}_i(X_i)\frac{du_{i1}}{dX_i}\right) + \tilde{\rho}_i(X_i)\Omega_{i0}^2 u_{i0} = 0, \qquad i = 2, 3, \tag{2.199}$$

subject to

$$\begin{aligned} \left.\frac{du_{31}}{dX_3}\right|_{X_3=-l_{13}-1} &= 0, \\ \tilde{E}_3(X_3)\left.\frac{du_{31}}{dX_3}\right|_{X_3=-l_{13}} &= E_{23} l_{32} \tilde{E}_1(X_1)\left.\frac{du_{10}}{dX_1}\right|_{X_1=-1}, \end{aligned} \tag{2.200}$$

and

$$\begin{aligned} \tilde{E}_2(X_2)\left.\frac{du_{21}}{dX_2}\right|_{X_2=l_{12}} &= \tilde{E}_1(X_1)\left.\frac{du_{10}}{dX_1}\right|_{X_1=1}, \\ \left.\frac{du_{21}}{dX_2}\right|_{X_2=l_{12}+1} &= 0, \end{aligned} \tag{2.201}$$

where due to (2.197)

$$\left.\frac{du_{10}}{dX_1}\right|_{X_1=\pm 1} = \frac{C_R - C_L}{\tilde{E}_1(\pm 1) e_1}. \tag{2.202}$$

Integrating (2.199) over X_2 ($l_{12} \le X_2 \le l_{12}+1$) and using (2.194) for u_{20}, we arrive at

$$\tilde{E}_2(X_2)\left.\frac{du_{21}}{dX_2}\right|_{X_2=l_{12}+1} - \tilde{E}_2(X_2)\left.\frac{du_{21}}{dX_2}\right|_{X_2=l_{12}} = -\Omega_{20}^2 C_R r_2, \tag{2.203}$$

where

$$r_2 = \int_{l_{12}}^{l_{12}+1} \tilde{\rho}_2(X_2) dX_2. \tag{2.204}$$

Next, adopting the conditions (2.201), we derive the expression for Ω_{20}^2 in the form

$$\Omega_{20}^2 = \frac{C_R - C_L}{e_1 r_2 C_R}. \tag{2.205}$$

The expression for Ω_{30}^2 is deduced similarly as

$$\Omega_{30}^2 = \frac{E_{23} l_{32} (C_L - C_R)}{e_1 r_3 C_L}, \tag{2.206}$$

where

$$r_3 = \int_{-l_{13}-1}^{-l_{13}} \tilde{\rho}_3(X_3) dX_3. \tag{2.207}$$

Combining the relation $\Omega_2 = l_{23} c_{32} \Omega_3$ and (2.206), we obtain the expression for Ω_{20}^2 in the form

$$\Omega_{20}^2 = \frac{l_{23} \rho_{23} (C_L - C_R)}{e_1 r_3 C_L}. \tag{2.208}$$

Therefore, from (2.205) and (2.208) we get $\Omega_{20} = 0$ associated with the rigid body motion as well as

$$\Omega_{20}^2 = \frac{1}{e_1} \left(\frac{1}{r_2} + \frac{\rho_{23} l_{23}}{r_3} \right), \tag{2.209}$$

with

$$C_L = -C_R \rho_{23} l_{23} \frac{r_2}{r_3}. \tag{2.210}$$

In case when E_i and ρ_i are independent of X_i, the expressions (2.209) and (2.210) can be simplified as

$$\Omega_{20}^2 = \frac{1}{2} (1 + \rho_{23} l_{23}), \tag{2.211}$$

with

$$C_L = -C_R \rho_{23} l_{23}, \tag{2.212}$$

respectively.

In case of a piecewise-homogeneous three-component rod studied previously in Section 2.2.2, $\rho_{23} = 1$, $l_{23} = 1$, and

$$\Omega_2^2 \sim \frac{E}{l}, \tag{2.213}$$

with

$$C_L = -C_R, \tag{2.214}$$

which matches the previous results, see (2.47).

2.3.2.2 "Weaker" outer parts

Next, we consider the small parameter $\epsilon = E_{21}l_{12}$. Setting $l_{12} = O(1)$, we get $E_2 \ll E_1$ and $E_3 \ll E_1$ as $E_{23}l_{32} = O(1)$. This implies a rod with "weaker" outer parts.

At leading order ϵ^0 the equation of motion (2.183) for a "stronger" inner part reduces to

$$\frac{d}{dX_1}\left(\tilde{E}_1(X_1)\frac{du_{10}}{dX_1}\right) = 0, \tag{2.215}$$

subject to

$$\left.\frac{du_{10}}{dX_1}\right|_{X_1=\pm 1} = 0, \tag{2.216}$$

which gives

$$u_{10} = C, \tag{2.217}$$

where C is a constant.

The leading order problem for the displacement of the outer parts can be written as

$$\frac{d}{dX_i}\left(\tilde{E}_i(X_i)\frac{du_{i0}}{dX_i}\right) = 0, \qquad i = 2, 3, \tag{2.218}$$

subject to

$$\begin{aligned} \left.\frac{du_{30}}{dX_3}\right|_{X_3=-l_{13}-1} &= 0, \\ u_{30}|_{X_3=-l_{13}} &= C, \end{aligned} \tag{2.219}$$

and

$$\begin{aligned} u_{20}|_{X_2=l_{12}} &= C, \\ \left.\frac{du_{20}}{dX_2}\right|_{X_2=l_{12}+1} &= 0. \end{aligned} \tag{2.220}$$

The result is

$$u_{30} = u_{20} = C. \tag{2.221}$$

The leading order displacement profile (2.217) and (2.221) matches the formula (2.73) in Section 2.2.3, which describes rigid body motion of a piecewise-homogeneous rod with free ends.

To obtain leading order estimates for frequencies we study the boundary value problem for a "stronger" part at next order ϵ. The equation of motion for the inner part is given by

$$\frac{d}{dX_1}\left(\tilde{E}_1(X_1)\frac{du_{11}}{dX_1}\right)+\tilde{\rho}_1(X_1)\Omega_{10}^2 u_{10}=0, \tag{2.222}$$

subject to

$$\begin{aligned}\tilde{E}_1(X_1)\left.\frac{du_{11}}{dX_1}\right|_{X_1=-1} &= \tilde{E}_3(X_3)\left.\frac{du_{30}}{dX_3}\right|_{X_3=-l_{13}},\\ \tilde{E}_1(X_1)\left.\frac{du_{11}}{dX_1}\right|_{X_1=1} &= \tilde{E}_2(X_2)\left.\frac{du_{20}}{dX_2}\right|_{X_2=l_{12}},\end{aligned} \tag{2.223}$$

where from (2.221) we deduce that

$$\begin{aligned}\left.\frac{du_{30}}{dX_3}\right|_{X_3=-l_{13}} &= 0,\\ \left.\frac{du_{20}}{dX_2}\right|_{X_2=l_{12}} &= 0.\end{aligned} \tag{2.224}$$

Next, we integrate (2.222) over X_1 ($-1\le X_1\le 1$) and substitute (2.217) for u_{10} to obtain

$$\tilde{E}_1(X_1)\left.\frac{du_{11}}{dX_1}\right|_{X_1=1}-\tilde{E}_1(X_1)\left.\frac{du_{11}}{dX_1}\right|_{X_1=-1}=-\Omega_{10}^2 C r_1, \tag{2.225}$$

where

$$r_1=\int_{-1}^{1}\tilde{\rho}_1(X_1)dX_1. \tag{2.226}$$

Then, $\Omega_{10}=0$ follows from (2.225) and (2.224).

The uniform solutions for the displacements of inner (2.217) and outer parts (2.221) together with zero-frequency correspond to the rigid body motion of a rod with free ends.

2.3.3 Fixed ends

Let us now consider low-frequency vibrations of a rod with variable material parameters and fixed ends.

2.3.3.1 "Weaker" inner part

Let us assume that $\epsilon = E_{12}l_{21}$, meaning that the rod has a "weaker" inner part. The leading order problem for the "stronger" outer parts is formulated as

$$\frac{d}{dX_i}\left(\tilde{E}_i(X_i)\frac{du_{i0}}{dX_i}\right) = 0, \qquad i = 2, 3, \tag{2.227}$$

subject to

$$\begin{aligned} u_{30}\,|_{X_3=-l_{13}-1} &= 0, \\ \left.\frac{du_{30}}{dX_3}\right|_{X_3=-l_{13}} &= 0, \end{aligned} \tag{2.228}$$

and

$$\begin{aligned} \left.\frac{du_{20}}{dX_2}\right|_{X_2=l_{12}} &= 0, \\ u_{20}\,|_{X_2=l_{12}+1} &= 0. \end{aligned} \tag{2.229}$$

Then, for the leading order displacement of the outer parts we arrive at

$$u_{30} = u_{20} = 0. \tag{2.230}$$

Next, we consider the boundary value problem for the inner part at ϵ^0. The equation of motion

$$\frac{d}{dX_1}\left(\tilde{E}_1(X_1)\frac{du_{10}}{dX_1}\right) = 0, \tag{2.231}$$

is subject to

$$u_{10}|_{X_1=\pm 1} = 0, \tag{2.232}$$

which results in

$$u_{10} = 0. \tag{2.233}$$

Thus, we can conclude that the limit $\epsilon = E_{12}l_{21} \ll 1$ in case of fixed ends does not allow low frequency vibrations.

2.3.3.2 "Weaker" outer parts

Now, the focus is on the small parameter $\epsilon = E_{21} l_{12}$ associated with a "stronger" inner part of the rod.

The ϵ^0 boundary value problem for the inner part is formulated similarly to (2.215) and (2.216) leading to

$$u_{10} = C. \tag{2.234}$$

For the displacement of the outer parts we have at leading order

$$\frac{d}{dX_i}\left(\tilde{E}_i(X_i)\frac{du_{i0}}{dX_i}\right) = 0, \qquad i = 2, 3, \tag{2.235}$$

subject to

$$\begin{aligned} u_{30}\,|_{X_3=-l_{13}-1} &= 0, \\ u_{30}\,|_{X_3=-l_{13}} &= C, \end{aligned} \tag{2.236}$$

and

$$\begin{aligned} u_{20}\,|_{X_2=l_{12}} &= C, \\ u_{20}\,|_{X_2=l_{12}+1} &= 0. \end{aligned} \tag{2.237}$$

The resulting displacement profile is derived by integrating (2.235) over X_3 ($-l_{13} - 1 \leq X_3 \leq -l_{13}$) and X_2 ($l_{12} \leq X_2 \leq l_{12} + 1$) and applying the boundary conditions (2.236) and (2.237). Thus, we have

$$\begin{aligned} u_{30} &= \int_{-l_{13}-1}^{X_3} \frac{C}{\tilde{E}_3(X_3)e_3} dX_3, \\ u_{20} &= C - \int_{l_{12}}^{X_2} \frac{C}{\tilde{E}_2(X_2)e_2} dX_2, \end{aligned} \tag{2.238}$$

where

$$e_3 = \int_{-l_{13}-1}^{-l_{13}} \tilde{E}_3^{-1}(X_3) dX_2, \qquad e_2 = \int_{l_{12}}^{l_{12}+1} \tilde{E}_2^{-1}(X_2) dX_3. \tag{2.239}$$

The solutions (2.234) and (2.238) are in agreement with the previously obtained results (2.120), see also Figure 2.18.

At next order ϵ the problem for the inner part is formulated as follows

$$\frac{d}{dX_1}\left(\tilde{E}_1(X_1)\frac{du_{11}}{dX_1}\right)+\tilde{\rho}_1(X_1)\Omega_{10}^2 u_{10}=0, \tag{2.240}$$

subject to

$$\begin{aligned}\tilde{E}_1(X_1)\left.\frac{du_{11}}{dX_1}\right|_{X_1=-1} &= E_{32}l_{23}\tilde{E}_3(X_3)\left.\frac{du_{30}}{dX_3}\right|_{X_3=-l_{13}},\\ \tilde{E}_1(X_1)\left.\frac{du_{11}}{dX_1}\right|_{X_1=1} &= \tilde{E}_2(X_2)\left.\frac{du_{20}}{dX_2}\right|_{X_2=l_{12}},\end{aligned} \tag{2.241}$$

where, according to (2.238),

$$\begin{aligned}\left.\frac{du_{30}}{dX_3}\right|_{X_3=-l_{13}} &= \frac{C}{\tilde{E}_3(X_3)e_3},\\ \left.\frac{du_{20}}{dX_2}\right|_{X_2=l_{12}} &= -\frac{C}{\tilde{E}_2(X_2)e_2}.\end{aligned} \tag{2.242}$$

We integrate (2.240) over X_1 ($-1\le X_1\le 1$), insert the uniform solution (2.234) for u_{10}, and adopt the conditions (2.241) to arrive at the expression for Ω_{10}^2 in the form

$$\Omega_{10}^2=\frac{1}{e_2r_1}+\frac{1}{e_3r_1}. \tag{2.243}$$

In case when E_i and ρ_i are constants the expression for the frequency Ω_1 transforms to

$$\Omega_1^2\sim\frac{l}{E}, \tag{2.244}$$

which coincides with the results for a piecewise-homogeneous rod with fixed ends, see (2.117).

2.3.4 Mixed boundary conditions

Finally, we consider low-frequency vibrations of an inhomogeneous rod subject to mixed boundary conditions.

2.3.4.1 "Weaker" inner part

Let us start with a "weaker" inner part assuming the small parameter $\epsilon = E_{12}l_{21}$.

The boundary value problem for the "stronger" parts at leading order ϵ^0 is formulated as

$$\frac{d}{dX_i}\left(\tilde{E}_i(X_i)\frac{du_{i0}}{dX_i}\right) = 0, \qquad i = 2, 3, \tag{2.245}$$

subject to

$$\begin{aligned} u_{30}|_{X_3=-l_{13}-1} &= 0, \\ \left.\frac{du_{30}}{dX_3}\right|_{X_3=-l_{13}} &= 0, \end{aligned} \tag{2.246}$$

and

$$\begin{aligned} \left.\frac{du_{20}}{dX_2}\right|_{X_2=l_{12}} &= 0, \\ \left.\frac{du_{20}}{dX_2}\right|_{X_2=l_{12}+1} &= 0. \end{aligned} \tag{2.247}$$

Thus, we arrive at the displacement profile for the outer parts in the form

$$\begin{aligned} u_{30} &= 0, \\ u_{20} &= C. \end{aligned} \tag{2.248}$$

At leading order ϵ^0 the equation of motion for the inner part

$$\frac{d}{dX_1}\left(\tilde{E}_1(X_1)\frac{du_{10}}{dX_1}\right) = 0, \tag{2.249}$$

subject to the boundary conditions

$$\begin{aligned} u_{10}|_{X_1=-1} &= 0, \\ u_{10}|_{X_1=1} &= C, \end{aligned} \tag{2.250}$$

provides the displacement in the form

$$u_{10} = \int_{-1}^{X_1} \frac{C}{\tilde{E}_1(X_1)e_1} dX_1. \tag{2.251}$$

The obtained leading order displacement (2.248) and (2.251) confirms the corresponding result (2.147), see also Figure 2.24 for $E/l \ll 1$.

At next order the problem for the outer right part with a non-zero displacement is written in the form

$$\frac{d}{dX_2}\left(\tilde{E}_2(X_2)\frac{du_{21}}{dX_2}\right) + \tilde{\rho}_2(X_2)\Omega_{20}^2 u_{20} = 0, \tag{2.252}$$

with

$$\begin{aligned} \tilde{E}_2(X_2)\left.\frac{du_{21}}{dX_2}\right|_{X_2=l_{12}} &= \tilde{E}_1(X_1)\left.\frac{du_{10}}{dX_1}\right|_{X_1=1}, \\ \left.\frac{du_{21}}{dX_2}\right|_{X_2=l_{12}+1} &= 0, \end{aligned} \tag{2.253}$$

where, using (2.251), we get

$$\left.\frac{du_{10}}{dX_1}\right|_{X_1=1} = \frac{C}{\tilde{E}_1(1)e_1}. \tag{2.254}$$

Integrating (2.252) over X_2 ($l_{12} \le X_2 \le l_{12}+1$) with (2.248) for u_{20} and using the conditions (2.253), we arrive at

$$\Omega_{20}^2 = \frac{1}{e_1 r_2}. \tag{2.255}$$

In case when E_i and ρ_i are independent of X_i, the frequency expression reduces to

$$\Omega_2^2 \sim \frac{E}{2l}. \tag{2.256}$$

This correlates with the formula (2.145) in Section 2.2.6.1.

2.3.4.2 "Weaker" outer parts

Next, we consider the small parameter $\epsilon = E_{21}l_{12}$ associated with the "weaker" outer parts.

The leading order boundary value problem for a "stronger" inner part is given by (2.215) and (2.216), which results in

$$u_{10} = C. \tag{2.257}$$

The equations of motion for the outer parts at ϵ^0 can be written as

$$\frac{d}{dX_i}\left(\tilde{E}_i(X_i)\frac{du_{i0}}{dX_i}\right)=0, \qquad i=2,3, \tag{2.258}$$

subject to

$$\begin{aligned} u_{30}|_{X_3=-l_{13}-1} &= 0, \\ u_{30}|_{X_3=-l_{13}} &= C, \end{aligned} \tag{2.259}$$

and

$$\begin{aligned} u_{20}|_{X_2=l_{12}} &= C, \\ \left.\frac{du_{20}}{dX_2}\right|_{X_2=l_{12}+1} &= 0. \end{aligned} \tag{2.260}$$

This provides the leading order displacements in the form

$$\begin{aligned} u_{30} &= \int_{-l_{13}-1}^{X_3} \frac{C}{\tilde{E}_3(X_3)e_3}dX_3, \\ u_{20} &= C. \end{aligned} \tag{2.261}$$

As in the previous case, (2.257) and (2.261) match the displacement profile (2.147) for mixed boundary conditions, see Figure 2.24 for $E/l \gg 1$.

The boundary value problem for the inner part at ϵ is derived as

$$\frac{d}{dX_1}\left(\tilde{E}_1(X_1)\frac{du_{11}}{dX_1}\right)+\tilde{\rho}_1(X_1)\Omega_{10}^2u_{10}=0, \tag{2.262}$$

subject to

$$\begin{aligned} \tilde{E}_1(X_1)\left.\frac{du_{11}}{dX_1}\right|_{X_1=-1} &= \tilde{E}_3(X_3)\left.\frac{du_{30}}{dX_3}\right|_{X_3=-l_{13}}, \\ \tilde{E}_1(X_1)\left.\frac{du_{11}}{dX_1}\right|_{X_1=1} &= \tilde{E}_2(X_2)\left.\frac{du_{20}}{dX_2}\right|_{X_2=l_{12}}, \end{aligned} \tag{2.263}$$

where, due to (2.261),

$$\begin{aligned} \left.\frac{du_{30}}{dX_3}\right|_{X_3=-l_{13}} &= \frac{C}{\tilde{E}_3(-l_{13})e_3}, \\ \left.\frac{du_{20}}{dX_2}\right|_{X_2=l_{12}} &= 0. \end{aligned} \tag{2.264}$$

Following the same procedure as in previous cases, we obtain the leading order estimate for the sought-for frequency as

$$\Omega_{10}^2 = \frac{1}{e_3 r_1}. \tag{2.265}$$

For a piecewise-homogeneous rod considered in Section 2.2.6, (2.265) becomes

$$\Omega_1^2 \sim \frac{l}{2E}, \tag{2.266}$$

which matches (2.144).

2.4 A multi-component rod

Finally, we present an asymptotic model of low-frequency vibrations of a piecewise-homogeneous multi-component rod.

2.4.1 Statement of the problem

We study a rod composed of two materials, having finite n number of components of length l_i and a periodic structure, such that the "stronger" parts alternate the "weaker" parts, see Figure 2.40. We set axis Ox such that the origin O is placed at the left end of the rod. Continuity conditions hold between the components. For the "weaker"/"stronger" outer component we assume the end to be fixed or free, respectively.

The dimensionless governing equations for the rod components are given by

$$\frac{d^2 u_i}{dX_i^2} + \Omega_i^2 u_i = 0, \qquad i = 1, 2, \ldots, n. \tag{2.267}$$

Let us introduce dimensionless quantities

$$B_i = \frac{l_0 + \ldots + l_{i-1}}{l_i}, \qquad \text{where} \quad l_0 = 0, \qquad i = 1, 2, \ldots, n, \tag{2.268}$$

Figure 2.40: A multi-component piecewise-homogeneous rod

such that the local variables are defined within

$$B_i \le X_i \le B_i + 1, \qquad i = 1, 2, \ldots, n. \tag{2.269}$$

The continuity conditions for displacements and stresses are written as

$$u_i|_{X_i=B_i+1} = u_{i+1}|_{X_{i+1}=B_{i+1}}, \tag{2.270}$$

and

$$\left.\frac{du_i}{dX_i}\right|_{X_i=B_i+1} = L^i_{i+1}\frac{E_2}{E_1}\left.\frac{du_{i+1}}{dX_{i+1}}\right|_{X_{i+1}=B_{i+1}}, \tag{2.271}$$

where $i = 1, 2, \ldots, n-1$ and $L^k_j = l_k/l_j$.

We assume free ends if outer parts are "stronger"

$$\begin{aligned} \left.\frac{du_1}{dX_1}\right|_{X_1=0} &= 0, \\ \left.\frac{du_n}{dX_n}\right|_{X_n=B_n+1} &= 0, \end{aligned} \tag{2.272}$$

or fixed ends if outer parts are "weaker"

$$\begin{aligned} u_1|_{X_1=0} &= 0, \\ u_n|_{X_n=B_n+1} &= 0. \end{aligned} \tag{2.273}$$

In addition, we denote $\epsilon = \dfrac{E_1}{E_2}$ if the fist part of the rod is "weaker" or $\epsilon = \dfrac{E_2}{E_1}$ if the fist part of the rod is "stronger". Below we focus on the global low-frequency

regime of the form $\Omega_1^2 \sim \Omega_2^2 \sim \ldots \sim \Omega_n^2 \sim \epsilon$. Similarly to the previous section, we expand the frequencies and the displacements as asymptotic series for the each part of the rod, see (2.188) and (2.189), respectively.

Noting that the relations between frequency parameters of the "stronger" and "weaker" parts can be formulated as

$$\Omega_i = L_{i+1}^i \frac{c_1}{c_2} \Omega_{i+1}, \tag{2.274}$$

we can conclude that $L_{i+1}^i \dfrac{c_1}{c_2} \sim 1$. Then, assuming that $L_{i+1}^i \sim 1$, we infer that $\dfrac{\rho_1}{\rho_2} \sim \epsilon$ if the fist part of the rod is "weaker" or $\dfrac{\rho_2}{\rho_1} \sim \epsilon$ if the fist part of the rod is "stronger". This conclusion coincides with the condition on parameters (2.48) for a three-component piecewise-homogeneous rod.

Displacements of the "stronger" components

To deduce the displacements for the "stronger" parts we substitute (2.189) into (2.267) and the conditions (2.271) and (2.272) at leading order to obtain the boundary value problem as equations

$$\frac{d^2 u_{i0}}{dX_i^2} = 0, \tag{2.275}$$

subject to the Neumann boundary conditions

$$\begin{aligned} \left.\frac{du_{i0}}{dX_i}\right|_{X_i=B_i} &= 0, \\ \left.\frac{du_{i0}}{dX_i}\right|_{X_i=B_i+1} &= 0. \end{aligned} \tag{2.276}$$

Thus, for the displacements of the "stronger" parts we have uniform solutions

$$u_{i0} = C_i, \tag{2.277}$$

where C_i are constants and

$$C_j = 0, \qquad \text{for} \quad j < 1 \quad \text{or} \quad j > n. \tag{2.278}$$

As we consider the rod having n number of parts, C_j with $j < 1$ or $j > n$ refers to the non existing parts. However, this notation allows us to formulate further boundary value problems without splitting them on separate cases for the inner and outer parts.

Displacements of the ‟weaker″ components

The leading order boundary value problem for the ‟weaker″ components follows from substitution of (2.189) into (2.267) and the conditions (2.270) and (2.273) as

$$\frac{d^2 u_{i0}}{dX_i^2} = 0, \tag{2.279}$$

subject to the Dirichlet boundary conditions

$$\begin{aligned} u_{i0}|_{X_i=B_i} &= C_{i-1}, \\ u_{i0}|_{X_i=B_i+1} &= C_{i+1}. \end{aligned} \tag{2.280}$$

This provides us with the displacements of the ‟weaker″ parts in the form

$$u_{i0} = C_{i-1} + (C_{i+1} - C_{i-1})(X_i - B_i). \tag{2.281}$$

The frequency estimation

To determine the leading order estimate of dimensionless frequencies we need to consider the boundary value problem for the ‟stronger″ parts at ϵ. The equations of motion are approximated to the form

$$\frac{d^2 u_{i1}}{dX_i^2} + \Omega_{i0}^2 u_{i0} = 0, \tag{2.282}$$

with the boundary conditions

$$\begin{aligned} \left.\frac{du_{i1}}{dX_i}\right|_{X_i=B_i} &= L_{i-1}^i \left.\frac{du_{(i-1)0}}{dX_{i-1}}\right|_{X_{i-1}=B_{i-1}+1}, \\ \left.\frac{du_{i1}}{dX_i}\right|_{X_i=B_i+1} &= L_{i+1}^i \left.\frac{du_{(i+1)0}}{dX_{i+1}}\right|_{X_{i+1}=B_{i+1}}, \end{aligned} \tag{2.283}$$

where, according to (2.281),

$$\begin{aligned} \left.\frac{du_{i1}}{dX_i}\right|_{X_i=B_i} &= L^i_{i-1}(C_i - C_{i-2}), \\ \left.\frac{du_{i1}}{dX_i}\right|_{X_i=B_i+1} &= L^i_{i+1}(C_{i+2} - C_i). \end{aligned} \tag{2.284}$$

Then, we can integrate equations (2.282) over X_i ($B_i \le X_i \le B_i + 1$), use (2.277) for u_{i0}, and with help of (2.283) derive the leading order estimations for the frequencies of the "stronger" parts as

$$\Omega^2_{i0} = \frac{(L^i_{i-1} + L^i_{i+1})C_i - L^i_{i-1}C_{i-2} - L^i_{i+1}C_{i+2}}{C_i}. \tag{2.285}$$

Keeping in mind that the relations between frequency parameters of the "stronger" parts are given by

$$\Omega_{k0} = L^k_j \Omega_{j0}, \tag{2.286}$$

we can use this model to find a solution for any particular number of components. The number of the low eigenfrequencies is equal to the number of "stronger" parts. Moreover, from (2.277) and (2.281) it can be observed that "stronger" parts at leading order always perform a rigid body motion, while "weaker" parts suffer an almost homogeneous deformation.

2.4.2 Examples

Further we provide several examples, describing the methodology developed in the previous section.

2.4.2.1 A three-component rod with two "stronger" parts

Let us now implement the model to find the low-frequency vibrations profile for a three-component rod with two "stronger" parts. In this case to keep periodic structure the rod should have the "stronger" outer components subject to the Neumann

boundary conditions. Using (2.285), we can write down for the "stronger" parts

$$\begin{aligned} \Omega_{10}^2 &= L_2^1 \frac{C_1 - C_3}{C_1}, \\ \Omega_{30}^2 &= L_2^3 \frac{C_3 - C_1}{C_3}, \end{aligned} \tag{2.287}$$

with

$$\Omega_{10} = L_3^1 \Omega_{30}. \tag{2.288}$$

The expressions (2.287) with (2.288) provide us with the relation between the constants and with the leading order estimation for the lowest eigenfrequencies

$$C_3 = (1-k)C_1, \quad \Omega_{10}^2 = kL_2^1, \tag{2.289}$$

where $k = 0$ or $k = 1 + L_3^1$.

If $l_1 = l_3$ as in Section 2.2, then $k = 0$ or $k = 2$ and

$$\Omega_1^2 = 0 \quad \text{or} \quad \Omega_1^2 = 2\epsilon L_2^1, \tag{2.290}$$

which correlates with the previous solutions (2.73) and (2.47), respectively.

Using (2.277) and (2.281) with (2.289) we can derive the scaled displacement profiles as

$$\begin{aligned} U_{10} &= 1, \\ U_{20} &= 1 - k(X_2 - B_2), \\ U_{30} &= 1 - k, \end{aligned} \tag{2.291}$$

see Figure 2.41 with a symmetric motion of the rod when $k = 0$ and an antisymmetric motion when $k = 2$.

2.4.2.2 A four-component rod with two "stronger" parts

For a four-component rod with two "stronger" parts we have

$$\begin{aligned} \Omega_{10}^2 &= L_2^1 \frac{C_1 - C_3}{C_1}, \\ \Omega_{30}^2 &= \frac{(L_2^3 + L_4^3)C_3 - L_2^3 C_1}{C_3}, \end{aligned} \tag{2.292}$$

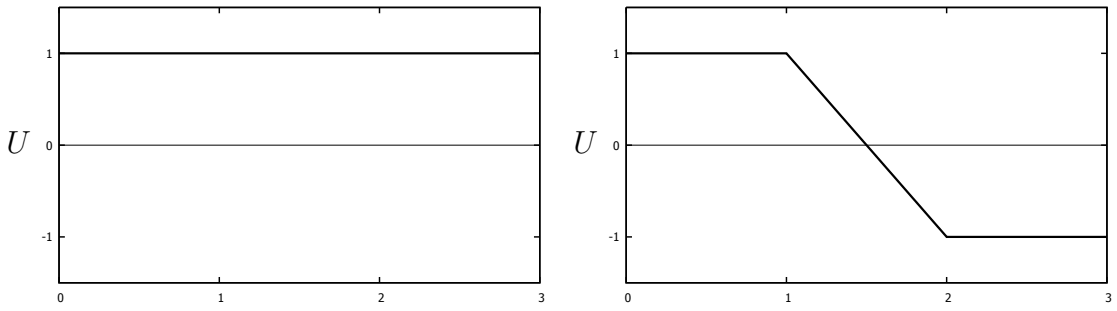

a) $k = 0$ b) $k = 2$

Figure 2.41: Displacement profiles (2.291); $l_1 = l_2 = l_3$

with

$$\Omega_{10} = L_3^1 \Omega_{30}. \tag{2.293}$$

Thus, the relation between constants and expression for the eigenfrequencies are deduced as

$$C_3 = (1-k)C_1, \quad \Omega_{10}^2 = kL_2^1, \tag{2.294}$$

where

$$k = \frac{1 + L_3^1 + L_3^1 L_4^2 \pm \sqrt{(1 + L_3^1 + L_3^1 L_4^2)^2 - 4L_3^1 L_4^2}}{2}. \tag{2.295}$$

In case when $l_1 = l_3$ and $l_2 = l_4$, we get a simplification $k = \dfrac{3 \pm \sqrt{5}}{2}$.

The eigenforms are given by

$$\begin{aligned} U_{10} &= 1, \\ U_{20} &= 1 - k(X_2 - B_2), \\ U_{30} &= 1 - k, \\ U_{40} &= (1-k)(1 - X_4 + B_4). \end{aligned} \tag{2.296}$$

On Figure (2.42) we can see that as the rod is subject to the mixed boundary conditions we can not separate symmetric and antisymmetric motions.

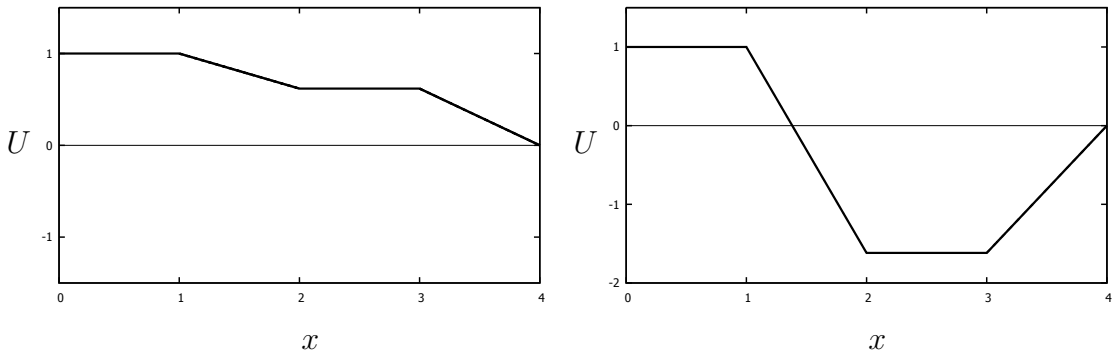

a) $k = \dfrac{3-\sqrt{5}}{2}$ b) $k = \dfrac{3+\sqrt{5}}{2}$

Figure 2.42: Displacement profiles (2.296); $l_1 = l_2 = l_3 = l_4$

2.4.2.3 A five-component rod with two "stronger" parts

As now we study a five-component rod with two "stronger" parts, it can be noted that the rod should have the "weaker" outer parts subject to the Dirichlet boundary conditions, thus,

$$\begin{aligned} \Omega_{20}^2 &= \frac{(L_1^2 + L_3^2)C_2 - L_3^2 C_4}{C_2}, \\ \Omega_{40}^2 &= \frac{(L_3^4 + L_5^4)C_4 - L_3^4 C_2}{C_4}, \end{aligned} \tag{2.297}$$

with the relation

$$\Omega_{20} = L_4^2 \Omega_{40}^2. \tag{2.298}$$

Then, the relation between constants and the leading order eigenfrequencies are followed as

$$C_4 = (1 + L_1^3 - k)C_2, \quad \Omega_{20}^2 = kL_3^2, \tag{2.299}$$

where

$$k = \frac{1 + L_1^3 + L_4^2 + L_4^2 L_5^3 \pm \sqrt{(L_4^2 L_5^3 + L_4^2 - L_1^3 - 1)^2 + 4L_4^2}}{2}. \tag{2.300}$$

Also, for the rod with $l_1 = l_3 = l_5$ and $l_2 = l_4$ we get $k = 1$ or $k = 3$.

The scaled displacement profiles are written in the form

$$U_{10} = X_1,$$

$$U_{20} = 1,$$

$$U_{30} = 1 + (L_1^3 - k)(X_3 - B_3), \tag{2.301}$$

$$U_{40} = 1 + L_1^3 - k,$$

$$U_{50} = (1 + L_1^3 - k)(1 - X_5 + B_5),$$

see Figure 2.43. Again, we can observe a symmetric motion when $k = 1$ and an antisymmetric motion when $k = 3$.

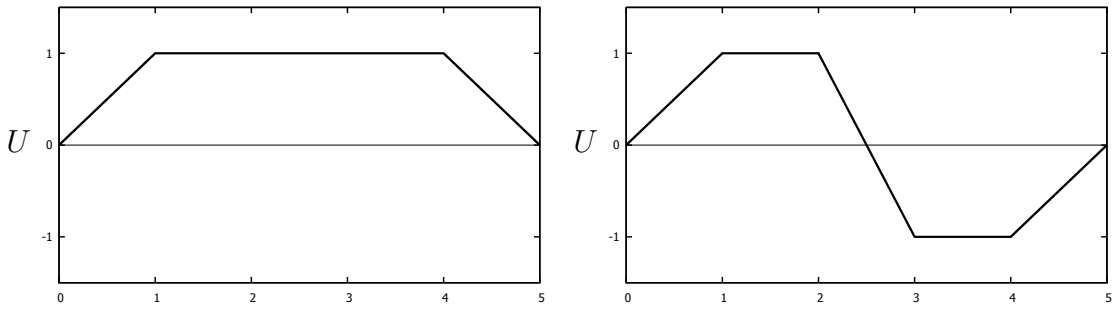

a) $k = 1$ b) $k = 3$

Figure 2.43: Displacement profiles (2.301); $l_1 = l_2 = l_3 = l_4 = l_5$

2.4.2.4 A five-component rod with three "stronger" parts

This example describes a behaviour of a five-component rod with three "stronger" parts. Thus, the rod has both ends subjected to the Neumann boundary conditions.

Then,

$$\Omega_{10}^2 = L_2^1 \frac{C_1 - C_3}{C_1},$$

$$\Omega_{30}^2 = \frac{(L_2^3 + L_4^3)C_3 - L_2^3 C_1 - L_4^3 C_5}{C_3}, \tag{2.302}$$

$$\Omega_{50}^2 = L_4^5 \frac{C_5 - C_3}{C_5},$$

with

$$\Omega_{10} = L_3^1 \Omega_{30} = L_5^1 \Omega_{50}. \tag{2.303}$$

The corresponding relations between the constants and the leading order frequency estimation are found in the form

$$C_3 = (1-k)C_1, \quad C_5 = \frac{1-k}{1 - L_2^4 L_1^5 k} C_1, \quad \Omega_{10}^2 = L_2^1 k, \tag{2.304}$$

where $k = 0$, and

$$k = \frac{L_5^1 L_4^2 + L_3^1 + L_3^1 L_4^2 + 1}{2} \pm$$

$$\pm \frac{\sqrt{(L_5^1 L_4^2 + L_3^1 + L_3^1 L_4^2 + 1)^2 - 4L_4^2(L_5^1 + L_3^1 + L_3^1 L_5^1)}}{2}. \tag{2.305}$$

Thus, for $l_1 = l_3 = l_5$ and $l_2 = l_4$ the coefficient is reduced to $k = 0$, $k = 1$, and $k = 3$.

The natural forms are derived as

$$\begin{aligned} U_{10} &= 1, \\ U_{20} &= 1 - k(X_2 - B_2), \\ U_{30} &= 1 - k, \\ U_{40} &= 1 - k + \frac{L_2^4 L_1^5 k(1-k)}{1 - L_2^4 L_1^5 k}(X_4 - B_4), \\ U_{50} &= \frac{1-k}{1 - L_2^4 L_1^5 k}, \end{aligned} \tag{2.306}$$

see Figure 2.44. Here, as the middle part is ″stronger″ and performs a rigid body behaviour, we have only a symmetric motion for each displacement profile.

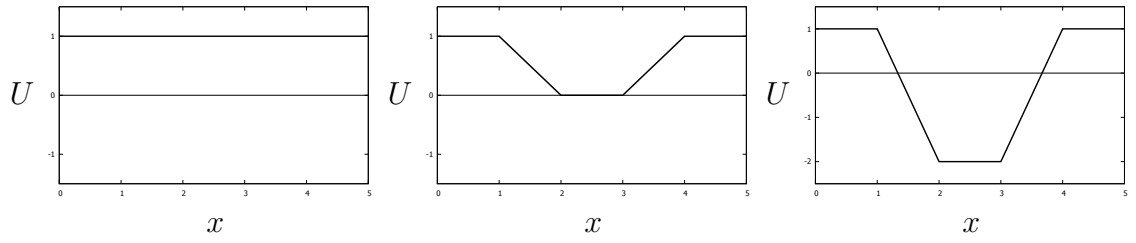

a) $k = 0$ b) $k = 1$ c) $k = 3$

Figure 2.44: Displacement profiles (2.306); $l_1 = l_2 = l_3 = l_4 = l_5$

2.4.2.5 A six-component rod with three "stronger" parts

Now, we consider a six-component rod with three "stronger" parts having free end of the "stronger" left outer part and fixed end of the "weaker" right outer part. Thus, we can write down

$$\Omega_{10}^2 = L_2^1 \frac{C_1 - C_3}{C_1},$$

$$\Omega_{30}^2 = \frac{(L_2^3 + L_4^3)C_3 - L_2^3 C_1 - L_4^3 C_5}{C_3}, \tag{2.307}$$

$$\Omega_{50}^2 = \frac{(L_4^5 + L_6^5)C_5 - L_4^5 C_3}{C_5},$$

with

$$\Omega_{10} = L_3^1 \Omega_{30} = L_5^1 \Omega_{50}. \tag{2.308}$$

The expressions (2.307) with the relations (2.308) provide us with

$$C_3 = (1-k)C_1, \quad \text{and} \quad C_5 = \frac{1-k}{1 + L_6^4 - L_2^4 L_1^5 k} C_1. \tag{2.309}$$

Also, we can derive the frequency equation for Ω_{10}^2 as

$$\Omega_{10}^6 - (L_2^1)^3 L_3^1 L_5^1 L_4^2 L_6^2 - \Omega_{10}^4 L_2^1 (L_5^1 (L_4^2 + L_6^2) + L_3^1 (1 + L_4^2) + 1) +$$

$$+ \Omega_{10}^2 (L_2^1)^2 (L_5^1 (L_4^2 + L_6^2) + L_3^1 L_4^2 + L_3^1 L_5^1 (L_4^2 + L_6^2 + L_4^2 L_6^2)) = 0. \tag{2.310}$$

We get the cubic equation, where it is possible to find a solution in the form $\Omega_{10}^2 = L_2^1 k$.

In case of $l_1 = l_3 = l_5$ and $l_2 = l_4 = l_6$ the equation (2.310) reduces to

$$\Omega_{10}^6 - 5L_2^1\Omega_{10}^4 + 6(L_2^1)^2\Omega_{10}^2 - (L_2^1)^3 = 0. \tag{2.311}$$

This equation has three distinct real roots. Thus, we can write down for the leading order frequency

$$\Omega_{10}^2 = kL_2^1, \quad \text{where} \quad k = 0.1981;\ 1.555;\ 3.247, \tag{2.312}$$

where k is calculated numerically.

We find the scaled displacement profiles in the form

$$\begin{aligned} U_{10} &= 1, \\ U_{20} &= 1 - k(X_2 - B_2), \\ U_{30} &= 1 - k, \\ U_{40} &= 1 - k - \frac{(1-k)(L_6^4 - L_2^4 L_1^5 k)}{1 + L_6^4 - L_2^4 L_1^5 k})(X_4 - B_4), \\ U_{50} &= \frac{1-k}{1 + L_6^4 - L_2^4 L_1^5 k}, \\ U_{60} &= \frac{1-k}{1 + L_6^4 - L_2^4 L_1^5 k}(1 - X_6 + B_6), \end{aligned} \tag{2.313}$$

see Figure 2.45. As the rod has mixed boundary conditions there are no symmetric or asymmetric vibrations.

2.4.2.6 A seven-component rod with three "stronger" parts

Finally, we study a rod with three "stronger" components out of seven. Therefore, both outer parts are "weaker" and the rod is subject to the Dirichlet boundary

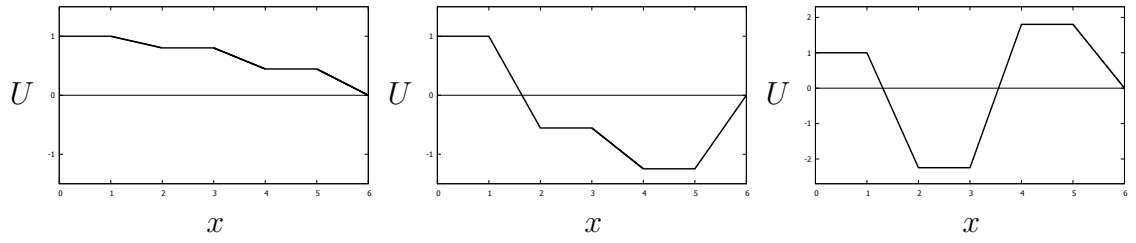

a) $k = 0.1981$ b) $k = 1.555$ c) $k = 3.247$

Figure 2.45: Displacement profiles (2.313); $l_1 = l_2 = l_3 = l_4 = l_5 = l_6$

conditions. We can write down for the frequencies of the ˝stronger˝ components

$$\Omega_{20}^2 = \frac{(L_1^2 + L_3^2)C_2 - L_3^2 C_4}{C_2},$$

$$\Omega_{40}^2 = \frac{(L_3^4 + L_5^4)C_4 - L_3^4 C_2 - L_5^4 C_6}{C_4}, \tag{2.314}$$

$$\Omega_{60}^2 = \frac{(L_5^6 + L_7^6)C_6 - L_5^6 C_4}{C_6},$$

with the relations

$$\Omega_{20} = L_4^1 \Omega_{40} = L_6^1 \Omega_{60}. \tag{2.315}$$

Then, the constants are connected as

$$C_4 = (1 + L_1^3 - k)C_2, \quad \text{and} \quad C_6 = \frac{1 + L_1^3 - k}{1 + L_7^5 - L_3^5 L_2^6 k} C_2, \tag{2.316}$$

with the frequency equation for Ω_{20}^2 deduced in the from

$$\Omega_{20}^6 - \Omega_{20}^4 L_3^2 (L_4^2 + L_4^2 L_5^3 + L_5^3 L_6^2 + L_6^2 L_7^3 + 1 + L_1^3) +$$

$$+ \Omega_{20}^2 (L_3^2)^2 (L_4^2 (L_1^3 + L_5^3 + L_1^3 L_5^3) + L_6^2 (L_5^3 + L_7^3 + L_1^3 L_5^3 + L_1^3 L_7^3) + L_4^2 L_6^2 (L_5^3 + L_7^3 + L_5^3 L_7^3)) -$$

$$- (L_3^2)^3 L_4^2 L_6^2 (L_1^3 L_5^3 + L_1^3 L_7^3 + L_5^3 L_7^3 + L_1^3 L_5^3 L_7^3) = 0. \tag{2.317}$$

The cubic equation (2.317) has real roots that could be derived in the form $\Omega_{20}^2 = L_3^2 k$.

If $l_1 = l_3 = l_5 = l_7$ and $l_2 = l_4 = l_6$ we can simplify (2.317) as

$$\Omega_{20}^6 - 6L_3^2\Omega_{20}^4 + 10(L_3^2)^2\Omega_{20}^2 - 4(L_3^2)^3 = 0. \tag{2.318}$$

This equation has three distinct real roots, that are given by

$$\Omega_{10}^2 = kL_3^2, \quad \text{where} \quad k = 0.5858;\ 2;\ 3.4142, \tag{2.319}$$

where k is calculated numerically.

The natural forms follow as

$$\begin{gathered}
U_{10} = X_1, \\
U_{20} = 1, \\
U_{30} = 1 + (L_1^3 - k)(X_3 - B_3), \\
U_{40} = 1 + L_1^3 - k, \\
U_{50} = 1 + L_1^3 - k - \frac{(1 + L_1^3 - k)(L_7^5 - L_3^5 L_2^6 k)}{1 + L_7^5 - L_3^5 L_2^6 k}(X_5 - B_5), \\
U_{60} = \frac{1 + L_1^3 - k}{1 + L_7^5 - L_3^5 L_2^6 k}, \\
U_{70} = \frac{1 + L_1^3 - k}{1 + L_7^5 - L_3^5 L_2^6 k}(1 - X_7 + B_7).
\end{gathered} \tag{2.320}$$

As the middle part of the rod is ″stronger″ we get only symmetric vibrations for the all scaled displacement profiles, see Figure 2.46.

We considered several cases of low-frequency vibrations of multi-component rods. In each case we provided the displacement profiles and expressions for the sought-for frequencies that depend on the number of the rod components and the boundary conditions.

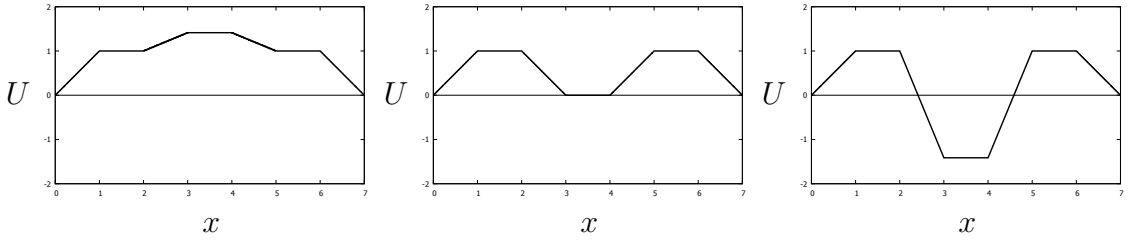

a) $k = 0.5858$ b) $k = 2$ c) $k = 3.4142$

Figure 2.46: Displacement profiles (2.320); $l_1 = l_2 = l_3 = l_4 = l_5 = l_6 = l_7$

3 Antiplane shear motion of a composite elastic circular cylinder

Antiplane shear motion of a composite elastic circular cylinder with an annular cross section is considered in this chapter focusing on low-frequency vibrations. First, we review the solution for a homogeneous single-component body. We assume two types of boundary conditions, namely free and fixed boundary. Next, we study antiplane shear motion of a two-component piecewise-homogeneous cylinder. For all considered problems we introduce appropriate scaling for the frequencies and the space variables and derive the sought-for frequency equations and the displacement profiles. The global low-frequency behaviour is studied and the general conditions allowing global low-frequency regimes are obtained. Antiplane shear motion of a two-component cylinder with variable material parameters is analysed for the low frequencies using a perturbation technique. Finally, a general asymptotic model for a circular cylinder with an arbitrary number of components is presented.

3.1 A homogeneous circular cylinder

Let us review antiplane shear motion of an elastic homogeneous circular cylinder. The body with the free or fixed boundary is specified by $r \leq l$. The axis Or is chosen such that the origin O is placed in the geometrical center of the cross section, see Figure 3.1.

The equation of motion is formulated as

$$r^2 \frac{d^2u}{dr^2} + r\frac{du}{dr} + (\omega^2 r^2 c^{-2} - m^2)u = 0, \tag{3.1}$$

where u is the out-of-plane displacement, ω is the vibration frequency, and $c = \sqrt{\mu/\rho}$ is the associated shear wave speed, where μ defines the Lamé shear modulus, and ρ is the density. Further we consider only $m = 0$.

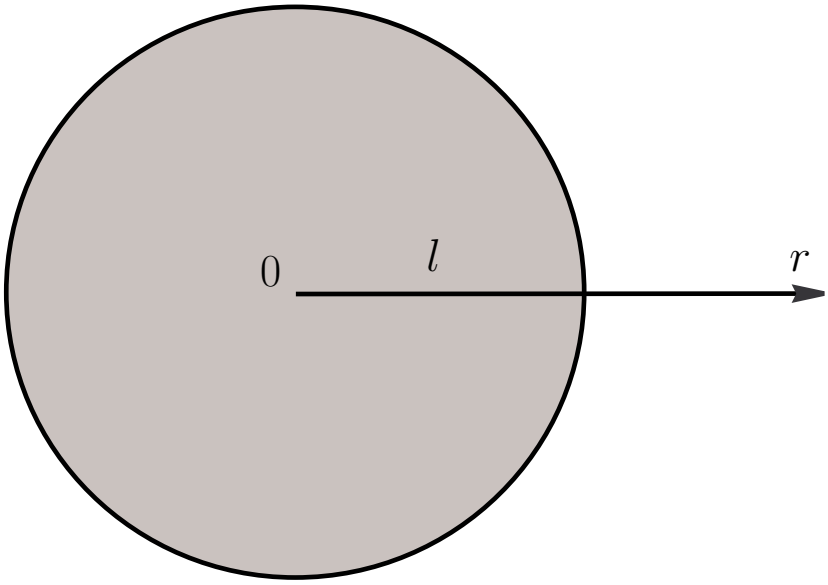

Figure 3.1: The cross section of a homogeneous circular cylinder

Two types of boundary conditions are allowed, namely fixed boundary

$$u|_{r=l} = 0, \tag{3.2}$$

and free boundary

$$\left.\frac{du}{dr}\right|_{r=l} = 0. \tag{3.3}$$

To solve the problem we present frequency and radial variable in dimensionless form as

$$\Omega = \frac{\omega l}{c}, \tag{3.4}$$

and

$$R = \frac{r}{l}. \tag{3.5}$$

Then, the equation of motion (3.1) can be transformed into the dimensionless form as

$$R\frac{d^2u}{dR^2} + \frac{du}{dR} + \Omega^2 Ru = 0, \tag{3.6}$$

with the boundary conditions (3.2) and (3.3) reformulated as

$$u|_{R=1} = 0, \tag{3.7}$$

and

$$\left.\frac{du}{dR}\right|_{R=1} = 0, \tag{3.8}$$

respectively.

The displacement can be found as

$$u = AJ_0(\Omega R), \tag{3.9}$$

where A is a constant and $J_m(x)$ is Bessel function of the first kind of order m, for details on properties of Bessel functions see e.g. Temme (2011). Substituting (3.9) into the boundary conditions (3.7) and (3.8), we arrive at the frequency equations

$$J_0(\Omega) = 0, \tag{3.10}$$

and

$$J_1(\Omega) = 0, \tag{3.11}$$

for the body with the fixed and free boundary, respectively.

3.2 A two-component piecewise-homogeneous circular cylinder

Antiplane shear motion of an elastic circular cylinder with annular cross section and two homogeneous domains is considered in this section.

3.2.1 Statement of the problem

Here we assume a finite two-component body with the free or fixed boundary of the outer domain and continuity of stresses and displacements between the domains. The origin O of axis Or is placed in the geometrical center of the inner domain. Then, the inner domain is placed between $0 \leq r \leq l_1$ and the outer one is located between $l_1 \leq r \leq l_1 + l_2$, see Figure 3.2.

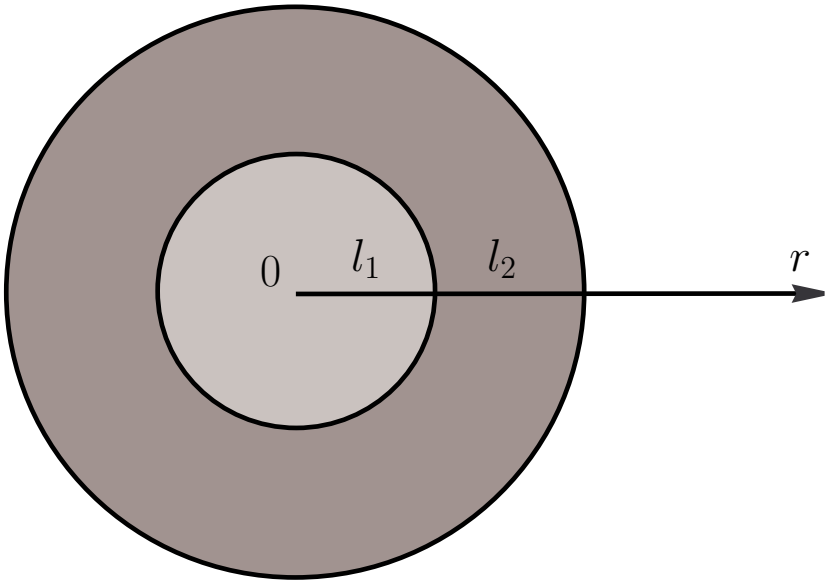

Figure 3.2: The cross section of a two-component circular cylinder

The equations of motion are provided as

$$r^2 \frac{d^2 u_i}{dr^2} + r \frac{du_i}{dr} + \omega^2 r^2 c_i^{-2} u_i = 0, \qquad i = 1, 2, \tag{3.12}$$

where u_i are the out-of-plane displacements, ω is the vibration frequency, and $c_i = \sqrt{\mu_i/\rho_i}$ are the shear wave speeds, with μ_i denote the Lamé shear moduli, and ρ_i are the densities. The indices 1 and 2 denote the inner and outer domains, respectively.

To analyse the problem further we need to present scaled frequencies and dimensionless radial variables

$$\Omega_i = \frac{\omega l_i}{c_i}, \quad R_i = \frac{r}{l_i}, \qquad i = 1, 2, \tag{3.13}$$

and transform parameters to the dimensionless form as

$$\mu = \frac{\mu_1}{\mu_2}, \qquad \rho = \frac{\rho_1}{\rho_2}, \qquad c = \frac{c_1}{c_2}, \qquad l = \frac{l_1}{l_2}. \tag{3.14}$$

Thus, the equations of motion (3.12) can be reformulated in the dimensionless form as

$$R_i \frac{d^2 u_i}{dR_i^2} + \frac{du_i}{dR_i} + \Omega_i^2 R_i u_i = 0, \qquad i = 1, 2. \tag{3.15}$$

The continuity conditions on displacements and stresses are formulated as

$$u_1|_{R_1=1} = u_2|_{R_2=l}\,, \tag{3.16}$$

and

$$\mu \frac{du_1}{dR_1}\bigg|_{R_1=1} = \frac{du_2}{dR_2}\bigg|_{R_2=l}, \tag{3.17}$$

respectively. The outer boundary can be fixed

$$u_2|_{R_2=l+1} = 0, \tag{3.18}$$

or free

$$\frac{du_2}{dR_2}\bigg|_{R_2=l+1} = 0. \tag{3.19}$$

In view of the equations (3.15), we employ for the displacements

$$\begin{aligned} u_1 &= AJ_0(\Omega_1 R_1), && 0 \le R_1 \le 1, \\ u_2 &= BJ_0(\Omega_2 R_2) + CY_0(\Omega_2 R_2), && l \le R_2 \le l+1, \end{aligned} \tag{3.20}$$

where $Y_m(x)$ is Bessel function of the second kind of order m.

3.2.2 Fixed boundary

The displacement profile (3.20) substituted into conditions (3.16), (3.17), and (3.18) leads to a set of linear algebraic equations

$$\begin{aligned} &AJ_0(\Omega_1) - BJ_0(\Omega_2 l) - CY_0(\Omega_2 l) = 0, \\ &A\frac{\mu}{c}J_1(\Omega_1) - BJ_1(\Omega_2 l) - CY_1(\Omega_2 l) = 0, \\ &BJ_0(\Omega_2(l+1)) + CY_0(\Omega_2(l+1)) = 0. \end{aligned} \tag{3.21}$$

The solvability of the latter gives the frequency equation

$$\begin{aligned} &\mu J_1(\Omega_1)\big[J_0(\Omega_2 l)Y_0(\Omega_2(l+1)) - Y_0(\Omega_2 l)J_0(\Omega_2(l+1))\big] - \\ &- cJ_0(\Omega_1)\big[J_1(\Omega_2 l)Y_0(\Omega_2(l+1)) - Y_1(\Omega_2 l)J_0(\Omega_2(l+1))\big] = 0. \end{aligned} \tag{3.22}$$

Then, using (3.21), we can present the scaled displacement profile as

$$\begin{aligned} U_1 &= J_0(\Omega_1 R_1), \\ U_2 &= J_0(\Omega_1)\frac{J_0(\Omega_2 R_2)Y_0(\Omega_2(l+1)) - Y_0(\Omega_2 R_2)J_0(\Omega_2(l+1))}{J_0(\Omega_2 l)Y_0(\Omega_2(l+1)) - Y_0(\Omega_2 l)J_0(\Omega_2(l+1))}. \end{aligned} \tag{3.23}$$

In case of $\Omega_1 \ll 1$ and $\Omega_2 \ll 1$ the frequency equation (3.22) can be simplified and the following approximations for the frequencies can be obtained

$$\Omega_1^2 = \frac{2\rho\mu^{-1}}{(\rho-1)\ln(l^{-1}+1) - 1}, \tag{3.24}$$

and

$$\Omega_2^2 = \frac{2l^{-2}}{(\rho-1)\ln(l^{-1}+1) - 1}. \tag{3.25}$$

Formulae (3.24) and (3.25) combined with $\Omega_1 \ll 1$ and $\Omega_2 \ll 1$ imply the following conditions on the parameters

$$\begin{aligned} &l \ll 1, \qquad \rho \gg \frac{l^{-2}}{\ln l^{-1}}, \qquad \mu \gg \frac{1}{\ln l^{-1}}, \\ &l \sim 1, \qquad \rho \gg 1, \qquad \mu \gg 1, \\ &l \gg 1, \qquad \rho \gg l, \qquad \mu \gg l. \end{aligned} \tag{3.26}$$

It can be seen that $\mu \gg l$ and $\rho \gg l$ for all possible values of l, i.e. $l \ll 1$, $l \sim 1$ and $l \gg 1$. Thus, (3.24) and (3.25) can be reduced to

$$\Omega_1^2 = \frac{\mu^{-1}}{\ln(l^{-1}+1)}, \tag{3.27}$$

and

$$\Omega_2^2 = \frac{l^{-2}\rho^{-1}}{\ln(l^{-1}+1)}. \tag{3.28}$$

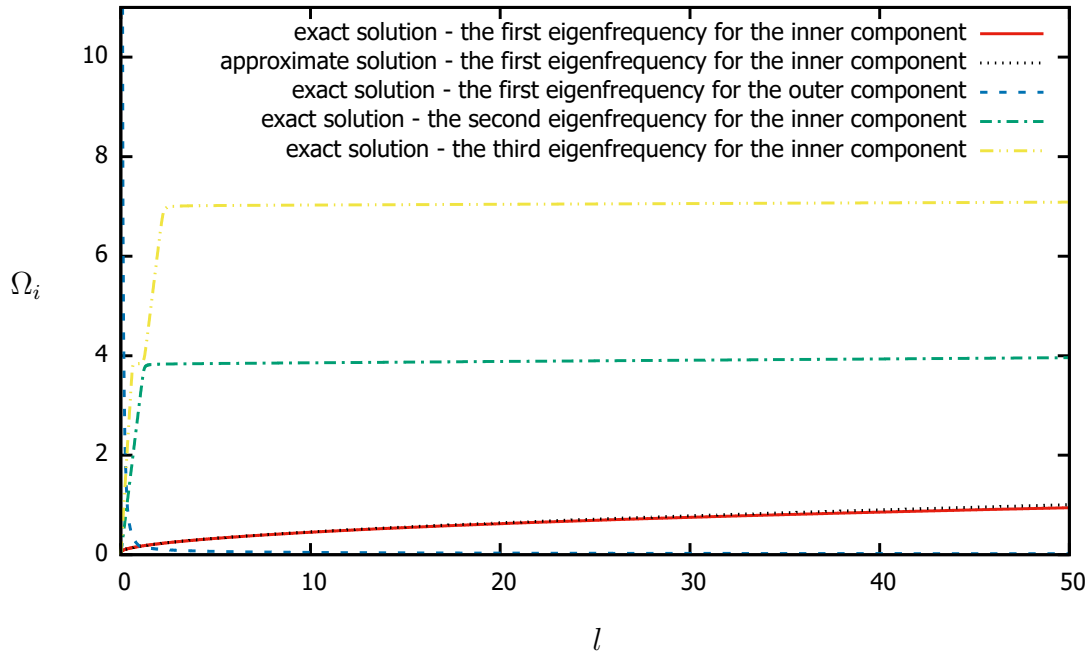

Figure 3.3: Frequency vs relative thickness l for antiplane shear motion of a two-component circular cylinder; $\mu = 100$, $\rho = 100$

Figure 3.3 shows scaled frequencies depending on the relative thickness l with known material properties μ and ρ. According to the conditions on parameters (3.26) we have $l \ll \mu$ and $l \ll \rho$ relations. It can be seen that if l is much smaller than μ and ρ then Ω_1 and Ω_2 are both small.

On Figure 3.3 the decreasing curve of the first scaled eigenfrequency for the outer domain and the increasing curves for the first three scaled eigenfrequencies of the inner domain are defined by (3.22) and represent exact solutions. There are also approximation (3.27) of the first eigenfrequency for the inner domain. We can observe good agreement between exact and approximate solutions. It may also be noticed that distance between the first and second eigenfrequencies is substantial. This replicates behaviour of a composite rod with high-contrast parameters, see Figure 2.3.

We arrive at the following approximate profile of the eigenform

$$\begin{aligned} U_1 &= 1, \\ U_2 &= \frac{\ln R_2 - \ln(l+1)}{\ln l - \ln(l+1)}. \end{aligned} \tag{3.29}$$

Figure 3.4 contains the scaled displacement profile (3.29) calculated at $l_1 = l_2 = 1$, with the overall axisymmetric plot and its axial cross section at $y = 0$. It is worth noting that the displacement variation of the softer domain is no longer polynomial, as was observed previously in 1D case for the rod with fixed ends, see Figure 2.18.

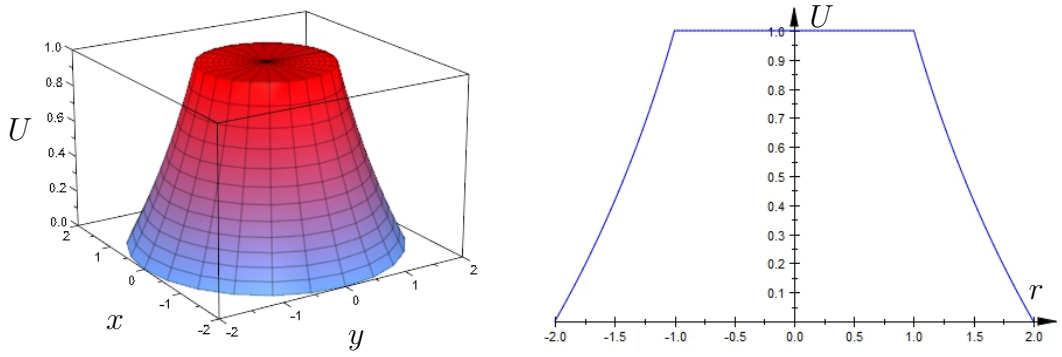

a) 3D b) 2D

Figure 3.4: Displacement profile (3.29); $l_1 = l_2$

3.2.3 Free boundary

Additionally, let us present the exact solution for the free outer boundary. Substituting (3.20) into conditions (3.16), (3.17), and (3.19), we have

$$\begin{gathered} AJ_0(\Omega_1) - BJ_0(\Omega_2 l) - CY_0(\Omega_2 l) = 0, \\ \Omega_2 \left[A\frac{\mu}{c} J_1(\Omega_1) - BJ_1(\Omega_2 l) - CY_1(\Omega_2 l) \right] = 0, \\ \Omega_2 \big[BJ_1(\Omega_2(l+1)) + CY_1(\Omega_2(l+1)) \big] = 0. \end{gathered} \tag{3.30}$$

Then, from the solvability of (3.30) we deduce the frequency equation

$$\begin{aligned} &\mu J_1(\Omega_1)\big[J_0(\Omega_2 l)Y_1(\Omega_2(l+1)) - Y_0(\Omega_2 l)J_1(\Omega_2(l+1))\big] - \\ &- cJ_0(\Omega_1)\big[J_1(\Omega_2 l)Y_1(\Omega_2(l+1)) - Y_1(\Omega_2 l)J_1(\Omega_2(l+1))\big] = 0. \end{aligned} \tag{3.31}$$

In view of (3.30), the scaled displacement profile takes the form

$$\begin{aligned} U_1 &= J_0(\Omega_1 R_1), \\ U_2 &= J_0(\Omega_1)\frac{J_0(\Omega_2 R_2)Y_1(\Omega_2(l+1)) - Y_0(\Omega_2 R_2)J_1(\Omega_2(l+1))}{J_0(\Omega_2 l)Y_1(\Omega_2(l+1)) - Y_0(\Omega_2 l)J_1(\Omega_2(l+1))}. \end{aligned} \tag{3.32}$$

Another solution for this system corresponding to the rigid body motion is

$$\Omega_1 = \Omega_2 = 0, \tag{3.33}$$

with $C = 0$ and $A = B$. Then, the eigenform is

$$U_1 = U_2 = 1. \tag{3.34}$$

In case of $\Omega_1 \ll 1$ and $\Omega_2 \ll 1$, the frequency equation (3.31) implies

$$\Omega_1^2 = \frac{4\rho(\rho - 1 - (l^{-1}+1)^2)}{\mu(l^{-1}+1)^2(\rho-1)(\ln(l^{-1}+1) - 1)}, \tag{3.35}$$

and

$$\Omega_2^2 = \frac{4(\rho - 1 - (l^{-1}+1)^2)}{(l+1)^2(\rho-1)(\ln(l^{-1}+1) - 1)}. \tag{3.36}$$

It may be observed that the obtained results (3.35) and (3.36) are outside of the considered low-frequency region $0 \le \Omega_i \ll 1$, $i = 1, 2$. Thus, there is no non-zero low natural frequency in this case.

3.3 A two-component circular cylinder with variable material parameters

In this section we study antiplane shear motion of a circular cylinder having two inhomogeneous domains.

3.3.1 Statement of the problem

In case when a cylinder having two inhomogeneous domains, the material parameters are dependent on the variable and are defined in the form

$$\mu_i = \mu_i^* \tilde{\mu}_i(R_i), \qquad \rho_i = \rho_i^* \tilde{\rho}_i(R_i), \qquad c_i = c_i^* \tilde{c}_i(R_i), \qquad i = 1, 2, \tag{3.37}$$

where μ_i^*, ρ_i^* and c_i^* are typical values of the associated quantities. Then, the dimensionless parameters along with the scaled frequencies are defined with use of material typical values as

$$\mu = \frac{\mu_1^*}{\mu_2^*}, \qquad \rho = \frac{\rho_1^*}{\rho_2^*}, \qquad c = \frac{c_1^*}{c_2^*}, \tag{3.38}$$

and

$$\Omega_i = \frac{\omega l_i}{c_i^*}, \qquad i = 1, 2. \tag{3.39}$$

Therefore, the dimensionless equations of motion can be rewritten as

$$R_i \frac{d}{dR_i}\left(\tilde{\mu}_i(R_i)\frac{du_i}{dR_i}\right) + \tilde{\mu}_i(R_i)\frac{du_i}{dR_i} + \tilde{\rho}_i(R_i)\Omega_i^2 u_i = 0, \qquad i = 1, 2. \tag{3.40}$$

The continuity conditions at the interface are given by

$$u_1|_{R_1=1} = u_2|_{R_2=l}\,, \tag{3.41}$$

and

$$\frac{\mu}{l}\tilde{\mu}_1(R_1)\frac{du_1}{dR_1}\bigg|_{R_1=1} = \tilde{\mu}_2(R_2)\,\frac{du_2}{dR_2}\bigg|_{R_2=l}. \tag{3.42}$$

The outer boundary is assumed to be fixed

$$u_2|_{R_2=l+1} = 0, \tag{3.43}$$

or free

$$\left.\frac{du_2}{dR_2}\right|_{R_2=l+1} = 0. \tag{3.44}$$

We employ a perturbation technique for the further analysis, starting with consideration of the global low-frequency regime of the form $\Omega_1^2 \sim \Omega_2^2 \sim \epsilon$ with the small parameter $\epsilon \ll 1$. Therefore, we expand the frequencies and the displacements as asymptotic series

$$\Omega_i^2 = \epsilon(\Omega_{i0}^2 + \epsilon\Omega_{i1}^2 + \epsilon^2\Omega_{i2}^2 + \ldots), \tag{3.45}$$

and

$$u_i = u_{i0} + \epsilon u_{i1} + \epsilon^2 u_{i2} + \ldots \ , \tag{3.46}$$

respectively. The small parameter ϵ is linked to the contrast properties of the domains. If $\epsilon = \dfrac{l}{\mu}$, we talk about the "stronger" inner domain, whether if $\epsilon = \dfrac{\mu}{l}$, it is associated with the "stronger" outer domain.

3.3.2 "Stronger" inner domain

We start with the analysis of a body with a "stronger" inner domain, when $\epsilon = \dfrac{l}{\mu}$.

3.3.2.1 Fixed boundary

Let us first consider a body with a "stronger" inner domain and a fixed outer boundary.

We start our analysis with the boundary value problem for the displacement of the "stronger" inner domain ($i = 1$). On substituting the expansion (3.46) into the dimensionless equation of motion (3.40) at leading order ϵ^0, we have

$$R_1\frac{d}{dR_1}\left(\tilde{\mu}_1(R_1)\frac{du_{10}}{dR_1}\right) + \tilde{\mu}_1(R_1)\frac{du_{10}}{dR_1} = 0, \tag{3.47}$$

subject to

$$\left.\frac{du_{10}}{dR_1}\right|_{R_1=1} = 0. \tag{3.48}$$

The equation (3.47) results in

$$\frac{du_{10}}{dR_1} = \frac{A_1}{R_1\tilde{\mu}_1(R_1)}, \tag{3.49}$$

where A_1 is a constant. From (3.48) we can conclude that $A_1 = 0$ and the inner displacement takes the form

$$u_{10} = C_1, \tag{3.50}$$

where C_1 is a constant.

Next, we can continue with consideration of the displacement of the outer domain ($i = 2$). The leading order boundary value problem is given by

$$R_2\frac{d}{dR_2}\left(\tilde{\mu}_2(R_2)\frac{du_{20}}{dR_2}\right) + \tilde{\mu}_2(R_2)\frac{du_{20}}{dR_2} = 0, \tag{3.51}$$

subject to

$$\begin{aligned} u_{20}|_{R_2=l} &= C_1, \\ u_{20}|_{R_2=l+1} &= 0. \end{aligned} \tag{3.52}$$

From (3.51) we deduce

$$\frac{du_{20}}{dR_2} = \frac{A_2}{R_2\tilde{\mu}_2(R_2)}, \tag{3.53}$$

and

$$u_{20} = C_2 + A_2\int_l^{R_2}\frac{1}{R_2\tilde{\mu}_2(R_2)}dR_2. \tag{3.54}$$

Thus, using the conditions (3.52), we can obtain the outer displacement in the form

$$u_{20} = C - \frac{C}{\tau_2}\int_l^{R_2}\frac{1}{R_2\tilde{\mu}_2(R_2)}dR_2, \tag{3.55}$$

where $C = C_1 = C_2$ and

$$\tau_2 = \int_l^{l+1}\frac{1}{R_2\tilde{\mu}_2(R_2)}dR_2. \tag{3.56}$$

At next order ϵ the analysis of the problem for the ‶stronger″ inner domain gives the estimates for frequencies. Then, the equation of motion for the inner domain is derived in the form

$$R_1\frac{d}{dR_1}\left(\tilde{\mu}_1(R_1)\frac{du_{11}}{dR_1}\right) + \tilde{\mu}_1(R_1)\frac{du_{11}}{dR_1} + \tilde{\rho}_1(R_1)\Omega_{10}^2 u_{10} = 0, \tag{3.57}$$

with the boundary conditions written as

$$\tilde{\mu}_1(R_1)\left.\frac{du_{11}}{dR_1}\right|_{R_1=1} = \tilde{\mu}_2(R_2)\left.\frac{du_{20}}{dR_2}\right|_{R_2=l}, \tag{3.58}$$

where, in a view of (3.55),

$$\left.\frac{du_{20}}{dR_2}\right|_{R_2=l} = -\frac{C}{l\tau_2\tilde{\mu}_2(l)}. \tag{3.59}$$

Integrating (3.57) over R_1 $(0 \leq R_1 \leq 1)$, we obtain the expression

$$R_1\tilde{\mu}_1(R_1)\left.\frac{du_{11}}{dR_1}\right|_{R_1=0}^{R_1=1} = -C\Omega_{10}^2 r_1, \tag{3.60}$$

where

$$r_1 = \int_0^1 \tilde{\rho}_1(R_1)dR_1. \tag{3.61}$$

Next, employing the condition (3.58), we find the estimate for Ω_{10}^2 as

$$\Omega_{10}^2 = \frac{l^{-1}}{\tau_2 r_1}. \tag{3.62}$$

Thus, we can infer that

$$\Omega_1^2 = \frac{\mu^{-1}}{\tau_2 r_1}. \tag{3.63}$$

If the material parameters are constant (3.63) can be simplified to a form

$$\Omega_1^2 = \frac{\mu^{-1}}{\ln(l^{-1}+1)}, \tag{3.64}$$

which correlates with the result (3.27) from the previous section.

3.3.2.2 Free boundary

Next, a body with a free outer boundary and a ˝stronger˝ inner domain is analysed.

The ϵ^0 boundary value problem for the inner domain is formulated similarly to (3.47)-(3.48) leading to

$$u_{10} = C. \tag{3.65}$$

At leading order for the outer displacement we infer

$$R_2\frac{d}{dR_2}\left(\tilde{\mu}_2(R_2)\frac{du_{20}}{dR_2}\right)+\tilde{\mu}_2(R_2)\frac{du_{20}}{dR_2}=0, \tag{3.66}$$

subject to

$$\begin{gathered} u_{20}|_{R_2=l}=C, \\ \left.\frac{u_{20}}{dR_2}\right|_{R_2=l+1}=0. \end{gathered} \tag{3.67}$$

This provides us with the displacement profile in the form

$$u_{20}=C. \tag{3.68}$$

We continue to analyse problem at next order ϵ for the ‶stronger″ inner domain to obtain the estimates for frequencies. The boundary value problem is written as

$$R_1\frac{d}{dR_1}\left(\tilde{\mu}_1(R_1)\frac{du_{11}}{dR_1}\right)+\tilde{\mu}_1(R_1)\frac{du_{11}}{dR_1}+\tilde{\rho}_1(R_1)\Omega_{10}^2u_{10}=0, \tag{3.69}$$

subject to

$$\tilde{\mu}_1(R_1)\left.\frac{du_{11}}{dR_1}\right|_{R_1=1}=\tilde{\mu}_2(R_2)\left.\frac{u_{20}}{dR_2}\right|_{R_2=l}, \tag{3.70}$$

where, according to (3.68),

$$\left.\frac{u_{20}}{dR_2}\right|_{R_2=l}=0. \tag{3.71}$$

Therefore, employing the condition (3.70), we derive the expression for the sought-for frequency as $\Omega_{10}^2=0$, which together with the displacement profile corresponds to rigid motions of a body with free face.

3.3.3 ‶Stronger″ outer domain

Consider now low-frequency vibrations of a body with a ‶stronger″ outer domain, which imply $\epsilon=\dfrac{\mu}{l}$.

3.3.3.1 Fixed boundary

A body with a "stronger" outer domain and a fixed boundary is studied in this section.

Now, we first consider the displacement of the "stronger" outer domain ($i = 2$). Thus, the leading order boundary value problem is taken as

$$R_2 \frac{d}{dR_2}\left(\tilde{\mu}_2(R_2)\frac{du_{20}}{dR_2}\right) + \tilde{\mu}_2(R_2)\frac{du_{20}}{dR_2} = 0, \tag{3.72}$$

subject to

$$\begin{aligned} \left.\frac{u_{20}}{dR_2}\right|_{R_2=l} &= 0, \\ u_{20}|_{R_2=l+1} &= 0. \end{aligned} \tag{3.73}$$

The resulting displacement profile is given by

$$u_{20} = 0. \tag{3.74}$$

Next, we proceed with the inner displacement, writing down the boundary value problem as

$$R_1 \frac{d}{dR_1}\left(\tilde{\mu}_1(R_1)\frac{du_{10}}{dR_1}\right) + \tilde{\mu}_1(R_1)\frac{du_{10}}{dR_1} = 0, \tag{3.75}$$

subject to

$$u_{10}|_{R_1=1} = 0. \tag{3.76}$$

The equation (3.75) together with the boundary condition (3.76) leads to

$$u_{10} = 0. \tag{3.77}$$

We can infer that a body with a "stronger" outer domain and a fixed face does not have low eigenfrequencies.

3.3.3.2 Free boundary

Finally, we consider a body with a "stronger" outer domain and a free boundary.

In this case the leading order boundary value problem for the outer domain takes the form

$$R_2\frac{d}{dR_2}\left(\tilde{\mu}_2(R_2)\frac{du_{20}}{dR_2}\right)+\tilde{\mu}_2(R_2)\frac{du_{20}}{dR_2}=0, \tag{3.78}$$

subject to

$$\begin{aligned}\left.\frac{u_{20}}{dR_2}\right|_{R_2=l}&=0,\\ \left.\frac{u_{20}}{dR_2}\right|_{R_2=l+1}&=0,\end{aligned} \tag{3.79}$$

which results in

$$u_{20}=C. \tag{3.80}$$

For the inner displacement the leading order equation of motion is formulated as

$$R_1\frac{d}{dR_1}\left(\tilde{\mu}_1(R_1)\frac{du_{10}}{dR_1}\right)+\tilde{\mu}_1(R_1)\frac{du_{10}}{dR_1}=0, \tag{3.81}$$

subject to

$$u_{10}|_{R_1=1}=C. \tag{3.82}$$

Thus, we get the uniform displacement of the inner domain as well

$$u_{10}=C. \tag{3.83}$$

To deduce the expression for the sought-for frequency we need to consider the boundary value problem for the "stronger" domain at next order. Therefore, at order ϵ the equation of motion for the outer domain is given by

$$R_2\frac{d}{dR_2}\left(\tilde{\mu}_2(R_2)\frac{du_{21}}{dR_2}\right)+\tilde{\mu}_2(R_2)\frac{du_{21}}{dR_2}+\tilde{\rho}_2(R_2)\Omega_{20}^2u_{20}=0, \tag{3.84}$$

subject to

$$\begin{aligned}\tilde{\mu}_2(R_2)\left.\frac{du_{21}}{dR_2}\right|_{R_2=l}&=\tilde{\mu}_1(R_1)\left.\frac{du_{10}}{dR_1}\right|_{R_1=1},\\ \left.\frac{du_{21}}{dR_2}\right|_{R_2=l+1}&=0,\end{aligned} \tag{3.85}$$

where, due to (3.83),

$$\left.\frac{du_{10}}{dR_1}\right|_{R_1=1} = 0. \tag{3.86}$$

Integrating (3.84) over R_2 ($l \le R_2 \le l+1$), we obtain the expression

$$R_2\tilde{\mu}_2(R_2)\left.\frac{du_{21}}{dR_2}\right|_{R_2=l}^{R_2=l+1} = -C\Omega_{20}^2 r_2, \tag{3.87}$$

where

$$r_2 = \int_l^{l+1} \tilde{\rho}_2(R_2)dR_2. \tag{3.88}$$

Substituting the conditions (3.85) into (3.87), we find the leading order estimate for Ω_2^2 as

$$\Omega_{20}^2 = 0. \tag{3.89}$$

The uniform displacement profile together with the zero eigenfrequency agrees with previous results and describes rigid motions of a body with free boundary.

3.4 A multi-component circular cylinder

Finally, an asymptotic model of low-frequency vibrations for a piecewise-homogeneous multi-component hollow circular cylinder with an annular cross section is developed in this section.

3.4.1 Statement of the problem

Consider a hollow circular cylinder composed of two materials having an annular cross-section with finite n number of domains of thickness l_i. The body has a periodic structure, such that the ″stronger″ domains alternate the ″weaker″ domains, see Figure 3.5. The origin O of axis Or is set in the middle of the inner hole. Continuity conditions are assumed between the domains. An outer domain has a free boundary if it is ″weaker″ or a fixed boundary in case if it is ″stronger″ .

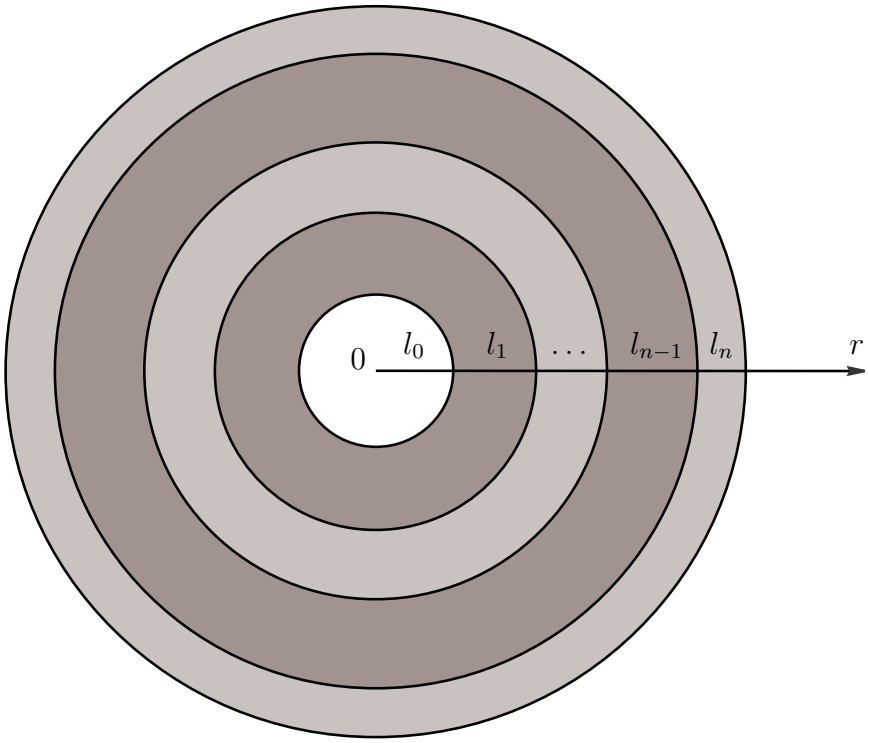

Figure 3.5: The cross section of a multi-component circular cylinder

The equations of motion are written in the form

$$R_i \frac{d^2 u_i}{dR_i^2} + \frac{du_i}{dR_i} + \Omega_i^2 R_i u_i = 0, \qquad i = 1, 2, \ldots, n. \tag{3.90}$$

We use dimensionless quantities

$$B_i = \frac{l_0 + \ldots + l_{i-1}}{l_i}, \tag{3.91}$$

defined such that

$$B_i \leq R_i \leq B_i + 1, \qquad i = 1, 2, \ldots, n. \tag{3.92}$$

The continuity conditions are given by

$$u_i|_{R_i = B_i + 1} = u_{i+1}|_{R_{i+1} = B_{i+1}}, \tag{3.93}$$

and

$$\left.\frac{du_i}{dR_i}\right|_{R_i=B_i+1} = L^i_{i+1}\frac{\mu_2}{\mu_1}\left.\frac{du_{i+1}}{dR_{i+1}}\right|_{X_{i+1}=B_{i+1}}, \tag{3.94}$$

where $i = 1, 2, \ldots, n-1$, and $L^k_j = l_k/l_j$.

We consider either free boundaries, i.e.

$$\begin{aligned} \left.\frac{du_1}{dR_1}\right|_{R_1=B_1} &= 0, \\ \left.\frac{du_n}{dR_n}\right|_{R_n=B_n+1} &= 0, \end{aligned} \tag{3.95}$$

or fixed boundaries, i.e.

$$\begin{aligned} u_1|_{R_1=B_1} &= 0, \\ u_n|_{R_n=B_n+1} &= 0. \end{aligned} \tag{3.96}$$

Developed asymptotic model is based on the small parameter ϵ and the global low-frequency regime of the form $\Omega_1^2 \sim \Omega_2^2 \sim \ldots \sim \Omega_n^2 \sim \epsilon$. If the first inner domain of the body is "stronger" , then, $\epsilon = \dfrac{\mu_2}{\mu_1}$, otherwise, $\epsilon = \dfrac{\mu_1}{\mu_2}$. As in the previous section, the frequencies and the displacements are expanded as asymptotic series, see (3.45) and (3.46), respectively.

Displacements of the "stronger" domains

At leading order the boundary value problems for the "stronger" domains are formulated as

$$R_i\frac{d^2u_{i0}}{dR_i^2} + \frac{du_{i0}}{dR_i} = 0, \tag{3.97}$$

subject to the Neumann boundary conditions

$$\begin{aligned} \left.\frac{du_{i0}}{dR_i}\right|_{R_i=B_i} &= 0, \\ \left.\frac{du_{i0}}{dR_i}\right|_{R_i=B_i+1} &= 0. \end{aligned} \tag{3.98}$$

Equations (3.97) lead to

$$\frac{du_{i0}}{dR_i} = \frac{A_i}{R_i}, \tag{3.99}$$

and

$$u_{i0} = A_i \ln R_i + C_i, \tag{3.100}$$

where A_i and C_i are constants. Thus, from (3.100) and the conditions (3.98) we can conclude that

$$A_i = 0, \tag{3.101}$$

and

$$u_{i0} = C_i, \tag{3.102}$$

with

$$C_j = 0, \qquad \text{for} \quad j < 1 \quad \text{or} \quad j > n. \tag{3.103}$$

Displacements of the "weaker" domains

The leading order boundary value problems for the "weaker" domains are derived as

$$R_i \frac{d^2 u_{i0}}{dR_i^2} + \frac{du_{i0}}{dR_i} = 0, \tag{3.104}$$

subject to the Dirichlet boundary conditions

$$\begin{aligned} u_{i0}|_{R_i=B_i} &= u_{(i-1)0}|_{R_{i-1}=B_{i-1}+1}, \\ u_{i0}|_{R_i=B_i+1} &= u_{(i+1)0}|_{R_{i+1}=B_{i+1}}. \end{aligned} \tag{3.105}$$

Then, using the solution for the "stronger" domains (3.102), we can write down the boundary conditions as

$$\begin{aligned} u_{(i-1)0}|_{R_{i-1}=B_{i-1}+1} &= C_{i-1}, \\ u_{(i+1)0}|_{R_{i+1}=B_{i+1}} &= C_{i+1}, \end{aligned} \tag{3.106}$$

which results in

$$u_{i0} = C_{i-1} + (C_{i+1} - C_{i-1}) \frac{\ln R_i - \ln B_i}{\ln(B_i + 1) - \ln B_i}. \tag{3.107}$$

The frequency estimation

Analysing the problem for the "stronger" domains at next order, we can write down the equations of motion

$$R_i \frac{d^2 u_{i1}}{dR_i^2} + \frac{du_{i1}}{dR_i} + \Omega_{i0}^2 R_i u_{i0} = 0, \tag{3.108}$$

and the boundary conditions

$$\begin{aligned} \left.\frac{du_{i1}}{dR_i}\right|_{R_i=B_i} &= L_{i-1}^i \left.\frac{du_{(i-1)0}}{dR_{i-1}}\right|_{R_{i-1}=B_{i-1}+1}, \\ \left.\frac{du_{i1}}{dR_i}\right|_{R_i=B_i+1} &= L_{i+1}^i \left.\frac{du_{(i+1)0}}{dR_{i+1}}\right|_{R_{i+1}=B_{i+1}}, \end{aligned} \tag{3.109}$$

where, in view of (3.107),

$$\begin{aligned} \left.\frac{du_{(i-1)0}}{dR_{i-1}}\right|_{R_{i-1}=B_{i-1}+1} &= \frac{1}{B_{i-1}+1} \frac{C_i - C_{i-2}}{\ln(B_{i-1}^{-1}+1)}, \\ \left.\frac{du_{(i+1)0}}{dR_{i+1}}\right|_{R_{i+1}=B_{i+1}} &= \frac{1}{B_{i+1}} \frac{C_{i+2} - C_i}{\ln(B_{i+1}^{-1}+1)}. \end{aligned} \tag{3.110}$$

Integrating the equations of motion over R_i ($B_i \le R_i \le B_i + 1$), we deduce

$$R_i \left.\frac{du_{i1}}{dR_i}\right|_{R_i=B_i+1} - R_i \left.\frac{du_{i1}}{dR_i}\right|_{R_i=B_i} = -C_i \Omega_{i0}^2 \frac{2B_i + 1}{2}. \tag{3.111}$$

Substituting the conditions (3.109) into (3.111), we arrive at the formulae for Ω_{i0}^2 in the form

$$\Omega_{i0}^2 = \frac{2}{C_i(2B_i+1)} \left(\frac{C_i - C_{i-2}}{\ln(B_{i-1}^{-1}+1)} + \frac{C_i - C_{i+2}}{\ln(B_{i+1}^{-1}+1)} \right). \tag{3.112}$$

Using (3.112) and the relation between frequency parameters of the "stronger" parts

$$\Omega_{k0} = L_j^k \Omega_{j0}, \tag{3.113}$$

we can build a system of equations for any particular number of domains. The number of equations in the system is equal to the number of the low eigenfrequencies and to the number of the "stronger" domains in the body.

3.4.2 Examples

Below we consider several examples, illustrating the method derived in the previous section.

3.4.2.1 A three-component cylinder with a single "stronger" domain

Now, we can implement the model to find the low-frequency and the eigenform for a three-component cylinder with an inner hole and the "stronger" inner domain. In this case to keep periodic structure the body should have the "weaker" outer domains subject to the Dirichlet boundary conditions. Using (3.112) we can write down for the inner "stronger" domain

$$\Omega_{20}^2 = \frac{2}{(2B_2+1)}\left(\frac{1}{\ln(B_1^{-1}+1)} + \frac{1}{\ln(B_3^{-1}+1)}\right). \tag{3.114}$$

Employing (3.102) and (3.107) we can derive the natural form as

$$\begin{aligned} U_{10} &= \frac{\ln R_1 - \ln B_1}{\ln(B_1+1) - \ln B_1}, \\ U_{20} &= 1, \\ U_{30} &= 1 - \frac{\ln R_3 - \ln B_3}{\ln(B_3+1) - \ln B_3}, \end{aligned} \tag{3.115}$$

see Figure 3.6.

3.4.2.2 A three-component cylinder with two "stronger" domains

Next, we consider a three-component cylinder with an inner hole and the "stronger" outer domains. Thus, the body has the "stronger" outer domains subject to the Neumann boundary conditions. Taking (3.112) for the "stronger" domains, we get

$$\begin{aligned} \Omega_{10}^2 &= \frac{2}{C_1(2B_1+1)}\frac{C_1 - C_3}{\ln(B_2^{-1}+1)}, \\ \Omega_{30}^2 &= \frac{2}{C_3(2B_3+1)}\frac{C_3 - C_1}{\ln(B_2^{-1}+1)}, \end{aligned} \tag{3.116}$$

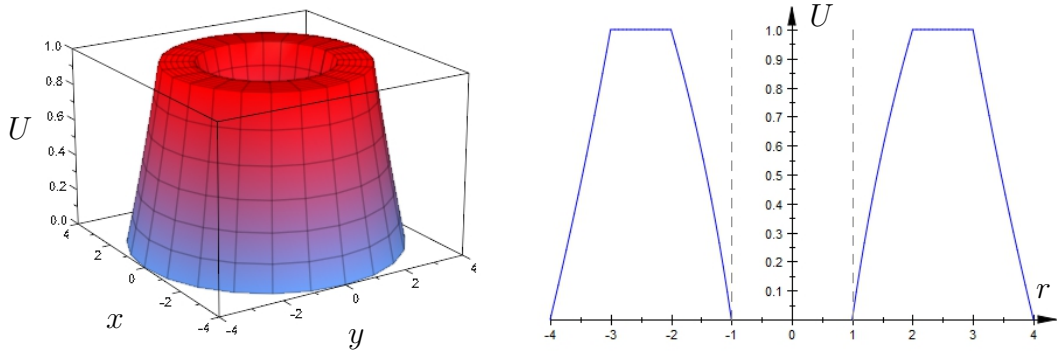

a) 3D b) 2D

Figure 3.6: Displacement profile (3.115); $l_0 = l_1 = l_2$

with the relation

$$\Omega_{10} = L_3^1 \Omega_{30}. \tag{3.117}$$

Therefore, expressions (3.116) with (3.117) result in the relations between the constants and the leading order estimations for the sought-for eigenfrequencies

$$C_3 = C_1, \qquad \Omega_{10}^2 = 0, \tag{3.118}$$

and

$$C_3 = -C_1 (L_3^1)^2 \frac{2B_1 + 1}{2B_3 + 1}, \qquad \Omega_{10}^2 = \frac{2}{\ln(B_2^{-1} + 1)} \left(\frac{1}{2B_1 + 1} + \frac{(L_3^1)^2}{2B_3 + 1} \right). \tag{3.119}$$

Substituting (3.118) and (3.119) into (3.102) and (3.107) we obtain the two displacement profiles. The first eigenform corresponds to the zero-frequency and the rigid body motion

$$U_{10} = U_{20} = U_{30} = 1. \tag{3.120}$$

We also have the second scaled displacement profile, where only outer domains perform

the uniform displacements

$$U_{10} = 1,$$
$$U_{20} = 1 - ((L_3^1)^2 \frac{2B_1 + 1}{2B_3 + 1} + 1) \frac{\ln R_2 - \ln B_2}{\ln(B_2 + 1) - \ln B_2}, \tag{3.121}$$
$$U_{30} = -(L_3^1)^2 \frac{2B_1 + 1}{2B_3 + 1},$$

see Figure 3.7.

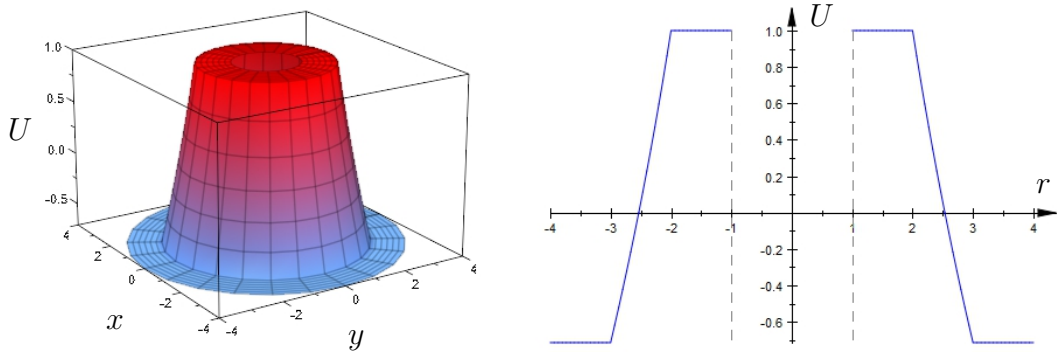

a) 3D b) 2D

Figure 3.7: Displacement profile (3.121); $l_0 = l_1 = l_2 = l_3$

The considered two examples show how the low-frequency profile of a three-component circular cylinder can vary depending on the number of "stronger" domains and boundary conditions.

4 Antiplane shear motion of a composite elastic body of arbitrary shape

In this chapter we study antiplane shear motion of a composite elastic body of arbitrary shape focusing on low frequency vibrations. We start with reviewing the solution for a single-component cylindrical body with a square cross section. Two types of boundary conditions are introduced, namely free boundary and fixed boundary. Seeking harmonic time-dependent solutions of the proposed boundary-value problems, we derive the appropriate frequency equations and displacement profiles. Next, antiplane shear motion of a two-component hollow cylindrical body with an annual arbitrary cross section is considered. The consideration is performed for either free or fixed inner and outer boundaries, together with perfect continuity conditions between domains. In this case the problem does not have an exact solution. Following the scheme of the previous chapter, we determine boundary conditions and contrast material properties of components allowing the low frequency vibration. A perturbation procedure is developed for evaluating the almost rigid body motions of stiffer components and the lowest vibration modes. Finally, the asymptotic model is implemented for two examples, deducing the estimates for the lowest natural frequencies and the displacement profiles for two-component bodies of standard geometric forms, that do not allow the exact solution.

4.1 A homogeneous body with a square cross section

Antiplane shear motion of a single-component cylindrical body with a square cross section is reviewed in this section.

4.1.1 Statement of the problem

Consider a homogeneous body with a square cross section, occupying a region D bounded by a closed boundary Γ with the origin of the Cartesian system $Oxyz$ located at the lower left corner of the square, see Figure 4.1. Both traction-free and fixed boundary conditions are considered.

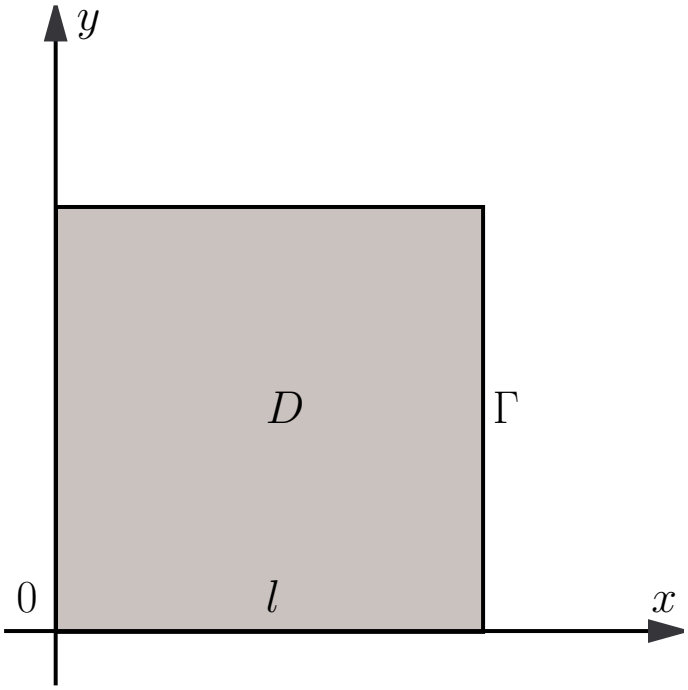

Figure 4.1: The square cross section of a homogeneous cylindrical body

For the components of the stress tensor independent of z, and in absence of body forces, the governing equation is given by the 2D Helmholtz equation

$$\frac{\partial^2 u}{\partial x^2} + \frac{\partial^2 u}{\partial y^2} + \frac{\omega^2}{c^2} u = 0, \tag{4.1}$$

where u is the out-of-plane displacement, ω is the vibration frequency, and $c = \sqrt{\mu/\rho}$

is the shear wave speed, with μ denoting the Lamé shear modulus, and ρ denoting the volume mass density.

Next, we introduce the scaled frequency

$$\Omega = \frac{\omega l}{c}, \tag{4.2}$$

where l is a side length of the square. Also, the Cartesian variables are converted into a dimensionless form as

$$X = \frac{x}{l}, \qquad Y = \frac{y}{l}. \tag{4.3}$$

Below we review both the case of a fixed boundary, i.e.

$$u|_{X=0} = u|_{X=1} = u|_{Y=0} = u|_{Y=1} = 0, \tag{4.4}$$

and the case of a traction-free boundary, i.e.

$$\left.\frac{\partial u}{\partial X}\right|_{X=0} = \left.\frac{\partial u}{\partial X}\right|_{X=1} = \left.\frac{\partial u}{\partial Y}\right|_{Y=0} = \left.\frac{\partial u}{\partial Y}\right|_{Y=1} = 0. \tag{4.5}$$

The equation (4.1) can be reformulated as

$$\frac{\partial^2 u}{\partial X^2} + \frac{\partial^2 u}{\partial Y^2} + \Omega^2 u = 0. \tag{4.6}$$

Applying separation of variables to (4.6), we adapt for the displacement

$$u = (A\cos\Omega_X X + B\sin\Omega_X X)(C\cos\Omega_Y Y + G\sin\Omega_Y Y), \tag{4.7}$$

where A, B, C and G are constants. Then, the vibration frequency is given as

$$\Omega^2 = \Omega_X^2 + \Omega_Y^2. \tag{4.8}$$

4.1.2 Fixed boundary

Substituting (4.7) into the boundary conditions (4.4), we arrive at

$$\begin{aligned} A\cos 0 + B\sin 0 &= 0, \\ A\cos\Omega_X + B\sin\Omega_X &= 0, \end{aligned} \tag{4.9}$$

and

$$\begin{aligned} C\cos 0 + G\sin 0 = 0, \\ C\cos\Omega_Y + G\sin\Omega_Y = 0. \end{aligned} \tag{4.10}$$

The frequency equations can be obtained by solving the linear algebraic systems (4.9) and (4.10) as

$$\begin{aligned} A = 0 \quad \text{and} \quad B\sin\Omega_X = 0, \qquad \text{with} \quad \Omega_X = \pi n, \\ C = 0 \quad \text{and} \quad G\sin\Omega_Y = 0, \qquad \text{with} \quad \Omega_Y = \pi m, \end{aligned} \tag{4.11}$$

respectively, where mode values $n, m = 1, 2, 3, \ldots$.

For the lowest natural frequency the displacement profile is given by

$$u = BG\sin\pi X\sin\pi Y. \tag{4.12}$$

4.1.3 Free boundary

The sought-for systems follow from substitution of (4.7) into the boundary conditions (4.5) resulting in

$$\begin{aligned} \Omega(A\sin 0 - B\cos 0) = 0, \\ \Omega(A\sin\Omega_X - B\cos\Omega_X) = 0, \end{aligned} \tag{4.13}$$

and

$$\begin{aligned} \Omega(C\sin 0 - G\cos 0) = 0, \\ \Omega(C\sin\Omega_Y - G\cos\Omega_Y) = 0. \end{aligned} \tag{4.14}$$

In this case, along with the set of eigenfrequencies (4.11), we observe at the zero eigenfrequency the solution

$$u = AC, \tag{4.15}$$

corresponding to a rigid motion typical for bodies with free faces. For the lowest non-zero natural frequency the displacement profile is derived as

$$u = AC\cos\pi X\cos\pi Y. \tag{4.16}$$

4.2 A two-component body of arbitrary shape

Antiplane shear motion of a two-component hollow cylindrical body with an annular arbitrary cross section is studied in this section.

4.2.1 Statement of the problem

Consider a hollow cylindrical body with an annular arbitrary cross section having inner and outer domains, D_1 and D_2, respectively, located between non-intersecting closed contours Γ_0, Γ_1 and Γ_2, see Figure 4.2. The origin of the Cartesian system $Oxyz$ set inside the inner hole. Both traction-free and fixed boundaries of the inner and outer domains are considered, assuming continuity of displacements and stresses along Γ_1.

The governing equations for the inner and outer domains are given as

$$\frac{\partial^2 u_i}{\partial x^2} + \frac{\partial^2 u_i}{\partial y^2} + \frac{\omega^2}{c_i^2} u_i = 0, \qquad i = 1, 2, \tag{4.17}$$

where u_i are the out-of-plane displacements, $c_i = \sqrt{\mu_i/\rho_i}$ are the associated shear wave speeds, μ_i are the Lamé shear moduli, ρ_i are the volume mass densities, and indices 1 and 2 correspond to the inner and outer domains, respectively.

As in the previous sections, the scaled frequencies for both domains are defined as

$$\Omega_i = \frac{\omega l_i}{c_i}, \qquad i = 1, 2, \tag{4.18}$$

where l_i is the contour length of the appropriate domain. The other parameters and variables transformed to the dimensionless form become

$$\mu = \frac{\mu_1}{\mu_2}, \qquad l = \frac{l_1}{l_2}, \qquad \rho = \frac{\rho_1}{\rho_2}, \qquad c = \frac{c_1}{c_2}, \tag{4.19}$$

and

$$X_i = \frac{x}{l_i}, \qquad Y_i = \frac{y}{l_i}, \qquad i = 1, 2. \tag{4.20}$$

The relation between two scaled frequencies following from (4.18) is

$$c\,\Omega_1 = l\,\Omega_2. \tag{4.21}$$

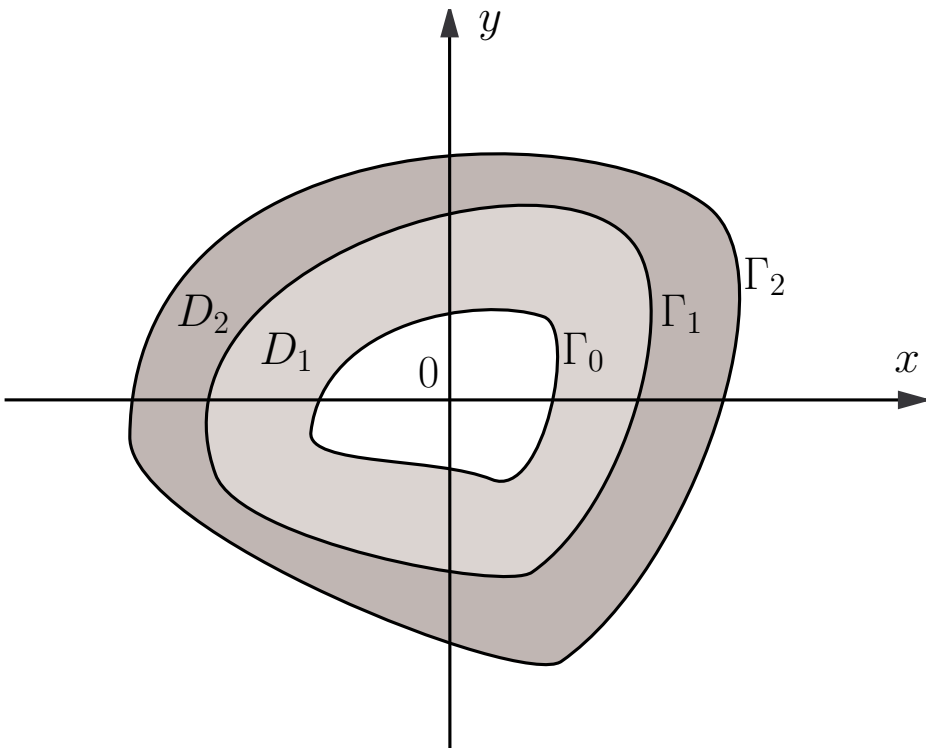

Figure 4.2: The cross section of a two-component cylindrical body of arbitrary shape

The governing equations in a dimensionless form are given by

$$\frac{\partial^2 u_i}{\partial X_i^2} + \frac{\partial^2 u_i}{\partial Y_i^2} + \Omega_i^2 u_i = 0, \qquad i = 1, 2, \tag{4.22}$$

with the conditions along fixed and traction-free contours for both inner and outer domains formulated as follow

$$u_i|_{\Gamma_j} = 0, \tag{4.23}$$

and

$$\left.\frac{\partial u_i}{\partial n}\right|_{\Gamma_j} = 0, \tag{4.24}$$

where $i = 1, 2$, as above, and n is the unit normal to the appropriate curve Γ_j, $j = 0, 2$. The continuity conditions on Γ_1 are written as

$$\frac{\mu}{l}\frac{\partial u_1}{\partial n}\bigg|_{\Gamma_1} = \frac{\partial u_2}{\partial n}\bigg|_{\Gamma_1}, \tag{4.25}$$

and

$$u_1|_{\Gamma_1} = u_2|_{\Gamma_1}. \tag{4.26}$$

To solve this problem a perturbation technique is implemented, focusing on the global low-frequency regime for which $\Omega_1^2 \sim \Omega_2^2 \sim \epsilon$, with $\epsilon \ll 1$ being a small parameter associated with contrast geometrical and material properties of the components. The displacements and frequencies are expanded as asymptotic series

$$\begin{aligned} u_i &= u_{i0} + \epsilon\, u_{i1} + \epsilon^2 u_{i2} + \ldots, \\ \Omega_i^2 &= \epsilon\,(\Omega_{i0}^2 + \epsilon\,\Omega_{i1}^2 + \epsilon^2\Omega_{i2}^2 + \ldots). \end{aligned} \tag{4.27}$$

The focus is on two contrast cases, namely $\epsilon = \dfrac{l}{\mu} \ll 1$ corresponding to the "stronger" inner domain, or $\epsilon = \dfrac{\mu}{l} \ll 1$ associated with the "stronger" outer domain of the body. It also can be noted that relations (4.21) imply

$$l \sim c. \tag{4.28}$$

4.2.2 "Stronger" outer domain

First, study a body with a "stronger" outer domain, where

$$\epsilon = \frac{\mu}{l} \ll 1. \tag{4.29}$$

Further we verify that the global low frequency regime $\Omega_1^2 \sim \Omega_2^2 \sim \epsilon$ is possible only for the fixed Γ_0 and free Γ_2 contours in case of a "stronger" outer domain.

4.2.2.1 Fixed inner and free outer boundaries

First, attention is drawn to a body with the "stronger" outer domain D_2, having the fixed inner and free outer contours.

In order to solve the problem for the "stronger" outer domain the expansions (4.27) are substituted into the dimensionless equation of motion (4.22) at $i = 2$ and the boundary conditions (4.24) and (4.25). As a result, at leading order the Laplace equation

$$\frac{\partial^2 u_{20}}{\partial X_2^2} + \frac{\partial^2 u_{20}}{\partial Y_2^2} = 0, \tag{4.30}$$

is obtained subject to the Neumann boundary conditions

$$\begin{aligned} \left.\frac{\partial u_{20}}{\partial n}\right|_{\Gamma_1} &= 0, \\ \left.\frac{\partial u_{20}}{\partial n}\right|_{\Gamma_2} &= 0. \end{aligned} \tag{4.31}$$

Hence, we arrive at

$$u_{20} = C, \tag{4.32}$$

where C is a constant, which corresponds to the rigid body motion of the "stronger" domain.

Then, the leading order boundary value problem for the inner domain is derived by substituting (4.27) into the dimensionless equation of motion (4.22) at $i = 1$ and the boundary conditions (4.23) and (4.26) with use of the previous result (4.32). Thus, the Laplace equation

$$\frac{\partial^2 u_{10}}{\partial X_1^2} + \frac{\partial^2 u_{10}}{\partial Y_1^2} = 0, \tag{4.33}$$

is subject to the Dirichlet boundary conditions

$$\begin{aligned} u_{10}|_{\Gamma_0} &= 0, \\ u_{10}|_{\Gamma_1} &= C. \end{aligned} \tag{4.34}$$

This leads to

$$u_{10} = C H_1(X_1, Y_1), \tag{4.35}$$

where $H_1(X_1, Y_1)$ is a harmonic function satisfying the conditions

$$\begin{aligned} H_1(X_1, Y_1)|_{\Gamma_0} &= 0, \\ H_1(X_1, Y_1)|_{\Gamma_1} &= 1. \end{aligned} \tag{4.36}$$

Treatment of the "stronger" domain D_2 at next order provides an estimate for the sought-for frequency. The analysed boundary value problem can be written as

$$\frac{\partial^2 u_{21}}{\partial X_2^2} + \frac{\partial^2 u_{21}}{\partial Y_2^2} = -\Omega_{20}^2 u_{20}, \tag{4.37}$$

subject to the Neumann boundary conditions

$$\begin{aligned} \left.\frac{\partial u_{21}}{\partial n}\right|_{\Gamma_1} &= \left.\frac{\partial u_{10}}{\partial n}\right|_{\Gamma_1}, \\ \left.\frac{\partial u_{21}}{\partial n}\right|_{\Gamma_2} &= 0, \end{aligned} \tag{4.38}$$

where, as follow from (4.35),

$$\left.\frac{\partial u_{10}}{\partial n}\right|_{\Gamma_1} = C \left.\frac{\partial H_1}{\partial n}\right|_{\Gamma_1}. \tag{4.39}$$

In view of (4.32), integration of (4.37) over the outer domain D_2 results in

$$\iint\limits_{D_2} \left(\frac{\partial^2 u_{21}}{\partial X_2^2} + \frac{\partial^2 u_{21}}{\partial Y_2^2} \right) dX_2 dY_2 = -\Omega_{20}^2 C \iint\limits_{D_2} dX_2 dY_2. \tag{4.40}$$

Let us now employ the Green's first identity, stating that for any function u and a bounded solid region D with a bounding surface Γ

$$\iint\limits_{D} \left(\frac{\partial^2 u}{\partial x^2} + \frac{\partial^2 u}{\partial y^2} \right) dx dy = \oint\limits_{\Gamma} \frac{\partial u}{\partial n}\, ds, \tag{4.41}$$

where the right hand side is a usual line integral, with n being the unit outer normal on Γ, e.g. see Strauss (1992). The Green's first identity originates in Stoke's theorem, see Grossman (2014).

On employing (4.41), we have

$$\oint\limits_{\Gamma_2} \frac{\partial u_{21}}{\partial n}\, ds - \oint\limits_{\Gamma_1} \frac{\partial u_{21}}{\partial n}\, ds = -\Omega_{20}^2 C A_2, \tag{4.42}$$

where A_2 is the area of the domain D_2.

Due to (4.38), the first term in the left hand side of (4.42) vanishes. Hence, on making use of (4.39), the leading order estimate for the sought-for frequency is given by

$$\Omega_{20}^2 = \frac{1}{A_2} \oint\limits_{\Gamma_1} \frac{\partial H_1}{\partial n}\, ds. \tag{4.43}$$

Then, in view of (4.21) and (4.29), the frequencies can be written as

$$\Omega_1^2 = \frac{\rho l}{A_2} \oint\limits_{\Gamma_1} \frac{\partial H_1}{\partial n}\, ds, \tag{4.44}$$

and

$$\Omega_2^2 = \frac{\mu}{l A_2} \oint\limits_{\Gamma_1} \frac{\partial H_1}{\partial n}\, ds. \tag{4.45}$$

4.2.2.2 Free inner and outer boundaries

Now, a body with the "stronger" outer domain D_2 and the free inner and outer contours is considered.

The leading order boundary value problem for the outer domain can be formulated as in the previous case, see (4.30) and (4.31). We arrive at the same result for the displacement of the outer domain

$$u_{20} = C. \tag{4.46}$$

Then, using (4.22) with (4.24), (4.26), and (4.46) we derive the leading order boundary value problem for the inner domain as Laplace equation

$$\frac{\partial^2 u_{10}}{\partial X_1^2} + \frac{\partial^2 u_{10}}{\partial Y_1^2} = 0, \tag{4.47}$$

subject to the mixed boundary conditions

$$\begin{aligned} \left.\frac{\partial u_{10}}{\partial n}\right|_{\Gamma_0} &= 0, \\ u_{10}|_{\Gamma_1} &= C. \end{aligned} \tag{4.48}$$

This implies

$$u_{10} = C. \tag{4.49}$$

At next order the equation of motion for the outer domain D_2 can be written as

$$\frac{\partial^2 u_{21}}{\partial X_2^2} + \frac{\partial^2 u_{21}}{\partial Y_2^2} = -\Omega_{20}^2 u_{20}, \tag{4.50}$$

subject to

$$\begin{aligned} \left.\frac{\partial u_{21}}{\partial n}\right|_{\Gamma_1} &= \left.\frac{\partial u_{10}}{\partial n}\right|_{\Gamma_1}, \\ \left.\frac{\partial u_{21}}{\partial n}\right|_{\Gamma_2} &= 0, \end{aligned} \tag{4.51}$$

where, according to (4.49),

$$\left.\frac{\partial u_{10}}{\partial n}\right|_{\Gamma_1} = 0. \tag{4.52}$$

Applying the same procedure as in (4.40)-(4.42), we get

$$\oint_{\Gamma_2} \frac{\partial u_{21}}{\partial n}\, ds - \oint_{\Gamma_1} \frac{\partial u_{21}}{\partial n}\, ds = -\Omega_{20}^2 C A_2, \tag{4.53}$$

where both terms in the left hand side vanish due to (4.51). Hence, the leading order estimate for frequency is given by

$$\Omega_{20}^2 = 0. \tag{4.54}$$

This case corresponds to the rigid motion of a body with free boundaries.

4.2.2.3 Fixed inner and outer boundaries

Next, study a body with the ˝stronger˝ outer domain and the fixed inner and outer boundaries.

The leading order boundary value problem for the outer domain includes the boundary conditions (4.23) and (4.25) in the form

$$\begin{aligned} \left.\frac{\partial u_{20}}{\partial n}\right|_{\Gamma_1} &= 0, \\ u_{20}|_{\Gamma_2} &= 0, \end{aligned} \tag{4.55}$$

along with the equation

$$\frac{\partial^2 u_{20}}{\partial X_2^2} + \frac{\partial^2 u_{20}}{\partial Y_2^2} = 0. \tag{4.56}$$

This is resulting at

$$u_{20} = 0. \tag{4.57}$$

The leading order boundary value problem for the inner domain is given by

$$\frac{\partial^2 u_{10}}{\partial X_1^2} + \frac{\partial^2 u_{10}}{\partial Y_1^2} = 0, \tag{4.58}$$

subject to the Dirichlet boundary conditions, originating from (4.23), (4.26), and (4.57), i.e.

$$\begin{aligned} u_{10}|_{\Gamma_0} &= 0, \\ u_{10}|_{\Gamma_1} &= 0. \end{aligned} \tag{4.59}$$

Hence, the solution for the inner displacement is again

$$u_{10} = 0, \tag{4.60}$$

due to the maximum principle for harmonic functions, see Strauss (2007). Thus, it is not possible to achieve the low-frequency regime in this case.

4.2.2.4 Free inner and fixed outer boundaries

Finally, a body with the ″stronger″ outer domain and free Γ_0 and fixed Γ_2 contours is considered.

At leading order the boundary value problem for the outer displacement is formulated in the same way as in the previous subsection, resulting in

$$u_{20} = 0. \tag{4.61}$$

The equation of motion for the inner domain D_1 at leading order becomes

$$\frac{\partial^2 u_{10}}{\partial X_1^2} + \frac{\partial^2 u_{10}}{\partial Y_1^2} = 0, \tag{4.62}$$

and the boundary conditions are obtained from (4.24), (4.26), and (4.61) in the form

$$\begin{aligned} \left.\frac{\partial u_{10}}{\partial n}\right|_{\Gamma_0} &= 0, \\ u_{10}|_{\Gamma_1} &= 0. \end{aligned} \tag{4.63}$$

Then, the leading order inner displacement is given by

$$u_{10} = 0, \tag{4.64}$$

indicating that the low-frequency regime is impossible for the considered boundary conditions.

4.2.3 "Stronger" inner domain

Let us now consider a body with a "stronger" inner domain, when

$$\epsilon = \frac{l}{\mu} \ll 1. \tag{4.65}$$

It can be verified that the global low frequency regime $\Omega_1^2 \sim \Omega_2^2 \sim \epsilon$ is possible only for free Γ_0 and fixed Γ_2 boundaries.

4.2.3.1 Fixed inner and free outer boundaries

First, we study a body with the "stronger" inner domain D_1, having fixed Γ_0 and free Γ_2 contours.

We begin with the "stronger" inner domain. In particular, the expansions (4.27) are substituted into the dimensionless equation of motion (4.22) at $i = 1$ and the boundary conditions (4.23) and (4.25) to arrive at the leading order boundary value problem. Thereby, the equation

$$\frac{\partial^2 u_{10}}{\partial X_1^2} + \frac{\partial^2 u_{10}}{\partial Y_1^2} = 0, \tag{4.66}$$

is subject to the mixed boundary conditions

$$\begin{aligned} u_{10}|_{\Gamma_0} &= 0, \\ \left.\frac{\partial u_{10}}{\partial n}\right|_{\Gamma_1} &= 0, \end{aligned} \tag{4.67}$$

leading to

$$u_{10} = 0. \tag{4.68}$$

The leading order boundary value problem for the outer domain follows from substitution of (4.27) into (4.22) at $i = 2$ and also involve the boundary conditions (4.24) and (4.26) along with the inner domain solution (4.68). Then, the Laplace equation

$$\frac{\partial^2 u_{20}}{\partial X_2^2} + \frac{\partial^2 u_{20}}{\partial Y_2^2} = 0, \tag{4.69}$$

is subject to the mixed boundary conditions

$$\begin{aligned} u_{20}|_{\Gamma_1} &= 0, \\ \left.\frac{\partial u_{20}}{\partial n}\right|_{\Gamma_2} &= 0. \end{aligned} \tag{4.70}$$

Therefore, at leading order the outer displacement is given by

$$u_{20} = 0, \tag{4.71}$$

meaning again that the low-frequency regime is impossible for these boundary conditions.

4.2.3.2 Fixed inner and outer boundaries

Now, attention is on a body having the ‶stronger″ inner domain and the fixed inner and outer boundaries.

In this case the leading order boundary value problem for the inner domain is formulated similarly to that in the previous subsection, see (4.66) and (4.67), with the same result for the inner displacement

$$u_{10} = 0. \tag{4.72}$$

Then, the leading order boundary value problem for the outer domain is given by

$$\frac{\partial^2 u_{20}}{\partial X_2^2} + \frac{\partial^2 u_{20}}{\partial Y_2^2} = 0, \tag{4.73}$$

subject to

$$\begin{aligned} u_{20}|_{\Gamma_1} &= 0, \\ u_{20}|_{\Gamma_2} &= 0, \end{aligned} \tag{4.74}$$

which leads to

$$u_{20} = 0, \tag{4.75}$$

due to the aforementioned maximum principle for harmonic functions. Thus, there is no low-frequency regime in this case.

4.2.3.3 Free inner and outer boundaries

The next set-up is a body with the "stronger" inner domain D_1 and free boundaries Γ_0 and Γ_2.

At leading order the boundary value problem for the inner domain is given by

$$\frac{\partial^2 u_{10}}{\partial X_1^2} + \frac{\partial^2 u_{10}}{\partial Y_1^2} = 0, \tag{4.76}$$

subject to

$$\begin{aligned} \left.\frac{\partial u_{10}}{\partial n}\right|_{\Gamma_0} &= 0, \\ \left.\frac{\partial u_{10}}{\partial n}\right|_{\Gamma_1} &= 0, \end{aligned} \tag{4.77}$$

following from (4.24) and (4.25). Then, the inner displacement is a constant, i.e.

$$u_{10} = C. \tag{4.78}$$

The leading order boundary value problem for the outer domain can be written as

$$\frac{\partial^2 u_{20}}{\partial X_2^2} + \frac{\partial^2 u_{20}}{\partial Y_2^2} = 0, \tag{4.79}$$

subject to

$$\begin{aligned} u_{20}|_{\Gamma_1} &= C, \\ \left.\frac{\partial u_{20}}{\partial n}\right|_{\Gamma_2} &= 0, \end{aligned} \tag{4.80}$$

following from (4.24) and (4.26). Hence, the solution for the outer displacement is

$$u_{20} = C. \tag{4.81}$$

At next order the equation of motion for the inner domain D_1 is given by

$$\frac{\partial^2 u_{11}}{\partial X_1^2} + \frac{\partial^2 u_{11}}{\partial Y_1^2} = -\Omega_{10}^2 u_{10}, \tag{4.82}$$

subject to the boundary conditions

$$\begin{aligned} \left.\frac{\partial u_{11}}{\partial n}\right|_{\Gamma_0} &= 0, \\ \left.\frac{\partial u_{11}}{\partial n}\right|_{\Gamma_1} &= \left.\frac{\partial u_{20}}{\partial n}\right|_{\Gamma_1}, \end{aligned} \tag{4.83}$$

where, according to (4.81),

$$\left.\frac{\partial u_{20}}{\partial n}\right|_{\Gamma_1} = 0. \tag{4.84}$$

Integrating (4.82) over the inner domain D_1 and applying the solution (4.78), we obtain

$$\iint\limits_{D_1} \left(\frac{\partial^2 u_{11}}{\partial X_1^2} + \frac{\partial^2 u_{11}}{\partial Y_1^2} \right) dX_1 dY_1 = -\Omega_{10}^2 C \iint\limits_{D_1} dX_1 dY_1. \tag{4.85}$$

Seeing the Green's first identity, (4.85) becomes

$$\oint\limits_{\Gamma_1} \frac{\partial u_{11}}{\partial n}\, ds - \oint\limits_{\Gamma_0} \frac{\partial u_{11}}{\partial n}\, ds = -\Omega_{10}^2 C A_1, \tag{4.86}$$

where both terms in the left hand side vanish due to (4.83) and (4.84). Therefore, we have at leading order

$$\Omega_{10}^2 = 0. \tag{4.87}$$

4.2.3.4 Free inner and fixed outer boundaries

Finally, attention is drawn to a body with the ˝stronger˝ inner domain, having free inner and fixed outer boundaries.

The leading order solution of the boundary value problem for the inner domain is similar to that in the previous subsection, see (4.76) and (4.77), giving the same result for the inner displacement

$$u_{10} = C. \tag{4.88}$$

The leading order boundary value problem for the outer domain is derived from the boundary conditions (4.23) and (4.26), using the previous solution (4.88). Thus, the Laplace equation

$$\frac{\partial^2 u_{20}}{\partial X_2^2} + \frac{\partial^2 u_{20}}{\partial Y_2^2} = 0, \tag{4.89}$$

is subject to the Dirichlet boundary conditions

$$\begin{aligned} u_{20}|_{\Gamma_1} &= C, \\ u_{20}|_{\Gamma_2} &= 0, \end{aligned} \tag{4.90}$$

resulting in

$$u_{20} = C H_2(X_2, Y_2). \tag{4.91}$$

Here $H_2(X_2, Y_2)$ is a harmonic function satisfying the conditions

$$\begin{aligned} H_2(X_2, Y_2)|_{\Gamma_1} &= 1, \\ H_2(X_2, Y_2)|_{\Gamma_2} &= 0. \end{aligned} \tag{4.92}$$

At next order the boundary value problem for the ˝stronger˝ domain can be formulated as

$$\frac{\partial^2 u_{11}}{\partial X_1^2} + \frac{\partial^2 u_{11}}{\partial Y_1^2} = -\Omega_{10}^2 u_{10}, \tag{4.93}$$

subject to

$$\begin{aligned} \left.\frac{\partial u_{11}}{\partial n}\right|_{\Gamma_0} &= 0, \\ \left.\frac{\partial u_{11}}{\partial n}\right|_{\Gamma_1} &= \left.\frac{\partial u_{20}}{\partial n}\right|_{\Gamma_1}, \end{aligned} \tag{4.94}$$

where, according to the solution (4.91),

$$\left.\frac{\partial u_{20}}{\partial n}\right|_{\Gamma_1} = C \left.\frac{\partial H_2}{\partial n}\right|_{\Gamma_1}. \tag{4.95}$$

In view of the solution (4.88), integration of (4.93) over the inner domain D_1 and employment of the Green's first identity yields

$$\oint\limits_{\Gamma_1} \frac{\partial u_{11}}{\partial n}\, ds - \oint\limits_{\Gamma_0} \frac{\partial u_{11}}{\partial n}\, ds = -\Omega_{10}^2 C A_1. \tag{4.96}$$

Due to (4.94), the second term in the left hand side of (4.96) vanishes. Hence, on making use of (4.95), the leading order estimate for frequency is given by

$$\Omega_{10}^2 \sim -\frac{1}{A_1} \oint\limits_{\Gamma_1} \frac{\partial H_2}{\partial n}\, ds. \tag{4.97}$$

Then, applying (4.21) and (4.65), the expressions for the frequency can be written as

$$\Omega_1^2 \sim -\frac{l}{\mu A_1} \oint\limits_{\Gamma_1} \frac{\partial H_2}{\partial n}\, ds, \tag{4.98}$$

and

$$\Omega_2^2 \sim -\frac{1}{l\rho A_1} \oint\limits_{\Gamma_1} \frac{\partial H_2}{\partial n}\, ds. \tag{4.99}$$

Thereby, it has been verified for all possible combinations of the boundary conditions, that a non-trivial low-frequency regime exists only for a body with a fixed boundary corresponding to a ‶weaker″ domain and a free boundary corresponding to a ‶stronger″ domain.

This formal conclusion has also a simple intuitive interpretation. Indeed, if one of the boundaries of a stronger domain is not clamped, its another domain is always almost free due to the contrast in the problem parameters. As a consequence, almost rigid body motion seems to be possible with a low natural frequency.

4.3 Examples

Now, we consider two examples illustrating the methodology developed in the previous section.

4.3.1 A two-component body with a "stronger" outer domain

First, we consider antiplane motion of a two-component solid cylindrical elastic body of a square cross section. The body has a circular inclusion with an inner hole of radius l_0, and the origin O lying in the geometrical center of the hole. The softer inner annular domain D_1 is specified in polar coordinates by $l_0 \leq r \leq l_0 + l_1$, whereas the stiffer outer domain D_2 is located between the circumference Γ_1 of radius $l_0 + l_1$ and the square Γ_2 with side length of $2(l_0 + l_1 + l_2)$, see Figure 4.3. This problem does not allow a straightforward analytical treatment leading to a closed-form solution.

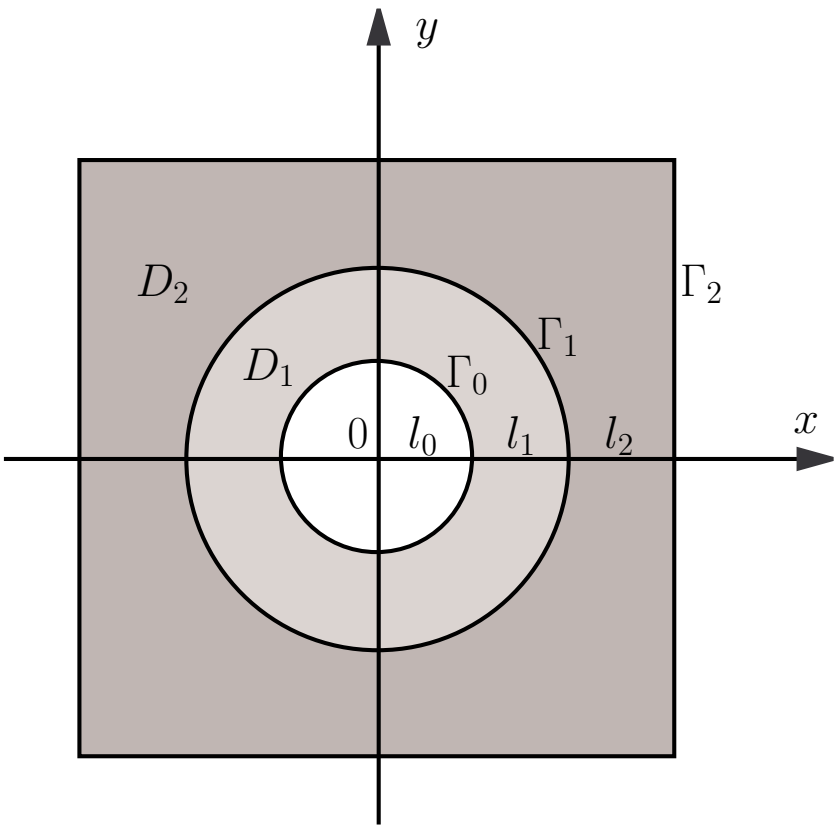

Figure 4.3: The cross section of a cylindrical body with the "stronger" outer domain

We introduce the dimensionless radial coordinates

$$R_i = \frac{r}{l_i}, \qquad i = 1, 2, \tag{4.100}$$

with the dimensionless boundaries for the domains, i.e.

$$L_1 = \frac{l_0}{l_1}, \qquad L_2 = \frac{l_0 + l_1}{l_2}. \tag{4.101}$$

The equation of axisymmetric motion is written for the inner domain as

$$R_1^2 \frac{d^2 u_1}{dR_1^2} + R_1 \frac{du_1}{dR_1} + R_1^2 \Omega_1^2 u_1 = 0, \tag{4.102}$$

and the equation of motion for the outer domain is given in the general form

$$\frac{\partial^2 u_2}{\partial X_2^2} + \frac{\partial^2 u_2}{\partial Y_2^2} + \Omega_2^2 u_2 = 0. \tag{4.103}$$

On adapting the general scheme of Section 4.2.2, consider the fixed inner

$$u_1|_{R_1 = L_1} = 0, \tag{4.104}$$

and free outer face contours

$$\left.\frac{\partial u_2}{\partial X_2}\right|_{|X_2| = L_2 + 1} = \left.\frac{\partial u_2}{\partial Y_2}\right|_{|Y_2| = L_2 + 1} = 0, \tag{4.105}$$

with the continuity conditions on stresses

$$\left.\frac{\mu}{l}\frac{du_1}{dR_1}\right|_{R_1 = L_1 + 1} = \left.\frac{du_2}{dR_2}\right|_{R_2 = L_2}, \tag{4.106}$$

and displacements

$$u_1|_{R_1 = L_1 + 1} = u_2|_{R_2 = L_2}. \tag{4.107}$$

Let us implement the same asymptotic method as in Subsection 4.2.2.1, relying on the small parameter $\epsilon = \dfrac{\mu}{l} \ll 1$. On expanding the displacements and frequencies as (4.27) and applying the procedure described in the previous section, we have for the leading order eigensolution

$$\begin{aligned} u_{10} &= C H_1(R_1), \\ u_{20} &= C, \end{aligned} \tag{4.108}$$

see (4.32) and (4.35). Here, H_1 is a harmonic function, satisfying

$$R_1 \frac{d^2 u_{10}}{dR_1^2} + \frac{du_{10}}{dR_1} = 0, \tag{4.109}$$

along with the conditions (4.36), which take the form

$$\begin{aligned} H_1|_{R_1=L_1} &= 0, \\ H_1|_{R_1=L_1+1} &= 1, \end{aligned} \tag{4.110}$$

thus

$$H_1(R_1) = \frac{\ln R_1 - \ln L_1}{\ln(L_1^{-1}+1)}. \tag{4.111}$$

The illustrations of the displacement profile (4.108) are shown in Figure 4.4, containing the overall axisymmetric plot along with its axial cross section at $y = 0$, calculated at $l_0 = l_1 = l_2 = 1$.

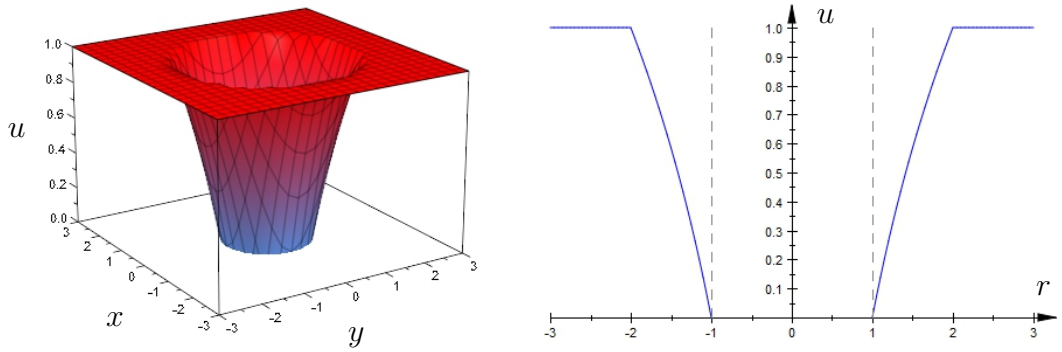

a) Displacement profile b) Axial cross section

Figure 4.4: Displacement profile (4.108); $l_0 = l_1 = l_2 = 1$

At next order it is sufficient to consider only the "stronger" domain to obtain an estimate for frequency. The boundary value problem is formulated as

$$\frac{\partial^2 u_{21}}{\partial X_2^2} + \frac{\partial^2 u_{21}}{\partial Y_2^2} + \Omega_{20}^2 u_{20} = 0, \tag{4.112}$$

subject to

$$\begin{aligned} \left.\frac{du_{21}}{dR_2}\right|_{R_2=L_2} &= \left.\frac{du_{10}}{dR_1}\right|_{R_1=L_1+1}, \\ \left.\frac{\partial u_{21}}{\partial X_2}\right|_{|X_2|=L_2+1} &= \left.\frac{\partial u_{21}}{\partial Y_2}\right|_{|Y_2|=L_2+1} = 0, \end{aligned} \tag{4.113}$$

where, making use of the solution (4.111), we have

$$\left.\frac{du_{10}}{dR_1}\right|_{R_1=L_1+1} = \frac{C(L_1+1)^{-1}}{\ln(L_1^{-1}+1)}. \tag{4.114}$$

Integrating (4.112) over the outer domain D_2 and using the solution (4.108) for u_{20}, we obtain

$$\iint\limits_{D_2} \left(\frac{\partial^2 u_{21}}{\partial X_2^2} + \frac{\partial^2 u_{21}}{\partial Y_2^2}\right) dX_2 dY_2 = -C\Omega_{20}^2 A_2, \tag{4.115}$$

where $A_2 = 4(L_2+1)^2 - \pi L_2^2$.

Then, on applying the Green's first identity, it can be deduced that

$$\begin{aligned} &\int\limits_{-(L_2+1)}^{L_2+1} \left.\frac{\partial u_{21}}{\partial X_2}\right|_{|X_2|=L_2+1} dY_2 + \int\limits_{-(L_2+1)}^{L_2+1} \left.\frac{\partial u_{21}}{\partial Y_2}\right|_{|Y_2|=L_2+1} dX_2 - \\ &-L_2 \int\limits_0^{2\pi} \left.\frac{\partial u_{21}}{\partial R_2}\right|_{R_2=L_2} d\varphi = -C\Omega_{20}^2 A_2. \end{aligned} \tag{4.116}$$

Finally, on substituting (4.113) with (4.114), the leading order estimate for the eigenfrequency is found as

$$\Omega_{20}^2 = \frac{2\pi l}{\ln(L_1^{-1}+1)(4(L_2+1)^2 - \pi L_2^2)}, \tag{4.117}$$

which coincides with the result in (4.43).

4.3.2 A two-component body with a "stronger" inner domain

As the next example, let us study antiplane motion of a circular cylinder with an annular cross section and stiffer inner and softer outer domains. Suppose, the

boundaries Γ_1 and Γ_2 are cylinders of radius $l_0 + l_1$ and $l_0 + l_1 + l_2$, respectively. The stronger domain D_1 has an inner hole with a square cross section and a side length of $2l_0$, situated such that the origin O lies in the geometrical center of the hole, see Figure 4.5. As in the previous example, an analytical solution can not be found for this problem.

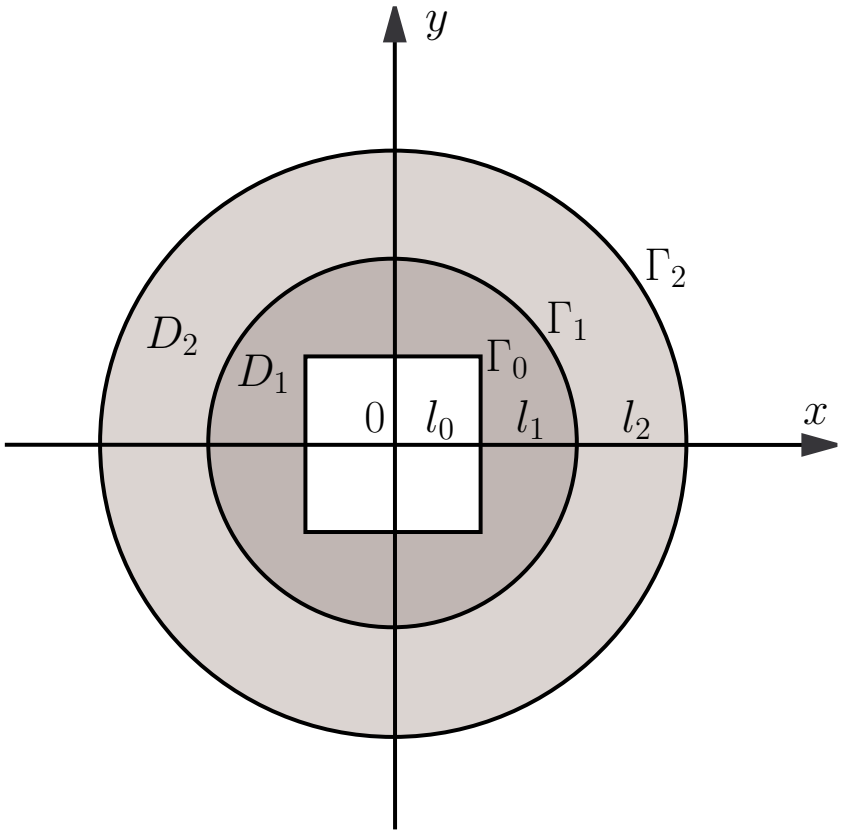

Figure 4.5: The cross section of a cylindrical body with the ˝stronger˝ inner domain

Here the equations of motion are taken in the form

$$\frac{\partial^2 u_1}{\partial X_1^2} + \frac{\partial^2 u_1}{\partial Y_1^2} + \Omega_1^2 u_1 = 0, \tag{4.118}$$

and

$$R_2^2\frac{d^2u_2}{dR_2^2}+R_2\frac{du_2}{dR_2}+R_2^2\Omega_2^2u_2=0, \tag{4.119}$$

for the inner and outer domains, respectively.

As follows from Section 4.2.3, in order to have the global low-frequency regime ($\Omega_1^2\sim\Omega_2^2\sim\epsilon$) with the small parameter $\epsilon=\dfrac{l}{\mu}$, we consider a free inner contour, i.e.

$$\left.\frac{\partial u_1}{\partial X_1}\right|_{|X_1|=L_1}=\left.\frac{\partial u_1}{\partial Y_1}\right|_{|Y_1|=L_1}=0, \tag{4.120}$$

and a fixed outer contour, i.e.

$$u_2|_{R_2=L_2+1}=0. \tag{4.121}$$

The continuity conditions on stresses and displacements are formulated as in (4.106) and (4.107), respectively.

As above, we arrive at the leading order eigenforms as

$$\begin{aligned} u_{10}&=C,\\ u_{20}&=CH_2(R_2), \end{aligned} \tag{4.122}$$

where the harmonic function

$$H_2(R_2)=\frac{\ln(L_2+1)-\ln R_2}{\ln(L_2^{-1}+1)}, \tag{4.123}$$

is the solution of (4.119) subject to

$$\begin{aligned} H_2|_{R_2=L_2}&=1,\\ H_2|_{R_2=L_2+1}&=0. \end{aligned} \tag{4.124}$$

The eigensolution (4.122) is shown in Figure 4.6, containing both the displacement profile and its cross section at $y=0$, calculated at $l_0=l_1=l_2=1$.

At next order the boundary value problem for the inner domain is given by

$$\frac{\partial^2u_{11}}{\partial X_1^2}+\frac{\partial^2u_{11}}{\partial Y_1^2}+\Omega_{10}^2u_{10}=0, \tag{4.125}$$

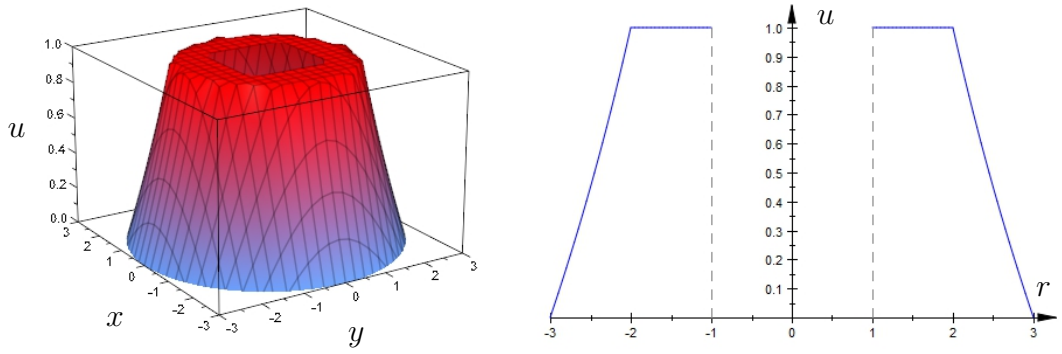

a) Displacement profile b) Axial cross section

Figure 4.6: Displacement profile (4.122); $l_0 = l_1 = l_2 = 1$

subject to

$$\begin{aligned} \left.\frac{\partial u_{11}}{\partial X_1}\right|_{|X_1|=L_1} &= \left.\frac{\partial u_{11}}{\partial Y_1}\right|_{|Y_1|=L_1} = 0, \\ \left.\frac{du_{11}}{dR_1}\right|_{R_1=L_1+1} &= \left.\frac{du_{20}}{dR_2}\right|_{R_2=L_2}, \end{aligned} \tag{4.126}$$

where, employing the solution (4.123), we have

$$\left.\frac{du_{20}}{dR_2}\right|_{R_2=L_2} = -\frac{CL_2^{-1}}{\ln(L_2^{-1}+1)}. \tag{4.127}$$

Thus, we integrate (4.125) over the inner domain D_1 and substitute the solution (4.122) for u_{10} to get

$$\iint\limits_{D_1} \left(\frac{\partial^2 u_{11}}{\partial X_1^2} + \frac{\partial^2 u_{11}}{\partial Y_1^2}\right) dX_1 dY_1 = -C\Omega_{10}^2 A_1, \tag{4.128}$$

where $A_1 = \pi(L_1+1)^2 - 4L_1^2$. Transforming integrals according to the Green's first

identity, we obtain

$$(L_1+1)\int_0^{2\pi}\left.\frac{\partial u_{11}}{\partial R_1}\right|_{R_1=L_1+1}d\varphi-\int_{-L_1}^{L_1}\left.\frac{\partial u_{11}}{\partial X_1}\right|_{|X_1|=L_1}dY_1- \\ -\int_{-L_1}^{L_1}\left.\frac{\partial u_{11}}{\partial Y_1}\right|_{|Y_1|=L_1}dX_1=-C\Omega_{10}^2A_1. \tag{4.129}$$

Thus, the leading order estimate for frequency follows from substitution of the boundary conditions (4.126) with (4.127) into (4.129), i.e.

$$\Omega_{10}^2=\frac{2\pi l^{-1}}{\ln(L_2^{-1}+1)(\pi(L_1+1)^2-4L_1^2)}, \tag{4.130}$$

which match the result in (4.97).

5 Conclusion

The low-frequency vibrations of composite elastic rods and cylindrical bodies with a high contrast in the material and geometric parameters have been investigated. The study proves that a high contrast may result in lowest natural frequencies tending to zero. For each of the considered problems we reveal boundary conditions and problem parameters supporting a non-zero low eigenfrequency and evaluate associated displacement profiles.

In cases of a piecewise-homogeneous three-component rod and a two-component circular cylinder exact solutions were studied. Then, the problems were analysed at the low-frequency asymptotic limit. The associated conditions on problem parameters, e.g see equations (2.48), (2.119), and (2.146) for a rod and equations (3.26) for a circular cylinder, are derived. Both the global and local low-frequency regimes were investigated for a three-component rod, see also Kaplunov et al (2016).

For a rod or a circular cylinder having variable material parameters, see Section 2.3 and Section 3.3, respectively, the related equations of motion usually do not allow explicit analytical solutions. The perturbation technique developed for these cases relies on the concept of the almost rigid body motion. It also has been used to develop the general perturbation procedure adapted for multi-component rods and cylinders. In Chapter 4 the obtained results have been extended to the antiplane low-frequency vibrations of two-layered cylindrical bodies of arbitrary cross sections, see also Kaplunov et al (2017b). To illustrate the efficiency of the proposed scheme the examples of a hollow cylinder of a square cross section with a circular annular inclusion and a two-component cylinder of a circular cross section with a square hole have been considered. It has been demonstrated that the perturbation technique in question enables tackling of mathematical problems that are beyond the scope of exact analysis.

The leading order approximations obtained for properly chosen boundary conditions show that uniform displacement variations corresponding to rigid body motions, occur across all stronger components. In this case, ‶weaker″ parts also experience

quasi-static deformation, which is homogeneous for composite rods. The estimations for the lowest natural frequencies follow from the solvability of boundary value problems for the stronger components at next order of the developed perturbation procedure. The proposed approach is similar in a sense to that presented in Kaplunov et al (2015) for low-frequency motions of viscoelastic bars without the assumption of a contrast.

We also mention several extensions and possible applications of the developed methodology. In particular, the derived asymptotic formulae have a clear relation to the evaluation of the lowest cut-off frequencies of high-contrast layered plates and shells, see Le (1999), Ryazantseva and Antonov (2012), and Kaplunov et al (2017a). In addition, the proposed perturbation approach can be expanded to more sophisticated 2D and 3D eigenfrequency problems for multi-layered strongly inhomogeneous structures with high contrast material and geometric properties, including but not restricted to the computation of higher order corrections to lowest eigenvalues. However, in the latter case, the solution procedure should apparently involve a numerical treatment, at least for weaker parts of studied structures. Even so, such hybrid procedures may be more preferable, then straightforward numerical methods, such as FEM.

Bibliography

Abramovici, F. and Alterman, Z. (1965). Computations pertaining to the problem of propagation of a seismic pulse in a layered solid. *Methods of Computational Physics*, 4:349–379.

Achenbach, J. (2012). *Wave propagation in elastic solids*, volume 16. Elsevier.

Adetona, O., Horta, L., Taleghani, B., Blandino, J., and Woods, K. (2003). Vibration studies of an inflatable/rigidizable hexapod structure with a tensioned membrane. In *Proceedings, 44th AIAA/ASME/ASCE/AHS Structures, Structural Dynamics, and Materials Conference, Norfolk, Virginia*.

Alsahlani, A. and Mukherjee, R. (2013). Dynamics of a circular membrane with an eccentric circular areal constraint: Analysis and accurate simulations. *Simulation Modelling Practice and Theory*, 31:149–168.

Altenbach, H., Eremeyev, V. A., and Naumenko, K. (2015). On the use of the first order shear deformation plate theory for the analysis of three-layer plates with thin soft core layer. *ZAMM-Journal of Applied Mathematics and Mechanics/Zeitschrift für Angewandte Mathematik und Mechanik*, 95(10):1004–1011.

Arbaoui, J., Schmitt, Y., Pierrot, J.-L., and Royer, F.-X. (2015). Comparison study and mechanical characterisation of a several composite sandwich structures. *International Journal of Composite Materials*, 5(1):1–8.

Aşık, M. Z. and Tezcan, S. (2005). A mathematical model for the behavior of laminated glass beams. *Computers & Structures*, 83(21):1742–1753.

Aßmus, M., Naumenko, K., and Altenbach, H. (2016). A multiscale projection approach for the coupled global–local structural analysis of photovoltaic modules. *Composite Structures*, 158:340–358.

Aßmus, M., Nordmann, J., Naumenko, K., and Altenbach, H. (2017). A homogeneous substitute material for the core layer of photovoltaic composite structures. *Composites Part B: Engineering*, 112:353–372.

Baker, A. A. B. (2004). *Composite materials for aircraft structures*. AIAA.

Baruh, H. (2001). Control of the elastic motion of lightweight structures. *AIAA Journal*, 1304:1–9.

Belingardi, G., Cavatorta, M., and Duella, R. (2003). Material characterization of a composite–foam sandwich for the front structure of a high speed train. *Composite structures*, 61(1):13–25.

Beral, B. (2007). *Airbus structure and technology–next steps and vision*. Proceedings of 16th international conference on composite materials. Kyoto.

Berthelot, J.-M. (2012). *Composite materials: mechanical behavior and structural analysis*. Springer Science & Business Media.

Borja, R. I. (2011). *Multiscale and Multiphysics Processes in Geomechanics*. Springer.

Chapman, C. (2013). An asymptotic decoupling method for waves in layered media. In *Proc. R. Soc. A*, volume 469, pages 56–59. The Royal Society.

Cheng, S. (1961). On the theory of bending of sandwich plates. Technical report, Wisconsin Univ Madison Mathematics Research Center.

Cherdantsev, M. and Cherednichenko, K. (2012). Two-scale γ-convergence of integral functionals and its application to homogenisation of nonlinear high-contrast periodic composites. *Archive for Rational Mechanics and Analysis*, 204(2):445–478.

Cherdantsev, M., Cherednichenko, K., and Neukamm, S. (2013). *Homogenisation in finite elasticity for composites with a high contrast in the vicinity of rigid-body motions*. arXiv preprint arXiv:1303.1224.

Cherednichenko, K., Smyshlyaev, V. P., and Zhikov, V. (2006). Non-local homogenized limits for composite media with highly anisotropic periodic fibres. *Proceedings of the Royal Society of Edinburgh Section A: Mathematics*, 136(1):87–114.

Cortinez, V. and Laura, P. (1992). Vibrations of non-homogeneous rectangular membranes. *Journal of sound and vibration*, 156(2):217–225.

Craster, R., Joseph, L., and Kaplunov, J. (2014). Long-wave asymptotic theories: the connection between functionally graded waveguides and periodic media. *Wave Motion*, 51(4):581–588.

Craster, R. V. and Guenneau, S. (2012). *Acoustic metamaterials: Negative refraction, imaging, lensing and cloaking*, volume 166. Springer Science & Business Media.

Dong, L., Grissom, M., and Fisher, F. T. (2015). Resonant frequency of mass-loaded membranes for vibration energy harvesting applications. *AIMS Energy*, 3(3):344–359.

Elishakoff, I. (2004). *Eigenvalues of inhomogeneous structures: unusual closed-form solutions*. CRC Press.

Elishakoff, I. and Perez, A. (2005). Design of a polynomially inhomogeneous bar with a tip mass for specified mode shape and natural frequency. *Journal of sound and vibration*, 287(4):1004–1012.

Elishakoff, I. and Yost, J. (2010). Design for a specified natural frequency of elastically constrained axially graded bars. *Acta Mechanica Sinica*, 26(2):313–316.

Eringen, A. C. (1951). Bending and buckling of rectangular sandwich plates. In *Journal of Applied Mechanics-Transactions of the ASME*, volume 18, pages 330–330. ASME-AMER soc Mechanical eng 345 E 47TH ST, New York, NY 10017.

Ewing, W. M., Jardetzky, W. S., Press, F., and Beiser, A. (1957). Elastic waves in layered media. *Physics Today*, 10:27–35.

Figotin, A. and Kuchment, P. (1998). Spectral properties of classical waves in high-contrast periodic media. *SIAM Journal on Applied Mathematics*, 58(2):683–702.

Gei, M., Movchan, A., and Bigoni, D. (2009). Band-gap shift and defect-induced annihilation in prestressed elastic structures. *Journal of Applied Physics*, 105(6):493–507.

Goldenveizer, A., Kaplunov, J., and Nolde, E. (1993). On timoshenko-reissner type theories of plates and shells. *International Journal of Solids and Structures*, 30(5):675–694.

Graff, K. (1975). *Wave motion in elastic solids, reprinted 1991*. Dover, Mineola, NY ed., Clarendon Press, Oxford.

Gridin, D., Craster, R. V., and Adamou, A. T. I. (2005). Correction for Gridin et al., Trapped modes in curved elastic plates. *Proceedings of the Royal Society of London A: Mathematical, Physical and Engineering Sciences*, 461(2064):4057–4061.

Grossman, S. I. (2014). *Multivariable calculus, linear algebra, and differential equations*. Academic Press.

Helsing, J., McPhedran, R. C., and Milton, G. W. (2011). Spectral super-resolution in metamaterial composites. *New Journal of Physics*, 13(11):115–125.

Hoff, N. J. (1950). *Bending and buckling of rectangular sandwich plates*. Polytechnic Institute of Brooklyn.

Horgan, C. and Chan, A. (1999). Vibration of inhomogeneous strings, rods and membranes. *Journal of Sound and Vibration*, 225(3):503–513.

Hsu, S., Ford, G., and Krimm, S. (1977). Longitudinal acoustic mode in polymers. ii. solution of the general composite perturbed elastic rod. *Journal of Polymer Science Part B: Polymer Physics*, 15(10):1769–1778.

Hsu, S. and Krimm, S. (1976). Longitudinal acoustic mode in polymers. *Journal of Applied Physics*, 47(10):4265–4270.

Kaplunov, J. (1995). Long-wave vibrations of a thinwalled body with fixed faces. *The Quarterly Journal of Mechanics and Applied Mathematics*, 48(3):311–327.

Kaplunov, J. and Nobili, A. (2017). Multi-parametric analysis of strongly inhomogeneous periodic waveguideswith internal cutoff frequencies. *Mathematical Methods in the Applied Sciences*, 40(9):3381–3392.

Kaplunov, J., Nolde, E., and Rogerson, G. (2002). An asymptotically consistent model for long-wave high-frequency motion in a pre-stressed elastic plate. *Mathematics and Mechanics of Solids*, 7(6):581–606.

Kaplunov, J., Prikazchikov, D., and Prikazchikova, L. (2017a). Dispersion of elastic waves in a strongly inhomogeneous three-layered plate. *International Journal of Solids and Structures*, 113:169–179.

Kaplunov, J., Prikazchikov, D., and Prikazchikova, L. (2017c). Dispersion of elastic waves in laminated glass. *Procedia engineering*, 199:1489–1494.

Kaplunov, J., Prikazchikov, D., and Sergushova, O. (2016). Multi-parametric analysis of the lowest natural frequencies of strongly inhomogeneous elastic rods. *Journal of Sound and Vibration*, 366:264–276.

Kaplunov, J., Prikazchikov, D. A., and Sergushova, O. (2017b). Lowest vibration modes of strongly inhomogeneous elastic structures. In *Mechanics for Materials and Technologies*, pages 265–277. Springer.

Kaplunov, J., Shestakova, A., Aleynikov, I., Hopkins, B., and Talonov, A. (2015). Low-frequency perturbations of rigid body motions of a viscoelastic inhomogeneous bar. *Mechanics of Time-Dependent Materials*, 19(2):135–151.

Kaplunov, J., Yu Kossovich, L., and Rogerson, G. (2000). Direct asymptotic integration of the equations of transversely isotropic elasticity for a plate near cut-off frequencies. *The Quarterly Journal of Mechanics and Applied Mathematics*, 53(2):323–341.

Kaplunov, J. D., Kossovich, L. Y., and Nolde, E. (1998). *Dynamics of thin walled elastic bodies*. Academic Press.

Kaplunov, J. D. and Markushevich, D. G. (1993). Plane vibrations and radiation of an elastic layer lying on a liquid half-space. *Wave Motion*, 17(3):199 – 211.

Kaplunov, J. D. and Nolde, E. V. (2002). Long-wave vibrations of a nearly incompressible isotropic plate with fixed faces. *The Quarterly Journal of Mechanics and Applied Mathematics*, 55(3):345–356.

Kaplunov, J. D., Rogerson, G. A., and Tovstik, P. E. (2005). Localized vibration in elastic structures with slowly varying thickness. *The Quarterly Journal of Mechanics and Applied Mathematics*, 58(4):645–664.

Kevorkian, J. and Cole, J. D. (2013). *Perturbation methods in applied mathematics*, volume 34. Springer Science & Business Media.

Kim, J.-S. and Chung, S.-K. (2007). A study on the low-velocity impact response of laminates for composite railway bodyshells. *Composite structures*, 77(4):484–492.

Kreja, I. (2011). A literature review on computational models for laminated composite and sandwich panels. *Open Engineering*, 1(1):59–80.

Kudaibergenov, A., Nobili, A., and Prikazchikova, L. (2016). On low-frequency vibrations of a composite string with contrast properties for energy scavenging fabric devices. *Journal of Mechanics of Materials and Structures*, 11(3):231–243.

Laura, P., Bambill, D., and Gutierrez, R. (1997). *A note on transverse vibrations of circular, annular, composite membranes*. Elsevier.

Laura, P., Ercoli, L., Grossi, R., Nagaya, K., and Sarmiento, G. S. (1985). Transverse vibrations of composite membranes of arbitrary boundary shape. *Journal of Sound and Vibration*, 101(3):299–306.

Le, K. C. (2012). *Vibrations of shells and rods*. Springer Science & Business Media.

Lee, J., Wang, Z., He, K., Shan, J., and Feng, P. X.-L. (2013). High frequency mos2 nanomechanical resonators. *ACS nano*, 7(7):6086–6091.

Lee, N. and Pellegrino, S. (2014). Multi-layered membrane structures with curved creases for smooth packaging and deployment. In *AIAA Spacecraft Structures Conference*.

Lee, P. and Chang, N. (1979). Harmonic waves in elastic sandwich plates. *Journal of Elasticity*, 9(1):51–69.

Lutianov, M. and Rogerson, G. A. (2010). Long wave motion in layered elastic media. *International Journal of Engineering Science*, 48(12):1856–1871.

Martin, T. P., Layman, C. N., Moore, K. M., and Orris, G. J. (2012). Elastic shells with high-contrast material properties as acoustic metamaterial components. *Physical Review B*, 85(16):103–161.

Milton, G. W. (2002). The theory of composites. *The Theory of Composites, by Graeme W. Milton, pp. 748. ISBN 0521781256. Cambridge, UK: Cambridge University Press, May 2002.*, pages 748–760.

Mindlin, R. (1959). Flexural vibrations of elastic sandwich plates. Technical report, Columbia Univ New York Dept of Civil Engineering and Engineering Mechanics.

Mines, R., Worrall, C., and Gibson, A. (1998). Low velocity perforation behaviour of polymer composite sandwich panels. *International Journal of Impact Engineering*, 21(10):855–879.

Mo, C., Davidson, J., and Clark, W. W. (2014). Energy harvesting with piezoelectric circular membrane under pressure loading. *Smart Materials and Structures*, 23(4):045–055.

Naumenko, K. and Eremeyev, V. A. (2014). A layer-wise theory for laminated glass and photovoltaic panels. *Composite Structures*, 112:283–291.

Nayfeh, A. H. (2011). *Introduction to perturbation techniques*. John Wiley & Sons.

Nobili, A. (2012). Superposition principle for the tensionless contact of a beam resting on a winkler or a pasternak foundation. *Journal of Engineering Mechanics*, 139(10):1470–1478.

Nobili, A. and Lanzoni, L. (2010). Electromechanical instability in layered materials. *Mechanics of Materials*, 42(5):581–591.

Noor, A. K. and Burton, W. S. (1989). Assessment of shear deformation theories for multilayered composite plates. *Appl. Mech. Rev*, 42(1):1–13.

Papa, A. and Pellegrino, S. (2008). Systematically creased thin-film membrane structures. *Journal of Spacecraft and Rockets*, 45(1):10–18.

Perrins, W. and McPhedran, R. (2010). Metamaterials and the homogenization of composite materials. *Metamaterials*, 4(1):24–31.

Piccolroaz, A. and Movchan, A. (2014). Dispersion and localisation in structured rayleigh beams. *International Journal of Solids and Structures*, 51(25):4452–4461.

Pichugin, A. V. and Rogerson, G. A. (2001). A two-dimensional model for extensional motion of a pre-stressed incompressible elastic layer near cut-off frequencies. *IMA Journal of Applied Mathematics*, 66(4):357–368.

Pichugin, A. V. and Rogerson, G. A. (2002). Anti-symmetric motion of a pre-stressed incompressible elastic layer near shear resonance. *Journal of Engineering Mathematics*, 42(2):181–202.

Prikazchikova, L., Ece Aydın, Y., Erbaş, B., and Kaplunov, J. (2018). Asymptotic analysis of an anti-plane dynamic problem for a three-layered strongly inhomogeneous laminate. *Mathematics and Mechanics of Solids*, pages 108–128.

Qatu, M. S. (2004). *Vibration of laminated shells and plates*. Elsevier.

Qin, Y., Wang, X., and Wang, Z. L. (2008). Microfibre-nanowire hybrid structure for energy scavenging. *nature*, 451(7180):809–816.

Ramakrishna, S., Mayer, J., Wintermantel, E., and Leong, K. W. (2001). Biomedical applications of polymer-composite materials: a review. *Composites science and technology*, 61(9):1189–1224.

Reddy, J. N. (2004). *Mechanics of laminated composite plates and shells: theory and analysis*. CRC press.

Reissner, E. (1947). On bending of elastic plates. *Quarterly of Applied Mathematics*, 5(1):55–68.

Renno, J. M. (2008). *Dynamics and control of membrane mirrors for adaptive optic applications*. PhD thesis, University Libraries, Virginia Polytechnic Institute and State University.

Rezaeisaray, M., El Gowini, M., Sameoto, D., Raboud, D., and Moussa, W. (2014). Wide-bandwidth piezoelectric energy harvester with polymeric structure. *Journal of Micromechanics and Microengineering*, 25(1):015–018.

Rion, J. (2008). *Ultra-light photovoltaic composite sandwich structures*. EPFL.

Romeo, G., Frulla, G., Cestino, E., and Corsino, G. (2004). Heliplat: design, aerodynamic, structural analysis of long-endurance solar-powered stratospheric platform. *Journal of Aircraft*, 41(6):1505–1520.

Ruffier, F., Benacchio, S., Expert, F., and Ogam, E. (2011). A tiny directional sound sensor inspired by crickets designed for micro-air vehicles. In *Sensors, 2011 IEEE*, pages 970–973. IEEE.

Ruzzene, M. and Baz, A. (2000). Attenuation and localization of wave propagation in periodic rods using shape memory inserts. *Smart materials and Structures*, 9(6):805–812.

Ryazantseva, M. Y. and Antonov, F. K. (2012). Harmonic running waves in sandwich plates. *International Journal of Engineering Science*, 59:184–192.

Salernitano, E. and Migliaresi, C. (2003). Composite materials for biomedical applications: a review. *Journal of Applied Biomaterials & Biomechanics*, 1(1):3–18.

Sayyad, A. S. and Ghugal, Y. M. (2015). On the free vibration analysis of laminated composite and sandwich plates: a review of recent literature with some numerical results. *Composite Structures*, 129:177–201.

Schlicke, H., Schröter, C. J., and Vossmeyer, T. (2016). Electrostatically driven drumhead resonators based on freestanding membranes of cross-linked gold nanoparticles. *Nanoscale*, 8(35):15880–15887.

Schulze, S.-H., Pander, M., Naumenko, K., and Altenbach, H. (2012). Analysis of laminated glass beams for photovoltaic applications. *International Journal of Solids and Structures*, 49(15):2027–2036.

Simmonds, J. G. and Mann, J. E. (2013). *A first look at perturbation theory*. Courier Corporation.

Smyshlyaev, V. P. (2009). Propagation and localization of elastic waves in highly anisotropic periodic composites via two-scale homogenization. *Mechanics of Materials*, 41(4):434–447.

Song, J., Zhou, J., and Wang, Z. L. (2006). Piezoelectric and semiconducting coupled power generating process of a single zno belt/wire. a technology for harvesting electricity from the environment. *Nano letters*, 6(8):1656–1662.

Sorokin, S. V. (2004). Analysis of wave propagation in sandwich plates with and without heavy fluid loading. *Journal of Sound and Vibration*, 271(3):1039–1062.

Sosa, M., Carneiro, A., Colafemina, J., and Baffa, O. (2001). A new magnetic probe to study the vibration of the tympanic membrane. *Journal of magnetism and magnetic materials*, 226:2067–2069.

Spence, J. and Horgan, C. (1983). Bounds on natural frequencies of composite circular membranes: integral equation methods. *Journal of Sound and Vibration*, 87(1):71–81.

Spencer, A. J. M. (2004). *Continuum mechanics*. Courier Corporation.

Strauss, W. A. (1992). *Partial differential equations*, volume 92. Wiley New York.

Tassicker, O. J. (1972). *Aspects of forces on charged particles in electrostatic precipitators*. PhD thesis.

Temme, N. M. (2011). *Special functions: An introduction to the classical functions of mathematical physics*. John Wiley & Sons.

Thorp, O., Ruzzene, M., and Baz, A. (2001). Attenuation and localization of wave propagation in rods with periodic shunted piezoelectric patches. *Smart Materials and Structures*, 10(5):979–988.

Titovich, A. S. (2015). *Acoustic and elastic waves in metamaterials for underwater applications*. Rutgers The State University of New Jersey-New Brunswick.

Torre, L. and Kenny, J. (2000). Impact testing and simulation of composite sandwich structures for civil transportation. *Composite structures*, 50(3):257–267.

Tovstik, P. E. and Tovstik, T. P. (2017). Generalized timoshenko-reissner models for beams and plates, strongly heterogeneous in the thickness direction. *ZAMM-Journal of Applied Mathematics and Mechanics/Zeitschrift für Angewandte Mathematik und Mechanik*, 97(3):296–308.

Vinson, J. R. (1999). *The behavior of sandwich structures of isotropic and composite materials*. CRC Press.

Wang, C., Reddy, J. N., and Lee, K. (2000). *Shear deformable beams and plates: Relationships with classical solutions*. Elsevier.

Wang, C. Y. and Wang, C. (2013). *Structural vibration: Exact solutions for strings, membranes, beams, and plates*. CRC Press.

Wang, W., Yang, T., Chen, X., and Yao, X. (2012). Vibration energy harvesting using a piezoelectric circular diaphragm array. *IEEE transactions on ultrasonics, ferroelectrics, and frequency control*, 59(9):1–9.

Yermolayev, B. (1992). The use of generalized functions in the problem of elastic oscillations of a composite rod. *Journal of Applied Mathematics and Mechanics*, 56(3):383–389.

Yu, Y.-Y. (1959). *Flexural vibrations of elastic sandwich plates*. United States Air Force, Office of Scientific Research.

Zenkert, D. (1995). *An introduction to sandwich construction*. Engineering materials advisory services.

Zhang, Y. and Yang, C. (2009). Recent developments in finite element analysis for laminated composite plates. *Composite Structures*, 88(1):147–157.

Zinno, A., Fusco, E., Prota, A., and Manfredi, G. (2010). Multiscale approach for the design of composite sandwich structures for train application. *Composite Structures*, 92(9):2208–2219.